Impact of Elastic Passage on the Peristaltic Transport of Williamson Fluid with Slip Effects

BY

Hadia Perveen

NATIONAL UNIVERSITY OF MODERN LANGUAGES
ISLAMABAD

December, 2025

Impact of Elastic Passage on the Peristaltic Transport of Williamson Fluid with Slip Effects

By

Hadia Perveen

MS MATH, NATIONAL UNIVERSITY OF MODERN LANGUAGES ISLAMABAD 2025.

A THESIS SUBMITTED IN PARTIAL FULFILMENT OF
THE REQUIREMENTS FOR THE DEGREE OF

MASTER OF SCIENCE
In MATHEMATICS

TO
FACULTY OF ENGINEERING AND COMPUTING

NATIONAL UNIVERSITY OF MODERN LANGUAGES ISLAMABAD

THESIS AND DEFENSE APPROVAL FORM

The undersigned certify that they have read the following thesis, examined the defense, are satisfied with overall exam performance, and recommend the thesis to the Faculty of Engineering and Computing for acceptance.

Thesis Title: Impact of Elastic Passage on the Peristaltic Transport of Williamson Fluid with Slip Effects

Submitted by: Hadia Perveen **Registration #:** 91MS/Math/F23

Master of Science in Mathematics
Title of the Degree

Mathematics
Name of Discipline

Dr. Hadia Tariq _____
Name of Research Supervisor Signature of Research Supervisor

Dr. Anum Naseem _____
Name of HOD (Math) Signature of HOD (Math)

Dr. Noman Malik _____
Name of Dean (FEC) Signature of Dean (FEC)

December 16th, 2025

AUTHOR'S DECLARATION

I Hadia Perveen

Daughter of Muhammad Hussain

Registration# 91MS/Math/F23

Discipline Mathematics

Candidate of **Master of Science in Mathematics (MS MATH)** at the National University of Modern Languages do hereby declare that the thesis **Impact of Elastic Passage on the Peristaltic Transport of Williamson Fluid with Slip Effects** submitted by me in partial fulfillment of MS Math degree, is my original work, and has not been submitted or published earlier. I also solemnly declare that it shall not, in future, be submitted by me for obtaining any other degree from this or any other university or institution. I also understand that if evidence of plagiarism is found in my thesis/dissertation at any stage, even after the award of a degree, the work may be cancelled and the degree revoked.

Hadia Perveen
Name of Candidate

_____
Signature of Candidate

Date: 16th December 2025

ABSTRACT

Title: Impact of Elastic Passage on the Peristaltic Transport of Williamson Fluid with Slip Effects

The main focus of this thesis is to investigates the impact of elastic wall properties on the peristaltic transport of Williamson fluid through a symmetric passage, incorporating the effects of slip boundary conditions. The mathematical model is developed under the assumptions of long wavelength and low Reynolds number, enabling the use of the lubrication approach. To address the nonlinear nature of the governing momentum and energy equations, a perturbation technique is applied to obtain approximate analytical solutions. The analysis explores variations in velocity distribution, pressure rise, and streamline patterns under the combined influence of wall elasticity and slip effects. Special emphasis is placed on extending the work where the peristaltic motion of Williamson fluid between concentric cylinders with an elastic outer wall was considered. In this framework, additional factors such as velocity slip at the boundaries, porosity, and magnetohydrodynamic (MHD) effects are incorporated into the model formulated in cylindrical coordinates. Solutions are derived using a regular perturbation method, while Mathematica software is employed for graphical representation of the results. The findings reveal that wall elasticity and slip conditions significantly modify the velocity profiles, shear stress, and trapping phenomena of the Williamson fluid. These results contribute to a deeper understanding of peristaltic transport mechanisms, with potential applications in physiological processes and industrial fluid systems.

TABLE OF CONTENTS

CHAPTER	TITLE	PAGE
	AUTHOR'S DECLARATION	**iii**
	ABSTRACT	**iv**
	TABLE OF CONTENTS	**v**
	LIST OF FIGURES	**x**
	LIST OF SYMBOLS	**xii**
	ACKNOWLEDGEMENT	**xiv**
	DEDICATION	**xv**

CHAPTER: 1……..……1

1. INTRODUCTION AND LITERATURE REVIEW 1

1.1 Introduction.....1

1.2 Peristalsis 1

1.3 Williamson Fluid..... 5

1.4 Wall Properties..... 6

1.5 Cylindrical Coordinates 8

1.6 Porosity..... 8

1.7 Magnetohydrodynamics 9

1.8 Slip Boundary Condition 10

1.9 Thesis Contribution..... 10

1.10 Thesis Organization 10

CHAPTER: 2 12

2. BASIC DEFINITIONS..... 12

2.1 Mechanics.....12

2.1.1 Statics 12

2.1.2 Dynamics.....12

2.2 Fluid.....12

2.2.1 Gas 12

2.2.2 Liquids.....13

2.3 Fluid Mechanics 13

2.4 Properties of Fluids 14

2.4.1 Compressibility..... 14

2.4.2 Density..... 14

2.4.3 Pressure 14

2.4.4 Temperature..... 15

2.4.5 Viscosity..... 15

2.4.6 Dynamic Viscosity 15

2.4.7 Kinematic Viscosity 15

2.4.8 Specific Heat 16

2.4.9 Heat Flux..... 16

2.4.10 Heat generation and Absorption 16

2.4.11 Thermal Conductivity..... 16

2.4.12 Thermal Diffusivity 17

2.4.13 Viscous Disspation ……. 17

2.5 Rheology 17

2.6 Flow..... 17

2.6.1 Steady and Unsteady Flow..... 18

2.6.2 Uniform and Non uniform 18
2.6.3 Compressible and Incompressible Flow 18
2.6.4 Rotational and Irrotational Flow 18
2.6.5 Laminar Turbulent Flow 19
2.7 Newton's Law of Viscosity 19
2.8 Types of Fluid 19
2.8.1 Ideal Fluid 20
2.8.2 Real Fluid 20
2.8.3 Newtonian Fluid 20
2.8.4 Non Newtonian Fluid 20
2.8.4.1 Rheopectic or Anti-Thixotropic Fluid 21
2.8.4.2 Thixotropic Fluid 21
2.8.4.3 Dilatant Fluid 22
2.8.4.4 Pseudo-plastic 21
2.8.4.5 Bingham- Plastic 22
2.9.1 Scalar Field 22
2.9.2 Tensor Field 22
2.9.3 Vector Field 22
2.9.4 Velocity Field 23
2.10 Dimensions Numbers 23
2.10.1 Prandtl Number 23
2.10.2 Eckert Number 23
2.10.3 Reynolds Number 24
2.10.4 Weissenberg Number 24
2.10.5 Grashof Number 25
2.10.6 Biot Number 25
2.10.5 Hartmann Number 25

2.11 Heat Transfer 26
2.11.1 Conduction 26
2.112 Convection 26
2.11.3 Radiation 26
2.12 Stress 27
2.12.1 Shear Stress 27
2.12.2 Normal Stress 27
2.12.3 Cauchy Stress Tensor 27
2.12.4 Extra Stress Tensor 28
2.112 Strain 28
2.13 Streamline 28
2.13.1 Stream Function 28
2.14 Darcy's Law 28
2.15 Basic Equations and Conservation Laws 29
2.15.1 Continuity Equation 29
2.15.2 Momentum Equation 29
2.15.3 Energy Equation 30
2.16 Perturbation Method 30

CHAPTER 3 31

3. THE PERISTALTIC FLOW OF WILLIAMSON FLUID THROUGH A FLEXIBLE CHANNEL 31

3.1 Introduction 31
3.2 Physical Model 31
3.3 Solution Methodology 38
3.3.1 System of Zero Order 38

3.3.2 First Order System 38

3.3.2 Second order System 39

3.4 Results and Discussion..... 40

CHAPTER 4..... 55

4. IMPACT OF ELASTIC PASSAGE ON THE PERISTALTIC TRANSPORT OF WILLIAMSON FLUID WITH SLIP EFFECTS…..55

4.1 Introduction..... 55

4.2 Physical Model..... 55

4.3 Solution and Methodology 61

4.3.1 System of Zero Order 61

4.3.2 First Order System..... 61

4.4 Results and Discussion 62

CHAPTER 5..... 77

5. CONCLUSION AND FUTURE WORK ……77

5.1 Conclusion.....77

5.2 Future Work…….. 78

REFERENCES 79

LIST OF FIGURES

FIGURE NO.	TITLE	PAGE
Fig. 1.1	Image of blood dialysis devices	2
Fig. 1.2	Movement of food through esophagus	2
Fig. 1.3	Image of Peristaltic Pump	3
Fig. 1.4	Characteristics Elastic Passage	7
Fig. 2.1	Classification of Fluid Mechanics	13
Fig. 3.1	The Geometry of the Problem	32
Fig. 3.2	Variation of φ on velocity field	47
Fig. 3.3	Variation of We on velocity field	47
Fig. 3.4	Variation of L_1 on velocity field	48
Fig. 3.5	Variation of L_2 on velocity field	48
Fig. 3.6	Variation of L_3 on velocity	49
Fig. 3.7	Variation of L_4 on velocity field	49
Fig. 3.8	Variation of L_5 on velocity field	50
Fig. 3.9	Variation of ϵ on velocity field	50
Fig. 3.10	Variation of φ on Shear-Stress	51
Fig. 3.11	Variation of L_1 on Shear-Stress	51
Fig. 3.12	Variation of L_2 on Shear-Stress	52

Fig. 3.13	Variation of L_3 on at Shear-Stress	52
Fig. 3.14	Variation of L_4 on Shear-Stress	53
Fig. 3.15	Variation of L_5 on Shear-Stress	53
Fig. 3.16	Variation of ϵ on Shear-Stress	54
Fig. 3.17	Variation of We on Shear-Stress	54
Fig. 4.1	Geometry of the Tube	56
Fig. 4.2	Streamlines for the diverse values of magnetic parameter	65
Fig. 4.3	Streamlines for the diverse values of Porosity parameter	66
Fig. 4.4	Streamlines for the diverse value of flexural stiffness of wall (L_1)	67
Fig. 4.5	Streamlines for the diverse of longitudinal tension per unit width (L_2)	68
Fig. 4.6	Streamlines for diverse of Mass per unit area (L_3)	69
Fig. 4.7	Streamlines for the diverse of coefficient of viscid damping (L_4)	70
Fig. 4.8	Streamlines for the diverse of Spring stiffness (L_5)	71
Fig. 4.9	Streamlines for the diverse values of slip parameter	72
Fig. 4.10	Velocity distribution for the diverse values of slip parameter	73
Fig. 4.11	Velocity distribution for the diverse values of Weissenberg number	73
Fig. 4.12	Velocity distribution for the diverse values of Magnetic Parameter	74
Fig. 4.13	Velocity distribution for the diverse values of Porosity Parameter	74
Fig. 4.14	Velocity distribution for the diverse values of Grashof Number	75
Fig. 4.15	Velocity distribution for the diverse values of B	75
Fig. 4.16	Velocity distribution for the diverse values of Wall Properties	76
Fig. 4.17	Temperature distribution for the diverse values of B	76

LIST OF SYMBOLS

S	Extra Stress Tensor
ρ	Density
T	Temperature
τ	Shear Stress Corresponding to the half Dynamic Viscosity
μ	Dynamic Viscosity
Π	Second Order Invariant of Stress Tensor
b	Amplitude of the peristaltic wave
a_1	Radius of inner region of tube
a_2	Average radius of the tube
t	Time
g	Gravity
R	Radial Direction

Z	Axial Direction
η	Inclination angle
s	Wave Speed
U_1	Velocity in Radial Direction
U_3	Velocity in Axial Direction
l	Wavelength
K	Thermal conductivity
Q_0	Heat generation
Pr	Prandlt number
B	Biot number
Gr	Grashof number
P	Pressure
Re	Reynold number
$\widetilde{K}$	Wall deformation operator
M	Hartmann Number
We	Weissenberg Number (Williamson Fluid parameter)
Da	Darcy Number

ACKNOWLEDGEMENT

I want to thank and honour Allah Ta'ala for making this study possible and fruitful. Without the sincere support provided by numerous sources for which I would want to sincerely thank you this project could not have been completed. However, a lot of people helped me succeed, and I will always be grateful for their support. I owe a debt of gratitude to Dr. Hadia Tariq, whose counsel, insight, and steadfast support have been invaluable to me during this study process. I consider myself extremely fortunate to have had her as my mentor because her knowledge and guidance have been helpful.

DEDICATION

This thesis work is dedicated to my parents and my teachers, whose steadfast encouragement and support have propelled me to pursue my academic goals. I am incredibly appreciative to my parents for their traits and contributions that have inspired and pushed me during this journey. Your advice and kindness have been a consistent source of support.

CHAPTER 1

INTRODUCTION AND LITERATURE REVIEW

1.1 Introduction

Fluid mechanics explores how liquids and gases behave, whether they are stationary (fluid statics) or in motion (fluid dynamics), and how they interact with surrounding surfaces or other fluids. This area of study is crucial in explaining every-day and industrial phenomena from how blood moves through the human body and air is exchanged during breathing, to how fish swim and how machines like pumps, turbines, and aircraft function. It also helps us understand natural events like river currents, wind behavior, and the movement of water through pipelines. The way that fluids and solids react to shear stresses is one of their main differences while solids can resist shape changes under stress, fluids do not even a slight shear force will cause a fluid to continuously deform and flow. This behavior stems from the way fluid molecules are arranged, allowing them to move freely and adapt their shape over time. Fluid mechanics brings together physical theories and real-world experiments to analyze and forecast how fluids will act under different conditions. Because fluid behavior is affected by various factors such as pressure, temperature and material properties, engineers and scientists rely on both mathematical models and laboratory testing to gain accurate insights (Farank, 1996).

1.2 Peristalsis

Peristaltic flow refers to the movement of fluid driven by wave-like contractions along a flexible tube or wall, typically following a sinusoidal pattern. This mechanism plays a key role in many natural and engineered systems, where it generates pressure changes that propel fluid forward often from regions of lower pressure to higher pressure. Peristalsis is particularly effective in handling complex, non-Newtonian fluids, making it suitable for a range of applications. In biological systems, it is essential for transporting fluids and particles through narrow channels or vessels. Peristaltic pumping transports a number of complex rheological fluids. In particular, peristaltic motion appears in urine transport from kidney to bladder

(Roshani *et al.*, 1999), dialysis devices (Fig. 1.1), ovum movement in the fallopian tube, the digestive, system male reproductive tract, bile duct, gastrointestinal tract, fallopian tube, worm locomotion, chyme motion in the small intestinal tract (Macagno & Christensen, 1980), (Nadeem *et al.*, 2012), roller and finger pumps cardiovascular flows the mechanical and neurological features of reflux, lymphatic vessel transfer. Peristaltic flow is also used for embryo movement in the uterus and early embryonic heart development, uterine cavities ,heart tubes(Taber et al., 2007), in swallowing food through the oesophagus (Paterson, 2006) (Fig. 1.2), and pharmaceutical delivery systems (Tripathi & Bég, 2014). Aggressive chemicals and sanitary fluids are also transported using the peristaltic transport mechanism. Peristalsis, which offers significantly higher efficiency and safety than traditional methods. The peristalsis principle is also used in the engineering of hose pumps, tube pumps, roller pumps (Fig. 1.3), and finger pumps. To put it briefly, peristaltic motion is how fluid moves naturally in living systems and is used by humans to their benefit when creating a variety of industrial and medical engineering instruments.

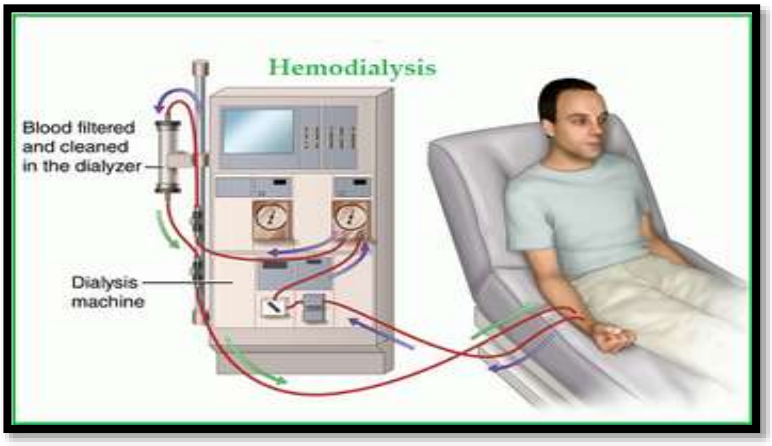

Fig. 1.1 Image of blood dialysis devices

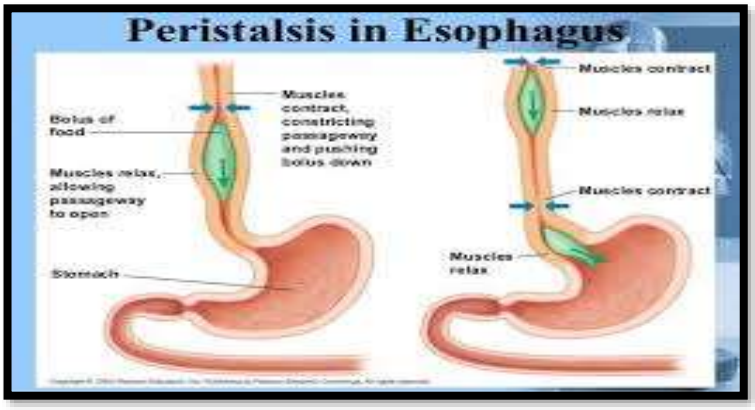

Fig. 1.2 Movement of food through esophagus.

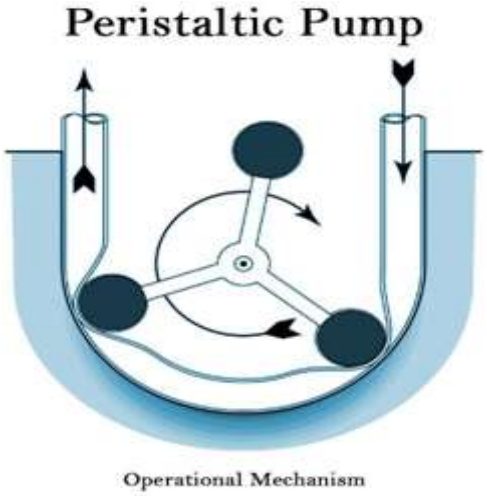

Fig. 1.3 Image of Peristaltic Pump

(Latham, 1966) researched into the mechanism behind peristaltic transfer. After then, there is a substantial body of research on Newtonian and non-Newtonian fluids' peristaltic mechanism.

Initial studies on peristaltic motion primarily revolved around understanding urine transport through the ureters, with foundational contributions from, (Weinberg, 1970), (Lykoudis, 1971), (Burns & Parkes, 1967), (Hanin, 1968) and (Jaffrin & Shapiro, 1971). These early efforts were largely theoretical, establishing essential frameworks to comprehend the mechanics of peristaltic flow without delving deeply into the underlying physiological processes.

In a notable advancement, (Jaffrin, 1973) applied regular perturbation methods to analyze peristaltic flow in a planar channel within the wave frame, particularly under conditions involving small wave numbers. This provided a more refined understanding of the wave-induced fluid motion. Building upon this, (Srivastava & Srivastava, 1985) investigated pulsatile flow in a cylindrical tube, demonstrating how varying flow patterns influence peristaltic transport in confined geometries. Meanwhile, (Gupta & Seshadri, 1976) addressed peristaltic movement in non-uniform tubes and channels, highlighting the complexities introduced by irregular geometries an issue frequently encountered in both biological tissues and industrial systems.

Additional numerical approaches to planar geometries were developed by (Gupta & Seshadri, 1976) and (Brown & Hung, 1977), while (Takabatake *et al.*, 1988) expanded the scope by

considering axisymmetric configurations. Later,(Afifi & Gad, 2001) explored peristaltic flow of magneto-fluids in porous media, building on the findings of Srivastava and Srivastava. (El Misery & El Shamy, 2004), using low Reynolds number approximations, analyzed peristaltic transport affected by endoscopic tools and variable-viscosity fluids. Their analytical formulation, based on the Weissenberg number, offered a new perspective on viscoelastic behaviors under medical conditions.

Research also began focusing on boundary slip and its influence on peristaltic behavior. (Kwang-Hua Chu & Fang, 2000) examined how slip at the tube walls affected the motion of viscous fluids, revealing implications for both physiological flows and engineered systems. (Mekheimer, 2005), employing the long wavelength and zero Reynolds number approximations, studied peristaltic motion in liquid confined between coaxial tubes both uniform and non-uniform. His findings highlighted how geometric irregularities significantly reduce pressure rise. Similarly, investigated the effect of suction on (El-Shehawey & Husseny, 2002) viscous flow in channels and presented analytical insights for low-amplitude waves using perturbation techniques.

A more intricate perspective on peristaltic transport in porous and asymmetric channels was introduced by (Elshehawey *et al.,* 2006), who applied the Adomian decomposition method to derive explicit stream functions for incompressible viscous fluids. Their findings were particularly relevant for biological and industrial settings involving porous media.(Hayat *et al.*, 2008) built upon this by incorporating partial slip effects especially important in micro-scale systems and non-ideal boundary conditions adding another layer of realism to the modelling of peristaltic systems.

These efforts collectively underline how channel geometry, porous structures, wall motion, and slip conditions substantially influence fluid behavior. While most of these models assumed Newtonian behavior, real-world applications often involve fluids that deviate from this assumption. Newton's law of viscosity, which formed the basis for many classical models, does not accurately describe the rheology of many biological and industrial fluids.

This realization prompted several researchers to investigate the peristaltic motion of non-Newtonian fluids using both analytical and computational approaches. (Raju & Devanathan,

1972) were among the first to address this, employing a fading memory model to study viscoelastic fluid transport. They derived solutions for peristaltic motion under small-amplitude oscillations using power-law assumptions. (Böhme & Friedrich, 1983) further explored peristaltic behavior in linear viscoelastic fluids, emphasizing the performance characteristics of peristaltic pumps a technology commonly used in medical applications.

(Siddiqui & Schwarz, 1994) examined the motion of a second-order fluid within an axisymmetric duct, deriving perturbation-based expressions to relate pressure gradients and flow rates. Their study accounted for parameters such as occlusion and fluid elasticity. (Misra & Pandey, 2001) developed a model of esophageal swallowing involving power-law fluids in finite-length circular channels. Later contributions by (Ali & Hayat, 2007) and (Hariharan *et al.*, 2008) analyzed peristaltic transport in diverging channels, discussing key behaviors like trapping, axial pressure distribution, and efficiency of pumping under non-Newtonian assumptions.

Additional studies considered yield-stress fluids, such as Casson models, within low Reynolds number and long wavelength long regimes, particularly in wave frames where fluid velocity matches wave propagations. Futhermore examined the effects of heat and mass transfer in an endoscope's peristaltic Eyring-Powell fluid flow by (Akbar & Nadeem, 2012).In another research in which the Weissenberg number includes the non-Newtonian coefficients relevant to shear thinning investigated by (Srinivas *et al.*, 2017).

The literature currently in publication provides an overview of numerous intriguing theoretical and experimental investigations on peristaltic flow mechanisms involving different fluids. These studies frequently make the assumption of long wavelengths and low Reynolds numbers. A few studies relevant to this mechanism are presented by (Rafiq *et al.*, 2023), (Yasmin & Nisar, 2023) and (Hafez, 2024). To gain a better understanding of peristalsis, we are investigating the mathematical models and mechanisms underlying it in our research.

1.3 Williamson Fluid

Williamson fluids are classified as non-Newtonian fluids with shear thinning characteristics, this means that their viscosity reduces as the rate of shear stress increases. The Williamson fluid

model was first presented experimentally by (Williamson, 1929). It is widely applied to the flow characterization of polymer solutions, biological fluids such as blood, and a wide range of industrial products, including dough and sauces, pharmaceutical gels, and cosmetic creams. By considering how these complex fluids flow during processes like food processing, product formulation, and medical diagnostics, the model helps predict and manage the flow behaviour of these fluids. A study by (Akbar *et al.,* 2012) investigated a Williamson fluid's peristaltic flow in an inclined asymmetric channel under conditions of velocity and thermal slip. Likewise analysis of Williamson fluids of three-dimensional peristaltic flow of rectangular channel with compliant walls by (Ellahi *et al.*, 2014).

Williamson fluids have been the subject of recent research on peristaltic transport in asymmetric channels and ducts. Heat transfer and magnetic fields are taken into consideration to study velocity, pressure gradient, and trapped bolus formation. Studies also look into the effects of heat and mass transfer that are relevant to industrial cooling and biological applications, such as heat generation, slip conditions, and buoyancy forces. The impact of slanted magnetic fields on temperature and velocity profiles in magneto hydrodynamics (MHD) and porous media flow has been investigated, with relevance to geophysical dynamics and filtration. The Williamson model is also applied in industrial processes involving polymeric solutions and food products, as well as in biomedical investigations of blood flow and drug delivery. A few recent studies are by (Tanveer *et al.,* 2024), (Abbas *et al.,* 2023) and (Alharbi *et al.,* 2023)**.** According to (El-Hamid *et al.,* 2025) the Williamson model, the carrier fluid, urine, is modelled as a non-Newtonian fluid. A stable magnetohydrodynamic non-Newtonian fluid is investigated theoretically and computationally in this work.

1.4 Wall Properties

Roughness and material selection are two factors that can regulate fluid movement in peristaltic flow. These factors have an impact on friction, wall deformation, and wall-fluid interaction. Walls must be waterproof for durability, and surface treatments can reduce friction and improve biological system compatibility. These wall characteristics also affect how well heat is transmitted in peristaltic systems. An important researched has been done on the peristaltic

transport of a Williamson nano fluid with compliant walls in a curved channel (Nadeem *et al.*, 2014). In this model includes the combined effects of thermal dissipation and channel curvature.

Williamson nano fluid's peristaltic flow in a flexible-walled, curved conduit has been examined by (Eldesoky *et al.,* 2019). An elastic passage is a stretchable, flexible tube or channel which enable fluid to flow through it. Microvasculature flow rates vary between normal and pathological conditions, the effects of blood flow through small arteries with elastic properties.

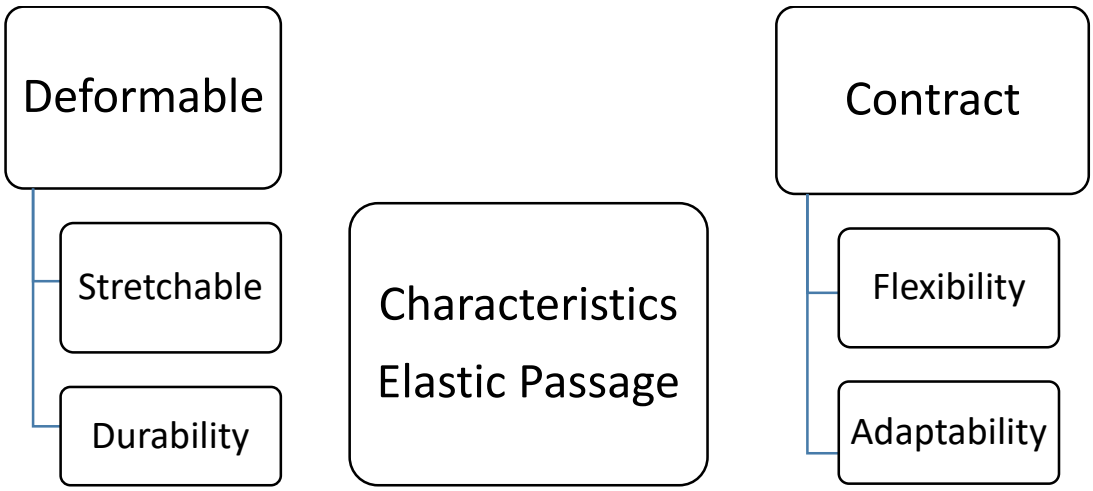

Fig. 1.4 Characteristics Elastic Passage

The fluid flow via flexible tubes is of importance because it dynamically resembles the fluid flow in veins, arteries, the urethra, and other comparable structures. Peristaltically transporting an incompressible non-Newtonian fluid in an elastic tube investigated by (Vajravelu *et al.*, 2016).

Similar to the effects of an elastic wall on the peristaltic flow of a Carreau fluid between two concentric cylinders, the outside wall of the inner tube has a regular elastic sine wave, while the inner tube has an inelastic wall that is cylindrical (Al-Khafajy & Majeed Mashhadi, 2023).

1.5 Cylindrical Coordinates

Cylindrical coordinates describe the motion and characteristics of fluids in systems with rotational symmetry around an axis. By superimposing a height (z) axis, two-dimensional polar coordinates can be generalized to three dimensions using cylindrical coordinates. Regretfully, the other two coordinates are represented by a variety of different notations. The radial coordinate is denoted by either r or ρ, and the azimuthal coordinates by either phi or theta. For example, Beyer (1987) uses (r, θ, z), whereas Arfken (1985) uses (ρ,φ,z). The notation (r,θ,z) is utilized in this work (Weisstein, 2005). The non-Newtonian fluid's peristaltic flow in a circular cylindrical tube is the subject by (Ali *et al.*, 2009). Low Reynolds number and long wavelength approximations are used in the problem definition. Using an iterative scheme and an appropriate finite-difference method, the governing nonlinear equation and boundary conditions are numerically solved. This coordinate system is especially effective for situations involving.

- Pipes
- Ducts
- Geometries in which the flow is naturally aligned with a cylindrical shape.

1.6 Porosity

A porous medium filled with fluid (liquid or gas) is defined as a material that contains pores (voids).

$$V = -\frac{K_1}{\mu}\nabla P,$$

K_1 is the permeability of the porous medium with dimensions (length),V is the Darcy velocity, ∇P represents pressure gradient and μ indicates the dynamic viscosity of the fluid and negative sign reflects the flow occurs from high to low pressure.

Porous media play a pivotal role in numerous engineering systems, where they serve as the foundation for various fluid and transport-related phenomena. These processes are inherently

complex due to the irregular geometry of the pore structure, the narrow spatial constraints, and the multifaceted interactions among the fluid, the solid matrix, and suspended particles. The study of transport phenomena in porous media provides a robust theoretical and computational framework for understanding how mass, momentum, energy, and species are transferred within these heterogeneous environments (Civan, 2011). This multidisciplinary approach integrates physical principles with mathematical modelling to address the challenges posed by the intricate microstructure and dynamic interactions present in porous systems.

Recent investigations that are related to engineering and biomedical as well as industrial and filtration chemical reactors by (Rafiq *et al.*, 2023), (Ajithkumar *et al.*, 2024) and (Abd-Alla *et al.*, 2025).

1.7 Magnetohydrodynamics

The study of magnetohydrody or MHD, examines the combination of fluid dynamics and electromagnetic dynamics. A fluid creates an electric current when it flows through a field of magnets.

This electric current may affect both the fluid's temperature and flow characteristics. MHD examines the dynamics of electrically conducting fluids, ionized gases, and liquid metals in the context of fluid mechanics when magnetic fields are present. The peristaltic MHD flow of an electrically conducting, Williamson fluid that is not compressible in a symmetric planar channel with mass and heat transfer when an angled magnetic field is present was covered by (Veera Krishna & Swarnalathamma, 2016). The interplay between electrically conducting fluids and magnetic fields opens up a wide range of research and creative possibilities. Applications of MHD range from space exploration to biomedical applications, allowing researchers to study a wide range of phenomena. Magnetohydrodynamic flows have a wide range of applications, such as separation devices, MHD energy generators, MHD drug targeting (Eldabe *et al.,* 2020), endoscope (Hayat *et al.,* 2017), materials processing, biomedical flow control (Nuwairan & Souayeh, 2022) , cancer treatment (Alqarni *et al.,* 2023), indusrial processes (Shaheen *et al.,* 2024), microfludic devices (Ridha & Solagh, 2025).

1.8 Slip Boundary Condition

The surface and fluid layer velocities are not equal in the slip boundary condition. Best example to understand slip flow is Mercury. A fluid flow known as "slip flow" occurs when a thin layer of fluid near a barrier moves in relation to the boundary or slips in that path. In contrast to the no slip scenrio, which occurs when fluid molecules adhere to the barrier and move at the same speed as the border, slip occurs when the fluid close to the boundary has a velocity differential.

The flow of a Newtonian and non-Newtonian Maxwellian fluid in an axisymmetric cylindrical tube (pore), where the movement is caused by propagating transversal oscillations along the tube wall, how slip boundaries affect fluid motion in media with pores investigated by (El-Shehawy *et al.*, 2006). Another worked by (Akram *et al.*, 2020) Impact of generated electromagnetic field and velocity second slip model on non- Newtonian transportation in tiny fluids with double-diffusivity convection.

1.9 Thesis Contribution

This thesis includes a thorough analysis of (Al-Khafajy & Al-Delfi, 2023) has been presented and then a flow analysis has been extended with impact of elastic passage on the peristaltic transport of Williamson fluid with slip effects. Williamson fluid trapped between two concentric cylinder. The main focus on effect of slip at the boundaries, porosity and MHD. The number of dependent variables has been reduced using an appropriate transformation technique, and solutions have been obtained using a perturbation technique. Mathematica software was used to evaluate the findings. At the end graphic results are provided for several important components, including wave frame streamlines, stress, and velocity distribution.

1.10 Thesis Organization

This thesis comprises the following chapters:

Chapter 1 covers a comprehensive and detailed analysis of the literature in accordance with recent published articles.

Chapter 2 examines the basic ideas, guidelines, and principles required to comprehend the upcoming work. An overview of the perturbation method and numerous terms that we are use in our research are provided in this chapter.

Chapter 3 provides a review of the work by (Al-Khafajy & Al-Delfi, 2023). The authors studied how an elastic wall affects the peristaltic flow of a non-Newtonian Williamson fluid between two concentric cylinders. The lubrication approach has been utilized to study the problem. Perturbation technique has been employed to obtain the analytical solution of the problem.

Chapter 4 is the extension work on research done by (Al-Khafajy & Al-Delfi, 2023). The effects of elastic wall properties on the Williamson fluid flowing past a symmetric passage with the slip boundary condition will are considered and by incorporating the effects of magnetohydrodynamics (MHD) and porous media.

Chapter 5 contains the conclusion drawn in chapter 4. Future recommendations are also included for the future researches.

In the end, the reference list is also incorporated.

CHAPTER 2

BASIC DEFINITIONS AND CONCEPTS

2.1 Mechanics

The oldest branch of physics that studies moving and stationary objects under the influence of forces is called mechanics. Statics and dynamics are the names of the branches of mechanics that deal with bodies at rest and in motion (Janna, 2009).

2.1.1 Statics

The study of fluid dynamics, also referred to as hydrostatics, examines how a fluid behaves at rest or very close to it (Rajput, 2010).

2.1.2 Dynamics

It examines the connections between fluid velocities and accelerations and the forces or energy that gives rise to them (Rajput, 2010).

2.2 Fluid

A fluid is defined as any substance with the ability to flow, that includes gases as well as liquids (Rajput, 2010).

According to density two categories of fluids are recognized.

2.2.1 Gas

Substances like hydrogen and nitrogen belong to a class of fluids that possess neither a fixed shape nor a constant volume; such fluids are known as gases (Rajput, 2010).

2.2.2 Liquids

Fluids that maintain a constant volume but do not retain a fixed shape are categorized as liquids. Examples include oil and water (Rajput, 2010).

2.3 Fluid Mechanics

One area of physics called fluid mechanics is focused on the characteristics and behavior of liquids and gases, whether they are moving or stationary. It helps understand how fluids interact with forces under varying conditions and is fundamental in several engineering and scientific areas like aerodynamics, hydrodynamics, and the development of devices such as turbines, pumps, and aircraft. This discipline also aids in understanding natural processes such as climate behavior, oceanic circulation, and blood circulation in the human body. It integrates principles from classical mechanics and thermodynamics to analyze how fluids behave across varying settings. The insights gained are highly valuable across diverse domains such as civil engineering, meteorology, biophysics, and aerospace research.

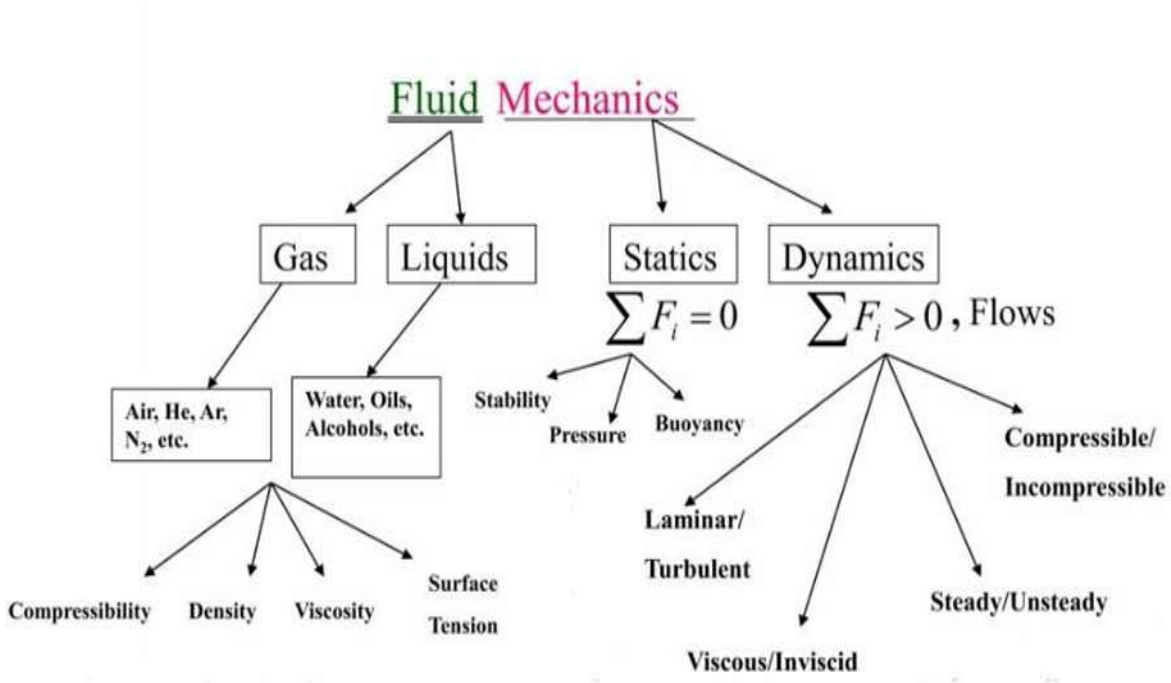

Fig. 2.1: Classification of Fluid Mechanics

Applications include analyzing bodily fluids, designing transport systems, forecasting weather patterns, and enhancing efficiency in industrial processes. Fluid mechanics research can be approached both macroscopically, focusing on average fluid behaviour, and microscopically, examining molecular-level interactions (Granger, 2012).

2.4 Properties of Fluid

2.4.1 Compressibility

A compressibility is a measure of how much its density changes in response to a change in pressure. It quantifies the fluid's ability to decrease in volume when subjected to an increase in pressure, reflecting how easily the fluid can be compressed (Bradford & Gupta, 1986).

2.4.2 Density

Density is the measure of mass per unit volume of a substance. Mathematically, it is expressed as the ratio of mass to volume, where ρ represents density, m is mass, and v is volume (Janna, 2009).

$$\rho = \frac{m}{v}. \tag{2.1}$$

The dimensions are $[ML^{-3}]$ and the SI units of density are $\frac{kg}{m^{-3}}$.

2.4.3 Pressure

Pressure is defined as the force exerted per unit area on a surface. It refers to the physical force applied to an object, and as a result of this force, stress is generated within the material (Raju, 2011).

$$P = \frac{F}{A}. \tag{2.2}$$

2.4.4 Temperature

A physical characteristic of matter that measures how hot or cold a body is a temperature. An object's temperature, typically expressed in degrees Celsius, Fahrenheit, or Kelvin. The kinetic energy of a substance's molecules or atoms is measured by its thermodynamic temperature (Raju, 2011).

2.4.5 Viscosity

A fluid's viscosity is a measurement of its internal friction. When two fluid layers move in relation to each other, the internal frictional force between them is related to viscosity. A fluid's state, which includes its temperature, pressure, and rate of deformation, typically affects its viscosity (Pritchard & Leylegian, 2011).

2.4.6 Dynamic Viscosity

Absolute or dynamic viscosity is the measure of a fluid's resistance to flow between two layers of fluid in motion. It is defined as the ratio of shear stress to the velocity gradient within the fluid, indicating how easily a fluid flows under an applied force (Pritchard & Leylegian, 2011).

$$\text{Viscosity} = \frac{\text{Shear stress}}{\text{velocity gradient}},$$

$$\mu = \frac{\tau}{\frac{du}{dy}}. \tag{2.3}$$

The SI units of $\frac{\text{Ns}}{\text{m}^2}$ or $\frac{\text{kg}}{\text{m}}$ are used to measure dynamic viscosity, and its dimensions are $\left[\frac{\text{M}}{\text{LT}}\right]$.

2.4.7 Kinematic Viscosity

Kinematic viscosity is determined by the ratio of fluid density to dynamic viscosity. This idea can be further developed mathematically as

$$v = \frac{\mu}{\rho}. \tag{2.4}$$

The units used to measure kinematic viscosity are $\frac{m^2}{s}$ and dimensions are $\left[\frac{L^2}{T}\right]$ (Pritchard & Leylegian, 2011).

2.4.8 Specific Heat

The amount of heat energy needed to increase a substance's temperature by one degree per unit mass is known as specific heat. It can be measured under different conditions, such as constant pressure (specific heat at constant pressure, c_p) or constant volume (specific heat at constant volume, c_v), depending on the temperature and pressure constraints (Raju, 2011).

2.4.9 Heat Flux

The heat flux is a measurement of the quantity of heat that moves across a surface in a specific amount of time. It is the rate of heat transfer per unit area across a surface. The unit of measurement is watts per square meter $\frac{W}{m^2}$ (Raju, 2011).

2.4.10 Heat generation and Absorption

Heat generation or absorption, is determined by the amount of heat generated or absorbed per unit volume (Raju, 2011).

2.4.11 Thermal Conductivity

The study of a material's ability to transfer heat is known as thermal conductivity. Heat can move in three different ways: conduction, convection, and radiation. In particular, we can demonstrate this mathematically as

$$\text{Thermal Conductivity} = \frac{\text{heat} \times \text{distance}}{\text{area} \times \text{temperature gradient}},$$

$$k = \frac{QL}{A\Delta T}, \tag{2.5}$$

In this case, ΔT is the temperature difference, the cross-sectional area is signified by A, k the thermal conductivity, Q the heat flow per unit time and SI unit is $\frac{kg.m}{s^3K}$ (Raju, 2011).

2.4.12 Thermal Diffusivity

It is defined as the ratio of specific heat to thermal diffusivity per unit density. In terms of math, it is expressed as

$$\alpha = \frac{K}{\rho c_p}, \tag{2.6}$$

where c_p stands for heat capacity, ρ for density, and K for thermal conductivity (Raju, 2011).

2.4.13 Viscous Dissipation

Viscous dissipation refers to the irreversible conversion of kinetic energy from fluid flow into internal energy due to the effects of viscosity. This process results in the generation of heat within the fluid, reducing the overall mechanical energy of the system (Rajput, 2010).

2.5 Rheology

The study of matter flow and modify in form, including elasticity, viscosity and plasticity is known as rheology (Raju, 2011).

2.6 Flow

The volume of fluid that moves through an area in a given amount of time is called flow (Pritchard & Leylegian, 2011).

Fluids are classified into based on their flow, which are

1. Compressible or incompressible flows.
2. Uniform and non-uniform flows.
3. Rotational / Irrotational flows.
4. Steady and unsteady flows.
5. Laminar and turbulent flows.

2.6.1 Steady and Unsteady Flows

A steady flow is one in which the fluid properties like pressure and velocity, remain persistent over time at a definite point. When these properties change with time at a given location, the flow is considered unsteady (Pritchard & Leylegian, 2011).

2.6.2 Uniform and Non uniform

When the velocity is the same in both direction and magnitude everywhere, the flow is considered uniform; when it is not, the flow is said to be non-uniform at any given time (Pritchard & Leylegian, 2011).

2.6.3 Compressible and Incompressible Flows

Compressible flow occurs when the fluid's density (ρ) fluctuates from one point to another in other words, the density is not constant for this flow. For example, gas flow via nozzles, gas turbines, orifices, etc. Incompressible flow where the fluid's density remains constant. In terms of mathematics, ρ = constant. For example, aerodynamics at subsonic speed (Pritchard & Leylegian, 2011).

2.6.4 Rotational and Irrotational Flows

Rotational flow refers to a type of flow in which fluid particles rotate around their own mass centres while moving in the direction of the flow. This typically occurs near solid boundaries.

An example of rotational flow is the movement of liquid in a rotating tank, where the fluid experiences both translational and rotational motion.

Irrotational flow occurs when fluid particles do not rotate around their mass centres while moving in the direction of the flow. Generally, the flow outside the boundary layer is considered irrotational, where the fluid particles follow a smooth path without any spin. For instance, Flow over a wash basin or stationary tank's drain hole (Pritchard & Leylegian, 2011).

2.6.5 Laminar and Turbulent Flows

Laminar flows are those in which fluid particles move in smooth layers, whereas turbulent flows are those in which random 3D velocity differences cause fluid particles to mix quickly as they move (Pritchard & Leylegian, 2011).

2.7 Newton's Law of Viscosity

As per this law, the rate of shear strain in a fluid element layer is directly related to the shear stress (τ), with the coefficient of viscosity serving as the constant of proportionality. This relationship describes how the fluid's viscosity resists deformation due to shear forces. The term Newtonian fluids refers to fluids that obey this law (Pritchard & Leylegian, 2011).

$$\tau = \mu \frac{du}{dy}. \tag{2.7}$$

2.8 Types of Fluid

Fluids are classified to according viscosity:

1. Ideal Fluid.
2. Real Fluid.
3. Newtonian Fluid.
4. Non-Newtonian fluid.

2.8.1 Ideal Fluid

These are hypothetical fluids with zero viscosity and no frictional forces. This implies they can flow without resistance and do not waste energy to friction. Ideal fluids are valuable for mathematical modelling, but they do not exist in reality. Ideal fluids include incompressible fluids, non-viscous fluids, perfect gas (Pritchard & Leylegian, 2011).

2.8.2 Real Fluid

These fluids experience frictional forces and have a viscosity that is not zero. Friction causes them to lose energy, and they can exhibit turbulence and other complicated behaviors. Real fluids include things like blood, oxygen, and water (Pritchard & Leylegian, 2011).

2.8.3 Newtonian Fluid

Fluid which follows the Newton's law of viscosity. For these fluids, the rate of deformation has no effect on μ. The viscosity of these fluids remains constant irrespective of the shear forces exerted on the fluid layers.

Newtonian fluids are defined as those whose shear stress versus shear rate plot at a specific temperature is a straight line with a constant slope, regardless of the shear rate. Examples. Air, kerosene, and water (Pritchard & Leylegian, 2011).

2.8.4 Non-Newtonian Fluid

Non-Newtonian fluids are fluids that do not exhibit a linear relationship between shear stress and the rate of deformation. These fluids are relatively rare and often consist of complex mixtures. Examples include suspensions or solutions (such as slurries), mud flows, polymer solutions, and blood. Non-Newtonian fluids are typically studied in the field of rheology, which focuses on the science of deformation and flow of materials (Pritchard & Leylegian, 2011).

Classifications for non-Newtonian fluid include

Fluids with Time Dependence

- Rheopectic or Anti-Thixotropic Fluids.
- Thixotropic Fluids.

Fluids that are Time Independent

- Dilatant Fluids
- Pseudo-plastic Fluids

2.8.4.1 Rheopectic or Anti-Thixotropic Fluids

As shear stress increases, the fluid's viscosity increases as well, and this relationship changes over time. One example of such a fluid would be gypsum paste (Pritchard & Leylegian, 2011).

2.8.4.2 Thixotropic Fluid

The fluid's viscosity decreases as shear stress increases, and the two variables' relationship varies over time. Paint and glue are two examples of thixotropic fluids (Pritchard & Leylegian, 2011).

2.8.4.3 Dilatant Fluid

A non-Newtonian fluid that experiences an increase in shear viscosity when shear stress is applied is called a dilatant. For example, mud slur and quicksand (Pritchard & Leylegian, 2011).

2.8.4.4 Pseudo-Plastic Fluid

Fluids Shear thinning fluids, such as paint and ketchup, are pseudo-plastic substances whose viscosity decreases with an increase in the rate of applied shear stress (Pritchard & Leylegian, 2011).

2.8.4.5 Bingham- Plastic Fluid

Bingham plastics are viscoelastic materials that behave like a rigid body under low stress and like a viscous fluid under high stress (Pritchard & Leylegian, 2011).

2.9 Scalar Field

A scalar field assigns a single numerical value to each point in a space, thereby characterizing the distribution of a scalar quantity. The only thing that a scalar quantity has is magnitude. The representation of scalar properties in fluid mechanics, like temperature and pressure, depends on scalar fields, mainly because they give a comprehensive picture of how these variables are distributed in a fluid. They aid in the analysis of fluid flow and support forecasts and optimizations in a range of engineering applications (Pritchard & Leylegian, 2011).

2.9.1 Tensor Field

A mathematical framework that allocates a tensor to every point in a space to analyze how physical properties vary across dimensions is termed as tensor field. In fluid mechanics, such fields are indispensable for understanding advanced concepts like stress, strain, and flow. They enable precise mapping of spatial changes and interactions between variables, offering deep insight into fluid behavior (Pritchard & Leylegian, 2011).

2.9.2 Vector Field

A vector field is a mathematical structure that allocates a vector to every point in a region to depict the direction and intensity of a physical quantity, such as velocity or force. These fields display both magnitude and direction. In fluid mechanics, vector fields play a central role in analyzing fluid motion, forces, and flow configurations. They simplify fluid behaviour, which aids in the design and advancement of technical applications such as aerodynamics and fluid flow in pipes (Pritchard & Leylegian, 2011).

2.9.3 Velocity Field

A velocity field describes the distribution of particle or fluid element velocities in a given space. A vector indicating the direction and speed of motion is used to represent each point in the field. Fields are essential to many areas of physics, such as electromagnetic, quantum, and general relativity. These mathematical fields can be used to represent and analyse physical phenomena in a variety of engineering and research fields. Three categories of fields exist: vector, tensor, and scalar fields (Pritchard & Leylegian, 2011).

2.10 Dimensionless Numbers

The inertia force, which is always present when any mass is in motion, is divided by the viscous, gravity, pressure, surface tension, or elastic forces to get the dimensionless numbers, also known as non-dimensional parameters (Raju, 2011).

2.10.1 Prandtl Number

The viscous-to-thermal diffusivity ratio is known as the Prandtl number.

$$\mathrm{Pr} = \frac{\text{Viscous diffusivity}}{\text{thermal diffusivity}},$$

$$\mathrm{Pr} = \frac{v}{\propto^*} = \frac{{}^{\mu}/_{\rho}}{{}^{k}/_{\rho c_p}} = \frac{c_{p\mu}}{k}, \tag{2.8}$$

where c_p is for specific heat at constant pressure, v is for kinematic viscosity (momentum diusivity), k is for thermal conductivity, and $\propto^*$is for thermal diusivity. Pr << 1 is dominated by thermal diffusivity, while Pr >> 1 is dominated by momentum diffusivity (Raju, 2011).

2.10.2 Eckert Number

The Eckert number (Ec) is a dimensionless parameter expressing the proportion between a fluid's kinetic energy and the variation in its enthalpy. It reflects how significantly kinetic

energy contributes to the thermal behavior of a flow and establishes a link between convective heat transfer and motion energy. It is particularly valuable in the study of high-velocity flows where heat transfer is influenced by dynamic forces (Raju, 2011).

$$\mathrm{Ec} = \frac{\mathrm{v}^2}{\mathrm{c_p\, T_0}}. \tag{2.10}$$

2.10.3 Reynolds Number

The Reynolds number is widely regarded as the most important dimensionless quantity in fluid flow, as it helps predict the flow regime, indicating whether the flow is laminar or turbulent. The inertial to effective viscous force ratio is how it is defined.

$$Re = \frac{\text{Inertial force}}{\text{Viscous force}},$$

$$Re = \frac{\mathrm{vL}}{\mathrm{v}^*}. \tag{2.9}$$

The symbols as μ , v, represent dynamic viscosity, and kinematic viscosity and v^*, L represent velocity, and characteristic length, respectively. A high Reynolds number indicates that viscous forces are negligible in the flow, leading to inviscid flow behavior. In contrast, low Reynolds numbers signify dominant viscous forces, resulting in laminar flow. For intermediate to high Reynolds numbers, inertial forces become more significant, often leading to turbulent flow where chaotic fluid motion prevails (Raju, 2011).

2.10.4 Weissenberg Number

The Weissenberg number is a dimensionless measure.In the study of rheology, We is used to quantify the relative importance of elastic vs viscous effects in a viscoelastic fluid or material. It can be represented mathematically as follows:

$$\mathrm{We} = \lambda\, \dot{\gamma}, \tag{2.11}$$

where $\dot{\gamma}$ is the shear rate, λ is the material's characteristic relaxation time, and We is the Weissenberg (Raju, 2011).

2.10.5 Grashof Number

It depicts how the buoyancy forces behave in a fluid that is flowing in opposition to the viscous forces. It is used to determine the laminar system's fluid boundary layer flow regime.

$$\mathrm{Gr} = \frac{\mathrm{L}^3}{\mathrm{v}^2}\mathrm{g}\beta(\mathrm{T} - \mathrm{T}_0), \tag{2.12}$$

where T and T_0 stand for fluid and ambient temperature, respectively, and β for volumetric thermal expansion coefficient, g for acceleration due to gravity, v for kinematic viscosity, and L for characteristic length (Raju, 2011).

2.10.6 Biot Number

Biot number is a dimensionless parameter that relates a solid's interior thermal resistance to its exterior convective resistance at the surface. It represents how quickly heat can travel within a substance in comparison to how easily it can be transferred to the surrounding fluid (Raju, 2011).

$$B = \frac{hL_c}{k} \tag{2.13}$$

Where L_c denote characteristic length of the solid, h for convective heat transfer coefficient and k represents thermal conductivity of the solid.

2.10.7 Hartmann Number

Hartmann number is a dimensionless magnetohydrodynamic quantity that compares the strength of the magnetic for (Lorentz force) to the viscous force in an electrically conducting

fluid. Its reflects how strongly a magnetic field may inhibit or influence fluid mobility (Raju, 2011).

$$M = B_0 L \sqrt{\frac{\sigma}{\mu}} \tag{2.14}$$

Where L denotes characteristic of length, B_0 for applied magnetic field, σ for electric conductivity of the fluid and μ represents dynamic viscosity of the fluid.

2.11 Heat Transfer

It is the transfer of energy between two surfaces as a result of temperature differences. Typically, heat moves from an area with a high temperature to one with a low temperature. Heat is transferred, for instance, from the stove to the cooking pan (Raju, 2011).

2.11.1 Conduction

When two objects come into physical contact, heat is transferred through the material through a process known as conduction. For instance, cooking vegetables in a pan, grabbing a steaming cup of tea, or a car's engine heating up after starting and using an automatic radiator (Raju, 2011).

2.11.2 Convection

The movement of heat-carrying fluid particles is known as convection, and it can occur spontaneously due to floatability caused by temperature changes or be induced by outside sources such as fans or pumps (Raju, 2011).

2.11.3 Radiation

Thermal radiation is the process through which heat is transferred from a body to its surroundings due to its temperature, without requiring a medium. Examples include the warmth

felt from the sun, the heat emitted by a lightbulb, or the thermal radiation from a toaster's heating element that toasts bread (Raju, 2011).

2.12 Stress

Stress is defined as the average force applied per unit area of a body's surface that is subjected to external forces or pressure. It quantifies the intensity of internal forces within a material in response to external loads (Pritchard & Leylegian, 2011).

$$\sigma = \frac{\text{Force}}{\text{Area}}. \tag{2.15}$$

2.12.1 Shear Stress

Shear stress is a type of stress where the applied force acts parallel to the surface or cross-sectional area of a material, causing layers of the material to slide past each other (Pritchard & Leylegian, 2011).

2.12.2 Normal Stress

Normal stress is a type of stress that occurs when a force is applied perpendicular to the cross-sectional area of a material, causing compression or tension within the material (Pritchard & Leylegian, 2011).

2.12.3 Cauchy Stress Tensor

The stress within a material at a particular position is described by the Cauchy stress tensor. It is essential for assessing and forecasting the mechanical behavior of materials under diverse circumstances and pertains to the force per unit area operating on numerous planes at that moment. The components of Cauchy stress tensor represents normal and shear stresses (Pritchard & Leylegian, 2011).

2.12.4 Extra Stress Tensor

The extra stress tensor is used to take into consideration extra stress contributions brought on by fluid motion. A common constitutive equation that governs the relationship between stress and strain in a fluid is the additional strain tensor (Pritchard & Leylegian, 2011).

2.12.5 Strain

Strain is the measure of the relative deformation or change in shape of a material when a force is applied. It is a dimensionless quantity, representing the ratio of the material's deformation to its original dimensions (Pritchard & Leylegian, 2011).

2.13 Streamline

A track that is always tangent to the velocity field at every point, representing the direction of fluid flow is termed as streamline. In two-dimensional flows, the slope of the streamline must be equal to the tangent of the angle between the velocity vector and the x-axis (Rajput, 2010).

2.13.1 Stream Function

A helpful tool for researching fluid dynamics is the stream function. Usually, the streamlines created by the stream function are used to realize the flow pattern surrounding an object. A function that solves the given equation is called a stream function (Rajput, 2010).

2.14 Darcy's Law

For water flowing through a saturated porous medium, Darcy's law provides a linear flow model. The renowned equation put forth by French engineer Henry P.G. Darcy in 1856 states that the hydraulic conductivity (k) and the pressure gradient (∇H) determine the flow rate (q) (Tanveer et al., 2017).

$$q = k\nabla H. \tag{2.16}$$

2.15 Basic Equations and Conservation Laws

2.15.1 Continuity Equation

The equation presents the rate of mass flow into and out of a given region, along with any accumulation within that region, must be balanced, ensuring the conservation of mass (Rajput, 2010).

Mathematically $$\frac{\partial \rho}{\partial t} + \nabla . (\rho \mathbf{V}) = 0, \quad (2.17)$$

where ρ is the fluid's density, t is time, and $\boldsymbol{V}$ is its velocity.

When incompressible flow occurs, then

$$\nabla \ . \mathbf{V} = 0. \quad (2.18)$$

2.15.2 Momentum Equation

The sum of the mass and velocity of a body is referred to as "linear momentum." Newton's second law states that a body's acceleration is proportional to the net force acting on it and inversely related to its mass. This is because the acceleration of a body is equal to the net force acting on it. The momentum of such systems is therefore conserved when there is no net force acting on them. This equation shows that the system's total momentum will always be conserved because it is physically related to the law of conservation of momentum. The equation is expressed as follows if incompressible fluid is considered.

$$\rho \frac{d\mathbf{V}^*}{dt} = \text{div}\boldsymbol{\tau} + \rho \mathbf{b}^* , \quad (2.19)$$

where $\mathbf{V}^*$ stands for velocity, ρ for density, $\mathbf{b}^*$ for body forces $\frac{d}{dt}$ material time derivative , div$\boldsymbol{\tau}$ for surface forces, and $\boldsymbol{\tau}$ characterizes the Cauchy stress tensor indicates the presence of inertial forces (Rajput, 2010).

2.15. 3 Energy Equation

The concept of energy conservation, also referred to as the first law of thermodynamics, is a natural rule. It states that energy can only change form during a process; it cannot be created or destroyed. The energy equation for the base fluid in a two-dimensional system can be written as T temperature.

$$(\rho c_p)\frac{dT}{dt} = \text{div } q^*, \tag{2.20}$$

$$q^* = -k\nabla T, \tag{2.21}$$

k is thermal conductivity, c_p is specific heat, q^* denotes heat flux, and ρ represents density $(\rho c_p)\frac{dT}{dt}$ for total internal energy, total heat flux $\text{div } q^*$ (Rajput, 2010).

2.16 Perturbation Method

Mathematical techniques known as perturbation methods are used to approximate solutions to challenging mathematical equations, particularly those involving large or small parameters.

The nonlinear differential equation's small parameters should be identified.

- Explain the answer using the perturbation expansion power series.
- Add the perturbation expansion to the equation system.
- Resolve the equation systems in various orders with small parameters.
- Integrate the solutions acquired at various orders to create the ultimate perturbation.

CHAPTER 3

THE PERISTALTIC FLOW OF WILLIAMSON FLUID THROUGH A FLEXIBLE CHANNEL

(Al-Khafajy & Al-Delfi, 2023)

3.1 Introduction

The research conducted by (Al-Khafajy & Al-Delfi, 2023) is thoroughly reviewed in this chapter. The main objective of research is to investigate the influence of flexible wall occur on the peristaltic transport of Williamson fluid. The suggested model is mathematically formulated using the continuity and momentum equation in cylindrical coordinates under the assumptions of a long wavelength and a low Reynolds number. Because the produced differential systems are non-linear, the series solutions are obtained using a regular perturbation method. The governing equations are solved using Mathematica software, which also examines the influence of critical parameters including wave amplitude, wall elasticity, and fluid rheology. The results demonstrate that significant variations in shear stress and velocity profiles are caused by the outer wall's elastic behavior.

3.2 Physical Model

The Williamson fluid's peristaltic flow travels through two concentric cylinders. There is a cylindrical inner tube and a regular elastic wall with a sinusoidal wave on the outside. As illustrated in Fig. 3.1. The cylindrical coordinates are represented as $\hat{Z}$ in synchrony with the tube's axis and $\hat{R}$ with the tube's radius. The wall surface's geometry is as follows:

$$\text{Inner wall} \quad \hat{r} = \hat{r}_1 = a_1, \tag{3.1}$$

$$\text{Outer wall} \quad \hat{r} = \hat{r}_2(\hat{Z}, \hat{t}) = a_2 + b\sin\left(\frac{2\pi}{l}(\hat{Z} - s\hat{t})\right), \tag{3.2}$$

where a_1 is the radius of the inner core region, a_2 is the average radius of the undisturbed tube, l is a wavelength, s is the wave propagation speed, $\hat{t}$ is time, and b is the amplitude of a peristaltic wave.

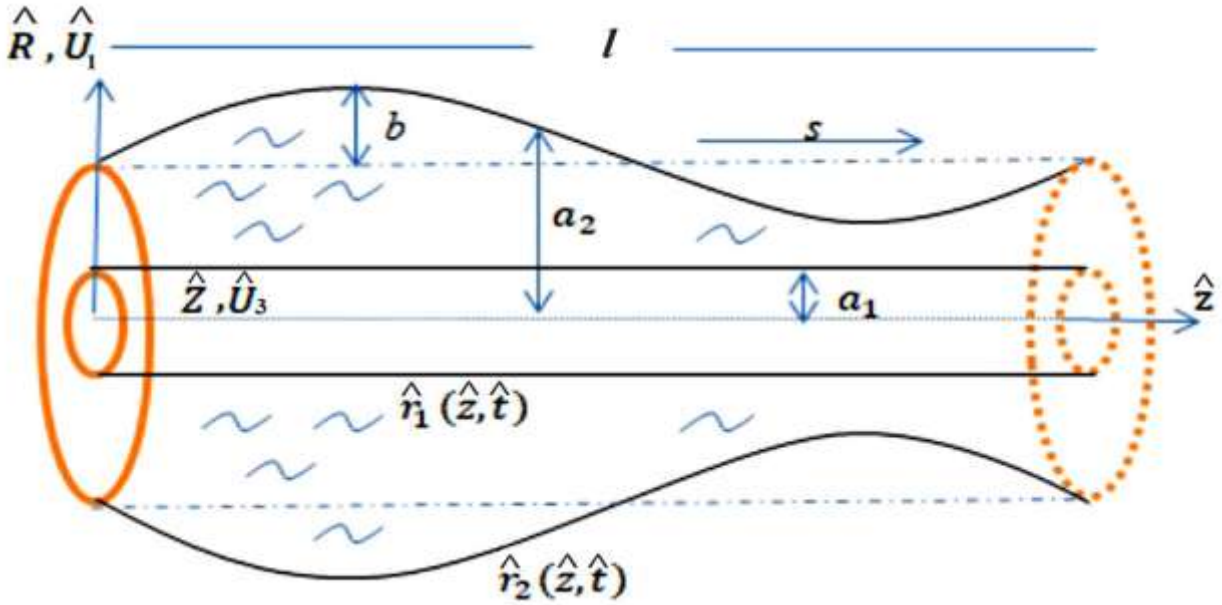

Fig. 3.1 The Geometry of the Problem

The basis for this system is the cylindrical coordinates system $(\hat{R}, \hat{Z})$, where the velocity field in an unstable two-dimensional flow is described as :

$$\hat{\mathbf{V}} = [\hat{U}_1(\hat{R}, \hat{Z}, \hat{t}), \hat{U}_3(\hat{R}, \hat{Z}, \hat{t})]. \tag{3.3}$$

The incompressible Williamson fluid, the basic governing continuity along momentum equations are

$$\text{div}\hat{\mathbf{V}} = 0, \tag{3.4}$$

$$\rho\left(\frac{d\hat{\mathbf{V}}}{dt}\right) = \text{div}\mathbf{S} + \rho\mathbf{f}, \tag{3.5}$$

where, the velocity field is denoted by $\hat{\mathbf{V}}$, the density by ρ, specific body force is denoted by **f**, and the material time derivative by $\frac{d}{dt}$.

For an incompressible fluid, the Cauchy stress tensor S can be written as follows:

$$S = [-\hat{P}\hat{I} + \hat{\tau}], \tag{3.6}$$

here the Cauchy stress tensor by S, pressure by $\hat{P}$, the identity tensor by $\hat{I}$, $\hat{\tau}$ extra stress tensor.The Williamson fluid constitutive equation is given as:

$$\hat{\tau} = [\mu_\infty + (\mu_0 + \mu_\infty)(1 - \Gamma|\hat{\alpha}|)^{-1}]\hat{\alpha}. \tag{3.7}$$

We examine the constitutive equation (3.7), where $\mu_\infty = 0$ and $\Gamma|\hat{\alpha}| < 1$.

The extra stress tensor component can be expressed as:

$$\hat{\tau} = \mu_0 [(1 - \Gamma|\hat{\alpha}|)^{-1}]\hat{\alpha}, \tag{3.8}$$

$$\hat{\tau} = \mu_0[1 + \Gamma|\hat{\alpha}|]\hat{\alpha}, \tag{3.9}$$

in which Γ is the time constant, μ_0 is a zero-shear rate viscosity, μ_∞ is an infinite shear viscosity, $\hat{\alpha}$ is shear strain which is define as:

$$\hat{\alpha} = \sqrt{\frac{1}{2}\sum_i \sum_j \hat{\alpha}_{ij}\hat{\alpha}_{ji}} \quad \text{or} \quad \hat{\alpha} = \sqrt{\frac{1}{2}\,\Pi}\,, i, j = 1,2. \tag{3.10}$$

The second invariant strain tensor is represented by Π and is given as:

$$\Pi = \left((\text{grad}\hat{V} + (\text{grad}\hat{V})^T\right)^2. \tag{3.11}$$

The components of tensor and magnitude are

$$\hat{\tau}_{\hat{R}\hat{R}} = 2\,\mu_0\,[1 + \Gamma|\hat{\alpha}|]\frac{\partial \hat{U}_1}{\partial \hat{R}}, \tag{3.12}$$

$$\hat{\tau}_{\hat{R}\hat{Z}} = \mu_0\,[1 + \Gamma|\hat{\alpha}|]\left(\frac{\partial \hat{U}_1}{\partial \hat{Z}} + \frac{\partial \hat{U}_3}{\partial \hat{R}}\right), \tag{3.13}$$

$$\hat{\tau}_{\hat{Z}\hat{Z}} = 2\,\mu_0\,[1 + \Gamma|\hat{\alpha}|]\frac{\partial \hat{U}_3}{\partial \hat{Z}}\,, \tag{3.14}$$

$$\hat{\alpha} = \sqrt{2\left(\frac{\partial \hat{U}_1}{\partial \hat{R}}\right)^2 + \left(\frac{\partial \hat{U}_1}{\partial \hat{Z}} + \frac{\partial \hat{U}_3}{\partial \hat{R}}\right)^2 + 2\left(\frac{\partial \hat{U}_3}{\partial \hat{Z}}\right)^2}\,. \tag{3.15}$$

An elastic wall's motion can be described by the following equation:

$$L^{\circ} = \hat{P} - \hat{P}_0. \tag{3.16}$$

Viscosity damping forces and the motion of a stretched membrane are represented by the operator L°

$$L^{\circ} = E\frac{\partial^4}{\partial \hat{Z}^4} - F\frac{\partial^2}{\partial \hat{Z}^2} + G\frac{\partial^2}{\partial \hat{t}^2} + H\frac{\partial^2}{\partial \hat{t}} + I_L\,, \tag{3.17}$$

where I_L is the spring stiffness, longitudinal tension per unit width is F, viscous damping coefficient is H, G is the mass per unit area and E is the flexural rigidity of a wall. For the properties of a flexible wall canal the governing equation at $\hat{r} = \hat{r}_2$ is

$$\frac{\partial \hat{P}}{\partial \hat{Z}} = \frac{\partial}{\partial \hat{Z}}\left(E\frac{\partial^4}{\partial \hat{Z}^4} - F\frac{\partial^2}{\partial \hat{Z}^2} + G\frac{\partial^2}{\partial \hat{t}^2} + H\frac{\partial^2}{\partial \hat{t}} + I_L\right)(\hat{r}_2). \tag{3.18}$$

The governing equations for fluid motion are obtained by replacing Williamson's fluid with the velocity components in the shear stress equations.

$$\frac{\partial \hat{U}_1}{\partial \hat{R}} + \frac{\hat{U}_1}{\hat{R}} + \frac{\partial \hat{U}_3}{\partial \hat{Z}} = 0, \tag{3.19}$$

$$\rho\left(\frac{\partial \hat{U}_1}{\partial \hat{t}} + \hat{U}_1\frac{\partial \hat{U}_1}{\partial \hat{R}} + \hat{U}_3\frac{\partial \hat{U}_1}{\partial \hat{Z}}\right) = -\frac{\partial \hat{P}}{\partial \hat{R}} + \frac{1}{\hat{R}}\frac{\partial}{\partial \hat{R}}\left(\hat{R}\hat{\tau}_{\hat{R}\hat{R}}\right) + \frac{\partial}{\partial \hat{Z}}(\hat{\tau}_{\hat{R}\hat{Z}}), \tag{3.20}$$

$$\rho\left(\frac{\partial \hat{U}_3}{\partial \hat{t}} + \hat{U}_1\frac{\partial \hat{U}_3}{\partial \hat{R}} + \hat{U}_3\frac{\partial \hat{U}_3}{\partial \hat{Z}}\right) = -\frac{\partial \hat{P}}{\partial \hat{Z}} + \frac{1}{\hat{R}}\frac{\partial}{\partial \hat{R}}\left(\hat{R}\hat{\tau}_{\hat{R}\hat{Z}}\right) + \frac{\partial}{\partial \hat{Z}}(\hat{\tau}_{\hat{Z}\hat{Z}}). \tag{3.21}$$

Using equation (3.18) in (3.21), we get

$$\frac{\partial}{\partial \hat{z}}\left(E\frac{\partial^4}{\partial \hat{Z}^4} - F\frac{\partial^2}{\partial \hat{Z}^2} + G\frac{\partial^2}{\partial \hat{t}^2} + H\frac{\partial^2}{\partial \hat{t}} + I_L\right)(\hat{r}_2) = \frac{1}{\hat{R}}\frac{\partial}{\partial \hat{R}}\left(\hat{R}\hat{\tau}_{\hat{R}\hat{Z}}\right) + \frac{\partial}{\partial \hat{Z}}(\hat{\tau}_{\hat{Z}\hat{Z}}) - \rho\left(\frac{\partial \hat{U}_3}{\partial \hat{t}} + \hat{U}_1\frac{\partial \hat{U}_3}{\hat{R}} + \hat{U}_3\frac{\partial \hat{U}_3}{\partial \hat{Z}}\right), \tag{3.22}$$

along with boundary conditions

$$\hat{U}_3 = \hat{U}_1 = 0, \text{ at } \hat{r} = \hat{r}_1\, a_1, \tag{3.23}$$

$$\hat{U}_3 = \hat{U}_1 = 0, \quad \text{at} \quad \hat{r} = \hat{r}_2(\hat{Z}, \hat{t}) = a_2 + b\sin\left(\frac{2\pi}{l}(\hat{Z} - s\hat{t})\right). \tag{3.24}$$

The following are the general and particular two-frame coordinate transformations:

$$\hat{r} = \hat{R}, \qquad \hat{z} = \hat{Z} - s\hat{t}, \qquad \hat{u}_1 = \hat{U}_1,$$
$$\hat{u}_3 = \hat{U}_3 - s, \qquad \hat{p} = \hat{P}(\hat{Z} - s\hat{t}, \hat{R}, \hat{t}). \tag{3.25}$$

These transformations give the following set of equations

$$\frac{\partial \hat{u}_1}{\partial \hat{r}} + \frac{\hat{u}_1}{\hat{r}} + \frac{\partial \hat{u}_3}{\partial \hat{z}} = 0, \tag{3.26}$$

$$\rho\left(\hat{u}_1 \frac{\partial \hat{u}_1}{\partial \hat{r}} + \hat{u}_3 \frac{\partial \hat{u}_1}{\partial \hat{z}}\right) = -\frac{\partial \hat{p}}{\partial \hat{r}} + \frac{1}{\hat{r}} \frac{\partial}{\partial \hat{r}}(\hat{r}\hat{\tau}_{\hat{r}\hat{r}}) + \frac{\partial}{\partial \hat{z}}(\hat{\tau}_{\hat{r}\hat{z}}), \tag{3.27}$$

$$\rho\left(\hat{u}_1 \frac{\partial \hat{u}_3}{\partial \hat{r}} + \hat{u}_3 \frac{\partial \hat{u}_3}{\partial \hat{z}}\right) = -\frac{\partial \hat{p}}{\partial \hat{z}} + \frac{1}{\hat{r}} \frac{\partial}{\partial \hat{r}}(\hat{r}\hat{\tau}_{\hat{r}\hat{z}}) + \frac{\partial}{\partial \hat{Z}}(\hat{\tau}_{\hat{z}\hat{z}}), \tag{3.28}$$

$$\left(E\frac{\partial^5}{\partial \hat{z}^5} - F\frac{\partial^3}{\partial \hat{z}^3} + G\frac{\partial^3}{\partial \hat{z}\,\partial \hat{t}^2} + H\frac{\partial^2}{\partial \hat{z}\,\partial \hat{t}} + I_L\frac{\partial}{\partial \hat{z}}\right)(\hat{r}_2) = \frac{1}{\hat{r}}\frac{\partial}{\partial \hat{r}}(\hat{r}\hat{\tau}_{\hat{r}\hat{z}}) + \frac{\partial}{\partial \hat{z}}(\hat{\tau}_{\hat{z}\hat{z}})$$
$$- \rho\left(\hat{u}_1 \frac{\partial \hat{u}_3}{\partial \hat{r}} + \hat{u}_3 \frac{\partial \hat{u}_3}{\partial \hat{z}}\right), \tag{3.29}$$

where

$$\hat{\tau}_{\hat{r}\hat{r}} = 2\mu_0\,[1 + \Gamma|\hat{\alpha}|]\frac{\partial \hat{u}_1}{\partial \hat{r}}, \tag{3.30}$$

$$\hat{\tau}_{\hat{r}\hat{z}} = \mu_0\,[1 + \Gamma|\hat{\alpha}|]\left(\frac{\partial \hat{u}_1}{\partial \hat{Z}} + \frac{\partial \hat{u}_3}{\partial \hat{r}}\right), \tag{3.31}$$

$$\hat{\tau}_{\hat{z}\hat{z}} = 2\,\mu_0\,[1 + \Gamma|\hat{\alpha}|]\frac{\partial \hat{u}_3}{\partial \hat{z}}, \tag{3.32}$$

and

$$\hat{\alpha} = \sqrt{2\left(\frac{\partial \hat{u}_1}{\partial \hat{r}}\right)^2 + \left(\frac{\partial \hat{u}_1}{\partial \hat{z}} + \frac{\partial \hat{u}_3}{\partial \hat{r}}\right)^2 + 2\left(\frac{\partial \hat{u}_3}{\partial \hat{z}}\right)^2}\,. \tag{3.33}$$

Following are non-dimensional quantities to be used in the above system of equations

$$u_1 = \frac{\hat{u}_1}{a_2 s},\ u_3 = \frac{\hat{u}_3}{s},\ r = \frac{\hat{r}}{a_2},\ z = \frac{\hat{z}}{l},\ \tau = \frac{a_2 \hat{\tau}}{s\mu_0},\ We = \frac{\Gamma s}{a_2},\ t = \frac{s\hat{t}}{l},\ p = \frac{a^2{}_2 \hat{P}}{sl\mu_0},$$

$$\alpha = \frac{\hat{\alpha} a_2}{s}, Re = \frac{\rho s a_2}{\mu_0}, r_1 = \frac{\hat{r}_1}{a_2} = \varepsilon < 1, \varphi = \frac{b}{a_2}, r_2 = \frac{\hat{r}_2}{a_2} = 1 + \varphi \sin(2\pi\hat{z}), \tag{3.34}$$

where, Re is Reynolds number, We is the Weissenberg number, δ the dimensionless wave number, and φ the amplitude ratio.

The dimensionless form of the ruling equations are

$$\frac{\partial u_1}{\partial r} + \frac{u_1}{r} + \frac{\partial u_3}{\partial z} = 0, \tag{3.35}$$

$$Re\delta^3\left(u_1\frac{\partial u_1}{\partial r} + u_3\frac{\partial u_1}{\partial z}\right) = -\frac{\partial p}{\partial r} + \frac{1}{r}\frac{\partial}{\partial r}(r\tau_{rz}) + \delta\frac{\partial}{\partial z}(\tau_{zz}), \tag{3.36}$$

$$Re\delta\left(u_1\frac{\partial u_3}{\partial r} + u_3\frac{\partial u_3}{\partial z}\right) = -\frac{\partial p}{\partial z} + \frac{1}{r}\frac{\partial}{\partial r}(r\tau_{rz}) + \delta\frac{\partial}{\partial z}(\tau_{zz}). \tag{3.37}$$

The equation of motion governing the elastic wall

$$\left(\left(\frac{Ea_2^3}{\mu_0 sl^5}\right)\frac{\partial^5 r_2}{\partial z^5} - \left(\frac{Fa_2^3}{\mu_0 sl^3}\right)\frac{\partial^3 r_2}{\partial z^3} + \left(\frac{Gsa_2^3}{\mu_0 l^3}\right)\frac{\partial^3 r_2}{\partial z\,\partial t^2} + \left(\frac{Hsa_2^3}{\mu_0 l^2}\right)\frac{\partial^2 r_2}{\partial z\,\partial t} + \left(\frac{I_L a_2^3}{\mu_0 sl}\right)\frac{\partial r_2}{\partial z}\right) = \frac{1}{r}\frac{\partial}{\partial r}(r\tau_{rz}) + \delta\frac{\partial}{\partial z}(\tau_{zz}) - Re\delta\left(u_1\frac{\partial u_1}{\partial r} + u_3\frac{\partial u_3}{\partial z}\right), \tag{3.38}$$

where

$$\tau_{rr} = 2\mu_0\ \delta[1 + We|\alpha|]\frac{\partial u_1}{\partial r}, \tag{3.39}$$

$$\tau_{rz} = \mu_0\,[1 + We|\alpha|]\left(\frac{\partial u_1}{\partial z} + \frac{\partial u_3}{\partial r}\right), \tag{3.40}$$

$$\tau_{rz} = 2\,\mu_0\,\delta[1 + We|\alpha|]\frac{\partial u_3}{\partial z}, \tag{3.41}$$

and

$$\alpha = \sqrt{2\delta^2\left(\frac{\partial u_1}{\partial r}\right)^2 + \left(\frac{\partial u_1}{\partial z}\delta^4 + \frac{\partial u_3}{\partial r}\right)^2 + 2\delta^2\left(\frac{\partial u_3}{\partial z}\right)^2}, \tag{3.42}$$

and the dimensionless boundary conditions are

$$u_3 = -1, \quad at \quad r = r_1 = \varepsilon,$$

$$u_3 = -1, \quad at \quad r = r_2 = 1 + \varphi\sin(2\pi z). \tag{3.43}$$

We assume an extremely small wavenumber, as solving the problem in its original form is exceedingly difficult ($\delta \ll 1$), hence equations (3.36-3.39) become

$$\frac{\partial p}{\partial r} = 0, \tag{3.44}$$

$$\frac{\partial p}{\partial z} = \frac{1}{r}\frac{\partial}{\partial r}(r\tau_{rz}), \tag{3.45}$$

$$\left(L_1\frac{\partial^5 r_2}{\partial z^5} - L_2\frac{\partial^3 r_2}{\partial z^3} + L_3\frac{\partial^3 r_2}{\partial z\,\partial t^2} + L_4\frac{\partial^2 r_2}{\partial z\,\partial t} + L_5\frac{\partial r_2}{\partial z}\right) = \frac{1}{r}\frac{\partial}{\partial r}(r\tau_{rz}), \tag{3.46}$$

where

$$L_1 = \frac{Ea_2^3}{\mu sl^5},\ L_2 = -\frac{Fa_2^3}{\mu sl^3},\ L_3 = \frac{Ga_2^3}{\mu l^3},\ L_4 = \frac{Ha_2^3}{\mu l^3},\ L_5 = \frac{I_l a_2^3}{\mu sl}. \tag{3.47}$$

$L_1$is flexural stiffness of the wall, L_2 is a longitudinal tension unit, L_3 is mass per unit area, L_4 is a coefficient of viscid damping and L_5 is spring stiffness and the components of extra stress are

$$\tau_{rr} = \tau_{zz} = 0 \quad and \quad \tau_{rz} = \left(\frac{\partial u_3}{\partial r} + We\left(\frac{\partial u_3}{\partial r}\right)^2\right), \tag{3.48}$$

$$r\frac{\partial^2 u_3}{\partial r^2} + \frac{\partial u_3}{\partial r} + We\left(\frac{\partial u_3}{\partial r}\right)^2 + 2rWe\left(\frac{\partial u_3}{\partial r}\right)\left(\frac{\partial^2 u_3}{\partial r^2}\right) = r\widetilde{K}, \tag{3.49}$$

where

$$\widetilde{K} = \mathrm{L}_1 \frac{\partial^5 \mathrm{r}_2}{\partial \mathrm{z}^5} - \mathrm{L}_2 \frac{\partial^3 \mathrm{r}_2}{\partial \mathrm{z}^3} + \mathrm{L}_3 \frac{\partial^3 \mathrm{r}_2}{\partial \mathrm{z}\, \partial \mathrm{t}^2} + \mathrm{L}_4 \frac{\partial^2 \mathrm{r}_2}{\partial \mathrm{z}\, \partial \mathrm{t}} + \mathrm{L}_5 \frac{\partial \mathrm{r}_2}{\partial \mathrm{z}}, \tag{3.50}$$

3.3 Solution Methodology

Equation (3.48) is nonlinear and may not have an exact solution, we apply the regular perturbation method in terms of a variant of the Weissenberg number for the second order to find the solution. Using the We, we extend

$$\mathrm{u}_3 = \mathrm{u}_{03} + \mathrm{We}\, \mathrm{u}_{13} + \mathrm{We}^2 \mathrm{u}_{23} + \mathrm{O}(\mathrm{We}^3). \tag{3.51}$$

3.3.1 Zero order system

$$\mathrm{r} \frac{\partial^2 \mathrm{u}_{03}}{\partial \mathrm{r}^2} + \frac{\partial \mathrm{u}_{03}}{\partial \mathrm{r}} = \mathrm{r}\widetilde{K}, \tag{3.52}$$

with boundary conditions as

$$\mathrm{u}_{03} = -1 \ \text{ at } \ r_1 = \varepsilon \ \text{ and } \ r_2 = 1 + \varphi \sin\big(2\pi(\mathrm{z} - \mathrm{t})\big). \tag{3.53}$$

3.3.2 First order system

$$\mathrm{r} \frac{\partial^2 \mathrm{u}_{13}}{\partial \mathrm{r}^2} + \frac{\partial \mathrm{u}_{13}}{\partial \mathrm{r}} = -2\mathrm{r}\left(\frac{\partial^2 \mathrm{u}_{03}}{\partial \mathrm{r}^2}\right)\left(\frac{\partial \mathrm{u}_{03}}{\partial \mathrm{r}}\right) - \left(\frac{\partial \mathrm{u}_{03}}{\partial \mathrm{r}}\right)^2, \tag{3.54}$$

with boundary conditions

$$\mathrm{u}_{23} = 0 \ \text{ at } \ r_1 = \varepsilon \ \text{ and } \ r_2 = 1 + \varphi \sin(2\pi z). \tag{3.55}$$

3.3.3 Second order system

$$\mathrm{r}\frac{\partial^2 \mathrm{u}_{23}}{\partial \mathrm{r}^2} + \frac{\partial \mathrm{u}_{23}}{\partial \mathrm{r}} = -2\mathrm{r}\left(\frac{\partial^2 \mathrm{u}_{03}}{\partial \mathrm{r}^2}\right)\left(\frac{\partial \mathrm{u}_{13}}{\partial \mathrm{r}}\right) - 2\mathrm{r}\left(\frac{\partial^2 \mathrm{u}_{13}}{\partial \mathrm{r}^2}\right)\left(\frac{\partial \mathrm{u}_{03}}{\partial \mathrm{r}}\right) - 2\left(\frac{\partial \mathrm{u}_{03}}{\partial \mathrm{r}}\right)\left(\frac{\partial \mathrm{u}_{13}}{\partial \mathrm{r}}\right), \qquad (3.56)$$

with boundary conditions:

$$\mathrm{u}_{23} = 0 \quad \text{at} \quad r_1 = \varepsilon \quad \text{and} \quad r_2 = 1 + \varphi \sin(2\pi z). \qquad (3.57)$$

3.5 Result and Discussion

This part shows results we obtained by using perturbation approach to solve the problem equations then drawing these results using a MATHEMATICA program.

Two section make up this part: The first part covers how parameters affect the fluid's through the flow channel, the second part covers how they affect shear stress.

3.5.1 Velocity Profile

Figures 3.2-3.9 shows the effect of parameters We, φ , L_1, L_2, L_3, L_4 , L_5 and ϵ on the velocity vs. r distribution. In the (Fig. 3.2) illustrates the axial velocity distribution u_3 versus radial position r for three different values of the amplitude ratio φ = 0.1, 0.125, and 0.15, under fixed values of other parameters (We = 0.01, ϵ = 0.15, L_1 = 0.1, L_2 = 0.5, L_3 = 0.1, L_4 = 0.1, L_5 = 0.1, z = 0.4, t = 0.1). As shown, the velocity profile is parabolic in shape, typical of peristaltic transport, peaking at the center of the channel and diminishing toward both the inner (rigid) and outer (elastic) walls. A key observation is that increasing the amplitude ratio φ that represents the strength of the peristaltic wave undulations on the elastic outer wall leads to a progressive rise in maximum velocity. This is evident from the upward shift in the curves from solid (φ = 0.1) to dotted (φ = 0.15). Physically, a larger φ increases the deformation of the elastic wall, effectively widening the flow path and intensifying the fluid pumping action. This greater wall motion amplifies the peristaltic driving force, especially near the central axis of the tube, causing higher axial velocities. where the increase in velocity to stronger peristaltic motion induced by a more undulating outer wall. Thus, the figure effectively demonstrates how elastic wall behavior, via the amplitude ratio, significantly influences fluid transport in peristaltic motion of Williamson fluid.

The (Fig. 3.3) illustrates the axial velocity component plotted against the radial coordinate r for varying values of the Weissenberg number We, that quantifies the degree of fluid elasticity in non-Newtonian flow, specifically during Williamson fluid. The three curves correspond to We = 0, (solid), We = 0.01 (dashed), and We = 0.02 (dotted). From the figure, it is evident that as the Weissenberg number increases, the velocity profile shifts upward, especially near the center of the channel, indicating that higher fluid elasticity enhances axial flow velocity. Physically,

this can be explained by the nature of elastic fluids higher We means that the fluid retains more of its deformation energy, that supports faster movement along the axis. This energy storage and release mechanism enhances the fluid's ability to accelerate during wave propagation. The parabolic shape of the velocity profile remains, but with a broader and taller peak as We increases. Thus, we conclude that elastic effects introduced by a higher Weissenberg number promote faster transport in peristaltic systems, that is crucial in engineering and biomedical applications where non-Newtonian behavior dominates, such as in blood flow, mucus transport, or industrial polymer pumping.

The (Fig. 3.4) illustrates the axial velocity distribution versus the radial coordinate r for three different values of the flexural rigidity L_1 parameter of the elastic outer wall during peristaltic flow of a Williamson fluid. As shown, increasing significantly enhances the peak velocity in the central region of the channel. Specifically, when increases from 0.05 to 0.15, the velocity profile becomes more pronouncedly parabolic and reaches higher maximum values at the center-line ≈ 0.6, suggesting a more vigorous axial flow. This behavior aligns with the physical interpretation that greater wall flexural stiffness allows the elastic outer wall to store and release more mechanical energy, amplifying the peristaltic wave-induced pumping effect. From a mechanical standpoint, the flexible wall behaves like a spring as increases, the wall's response to peristaltic undulation becomes stronger, generating greater forward momentum in the fluid. The amplification effect is especially relevant in biomedical applications (e.g., blood transport), where wall elasticity can be tuned to control flow rates. Therefore, this figure demonstrates how increasing flexural rigidity enhances the propane strength of peristaltic pumping in non-Newtonian fluids within deformable geometries.

In the (Fig. 3.5) depicts the axial velocity component as a function of the radial coordinate r, under different values of the longitudinal tension L_2 parameter ,that represents the axial tension per unit width in the flexible outer wall of the cylindrical channel. The profiles demonstrate a clear decrease in peak velocity as increases from 0.2 (solid line) to 0.6 (dotted line). The parabolic shape of the velocity remains, with symmetry about the center, but the amplitude of the velocity diminishes progressively. This indicates that higher longitudinal tension restricts the dynamic deformation of the elastic wall, thereby limiting the transmission of peristaltic wave energy into forward fluid motion. Physically, a larger means a stiffer axial stretch of the wall, resisting the sinusoidal wave's ability to expand and contract the channel effectively. As

a result, the peristaltic pumping weakens, leading to a lower induced axial velocity. This insight is particularly important in bio fluid dynamics, where tunable wall stiffness can modulate flow characteristics in artificial or physiological conduits, such as arteries or ureters. The figure highlights a dampening effect of axial wall tension on the efficiency of peristaltic transport, a crucial design consideration in fluidic systems employing elastic conduits.

The (Fig. 3.6) illustrates the velocity distribution versus the radial position r for different values of the parameter, that represents the mass per unit area L_3 of the elastic wall in the peristaltic flow of Williamson fluid. The three curves (solid, dashed, and dotted) correspond to L_3 = 0.1, 0.3 and 0.5. From the fig, seen that as increases, the peak velocity in the centre of the channel decreases noticeably. This implies that a heavier elastic wall (higher) resists the deformation caused by the peristaltic wave, resulting in lower fluid transport efficiency through the channel. Physically, this makes sense because a heavier wall has greater inertia and requires more force to achieve the same level of deformation thus, it transmits less energy to the fluid. As a result, the parabolic velocity profile flattens, and the maximum velocity achieved at the centreline reduces. Therefore, it can be concluded that increasing the wall's mass per unit area leads to a suppression of peristaltic pumping strength and a reduction in fluid flow velocity throughout the channel.

The (Fig. 3.7) illustrates how the axial velocity component varies along the radial direction r within a flexible cylindrical channel, under the influence of different values of the viscous damping coefficient L_4. The solid, dashed, and dotted lines represent L_4 = 0.1, 0.2, and 0.4. The velocity profile is parabolic in nature peaking at the center of the channel and reducing symmetrically toward the walls. The maximum velocity decreases progressively as increases.

Physically, this reflects the damping effect a higher viscous damping coefficient introduces more resistance to motion from the flexible wall, thereby suppressing the velocity. This trend is consistent with the theoretical modelling presented in the study, that shows that damping resists the amplitude of wave-induced deformation of the wall, leading to a weaker driving force for fluid motion. The system with L_4 = 0.4 exhibits the most suppressed flow, while L_4 = 0.1 permits the highest velocity peak. This demonstrates the inverse relationship between viscous damping and axial velocity magnitude in peristaltic transport of Williamson fluid through an elastic-walled channel.

The (Fig. 3.8) shows the velocity profile versus the radial coordinate r for different values of the parameter, that represents the spring stiffness L_5 of the elastic wall in the peristaltic transport of Williamson fluid. The curves correspond to L_5 = 0, 0.1, and 1.1 and all exhibit a classic parabolic velocity distribution, peaking at the center of the flow channel. A careful observation reveals that its increases, the velocity profile shows a slight but consistent rise, indicating that the spring stiffness enhances the wall's ability to push fluid more effectively. Physically, a stiffer spring attached to the elastic wall leads to more efficient restoration and propagation of the wall's peristaltic wave, that in turn transmits greater mechanical energy into the fluid. This increased wall motion boosts axial fluid momentum, especially in the core region, resulting in the observed higher peak velocity. While the difference between the curves is relatively subtle, it shows that spring stiffness plays a supportive role in enhancing flow rate, especially in applications where precise fluid control is critical, such as in biomedical devices or microfluidic systems.

The (Fig. 3.9) shows the velocity distribution versus radial position for different values of the parameter ε, that represents the inner radius ratio (i.e., the relative size of the inner cylinder within the channel). The solid, dashed, and dotted lines correspond to ε = 0.1, 0.125, and 0.15 from the figure, it is evident that increasing and leads to a significant decrease in the maximum velocity within the channel. where the inner cylinder radius increases, it constricts the flow domain, leaving less space for the fluid to move, thereby reducing axial velocity. Physically, this makes intuitive sense a thicker inner wall reduces the available flow area and introduces greater resistance to fluid motion. The figure also shows that the velocity profiles remain parabolic in shape, but the peak shifts downward as and increases. Thus, increasing the inner wall size higher and leads to more constricted flow and reduced pumping efficiency in peristaltic motion, an important consideration in applications such as biomedical fluid transport and microchannel design.

3.5.2 Shear Stress

Figures 3.10 - 3.17 shows the effect of parameters φ, L_1, L_2, L_3, L_4, L_5, ϵ and We on the shear stress. In the (Fig. 3.10) shows the shear stress as a function of radial position r for various values of the amplitude ratio φ , that characterizes the height of the wave on the outer elastic wall in a peristaltic channel. The solid, dashed, and dotted curves represent φ = 0.1, 0.125, and

0.15. As seen, increasing the amplitude ratio leads to a significant rise in shear stress near the inner wall (lower r) where the stress values are strongly positive. However, as r increases towards the outer wall, the shear stress decreases and eventually becomes negative, indicating a change in shear direction. This trend is consistent with highlights that increasing and intensifies wall deformation, thereby generating stronger velocity gradients near the solid wall, resulting in higher positive shear stress there. The physical explanation lies in the fact that a larger wave amplitude enhances the wall's peristaltic pumping action, increasing the strain rate and hence shear stress in the fluid near the inner boundary. As the wave effect tapers off towards the elastic outer wall, the stress declines and becomes negative due to the wall's flexibility absorbing some of the energy. Therefore, larger wave amplitudes amplify shear near the solid wall and intensify the stress reversal across the channel, that is a key consideration in designing peristaltic pumps or understanding biological flow phenomena where wave amplitude impacts shear-driven transport and mixing.

The (Fig. 3.11) displays the shear stress as a function of radial position for different values of the flexural rigidity L_1 parameter, that characterizes the stiffness of the outer elastic wall in response to bending in peristaltic flow. The curves correspond to L_1= 0.1, 0.15, and 0.2 for the solid, dashed, and dotted lines. The figure shows in that increasing significantly enhances the shear stress near the inner wall (lower r), where the stress is strongly positive. As r increases toward the outer elastic wall, the stress declines, crosses zero, and becomes increasingly negative with higher. Its explained that a stiffer elastic wall (higher flexural rigidity) transmits more mechanical energy to the fluid, thereby increasing the velocity gradient and, consequently, the shear stress. From a physical standpoint, a stiffer wall is less prone to damping, and its deformation more effectively drives the fluid, especially near the rigid inner boundary. However, the outer flexible wall absorbs some of this energy, causing the shear stress to flip sign as it adjusts to the wave-induced motion.

In the (Fig. 3.12) shows the variation of shear stress along the radial coordinate r for different values of the longitudinal tension parameter , that characterizes the tensile force per unit width acting along the elastic wall in the peristaltic flow of a Williamson fluid. The solid, dashed, and dotted lines represent increasing values of at L_2 = 0.1, 0.5, and 0.9. It is clear that as increases, the magnitude of shear stress near the inner wall (lower r) becomes significantly higher (positive), while the stress decreases toward the outer elastic wall, eventually becoming

negative. where increasing L_2 enhances the stretching ability of the wall, leading to more effective fluid-wall interaction and greater deformation, that in turn produces higher velocity gradients near the inner wall. Physically, greater longitudinal tension strengthens the elastic wave's ability to transmit force into the fluid, increasing the shear effect in regions closest to the rigid boundary. As the wave moves outward, the stress declines due to energy absorption by the elastic wall and reduced velocity gradient. The point at that the stress crosses zero shifts slightly depending on, illustrating the dynamic balance between the solid and elastic walls in transferring momentum. Increased longitudinal wall tension enhances shear stress intercity and steepens the radial gradient, making a key control parameter in fine-tuning flow behavior for efficient transport in peristaltic pumping systems.

The (Fig. 3.13) demonstrates the impact of the wall mass parameter on the radial distribution of shear stress in the peristaltic flow of Williamson fluid through a cylindrical channel with an elastic outer wall. As seen, the shear stress is maximal near the solid inner wall (small r) and declines toward the elastic outer wall (higher r), eventually crossing into negative territory. With a small wall mass (L_3 = 0.1), the fluid-wall interaction is more pronounced, producing higher stress values. However, as increases to 0.5 and 0.9 the wall's inertial resistance increases, that causes the magnitude of shear stress near the inner wall to drop significantly. The smoothening of the curve and shallower stress gradient indicate a buffering effect caused by the heavier wall, that absorbs and redistributes the shear more evenly across the flow domain. This matches the description that explains that an increase in leads to a decrease in shear stress near the inner wall and a rise at the elastic wall. Overall, this behavior is a reflection of the damping role played by wall mass in modulating peristaltic stresses within the fluid, and it shows how structural parameters directly affect flow behavior in biological or industrial applications involving flexible conduits.

The (Fig. 3.14) effectively illustrates how the coefficient of viscous damping, a critical wall property, influences the distribution of shear stress during peristaltic transport of Williamson fluid. As seen the value of increases, there is a clear reduction in the peak stress near the solid inner wall, and the decay of stress across the radius becomes more gradual. Physically, this means a wall with higher internal friction or damping capacity resists rapid motion changes, thereby absorbing part of the mechanical stress transmitted by the fluid flow. This results in smoother stress transitions and less energy being transmitted to the fluid. Noted this inverse

relationship, where increased leads to decreased stress at the inner wall and increased stress at the elastic outer wall, due to redistribution. This trend is relevant in bio fluid applications where tissue or membrane damping can regulate stress propagation such as in arteries or soft conduits. Ultimately, underscores the role of damping as a stress moderator in peristaltic systems, helping to shield the channel walls from extreme shear conditions and stabilizing the flow.

The (Fig. 3.15) illustrates the variation of the shear stress component with respect to the radial coordinate r, for different values of the parameter (spring stiffness of the outer elastic wall). Specifically, the Fig. 3.15 shows curves for L_5 = 0.1, 1.1, and 2.1. As observed, the shear stress is maximum and positive near the inner rigid wall (small r), and it steadily decreases as we move radially outward toward the elastic outer wall. The stress even becomes negative near the outer edge. According to the study, an increase in (spring stiffness) intensifies the resistance offered by the elastic wall, thereby altering the stress distribution inside the fluid domain. However, in this particular figure, all curves appear similar and almost overlap, suggesting that changes in may have a subtle effect in this range or for this particular case. Physically, a higher spring stiffness makes the outer wall more resistant to deformation, that stabilizes the wall shape and hence restricts large variations in shear stress. Near the inner wall, the positive stress indicates stronger interaction and push of the fluid against the rigid boundary, while the negative values near the elastic wall suggest a pull or suction-like effect due to wall elasticity.

The (Fig. 3.17) shows how the shear stress changes with the radial position r for different values of the Weissenberg number We, which reflects the fluid's elastic behavior. As r increases from the inner to the outer wall, shear stress decreases from a high positive value to a negative one, indicating a change in shear direction near the elastic wall. When We increases from 0 to 0.02, the stress near the center of the channel increases slightly, showing that elasticity enhances shear strength in that region. The results suggest that a higher We strengthens the fluid's resistance and flow near the center while increasing stress variation across the channel. This behavior matches the findings in the article, where a rise in We increases stress near the solid wall and deepens the negative stress near the elastic boundary.

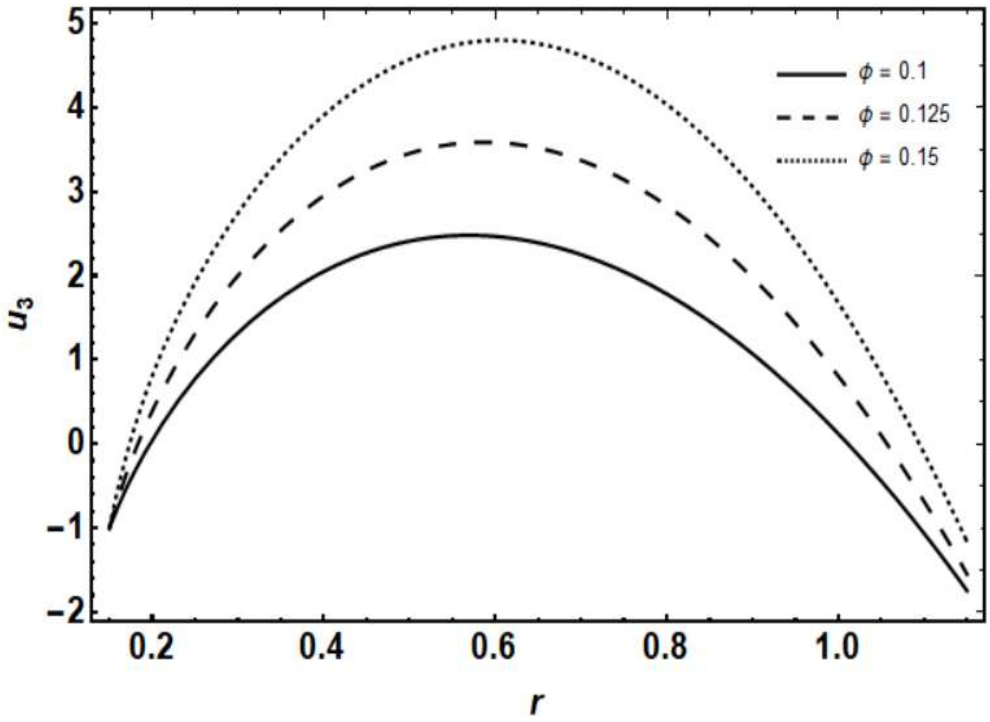

Fig. 3.2 Variation of φ on velocity field at φ = 0.1, 0.125, 0.15 with We = 0.01, ϵ = 0.15, L_1 = 0.1, z = 0.4, L_2 = 0.5, L_3 = 0.1, L_4 = 0.1, L_5 = 0.1, t = 0.1.

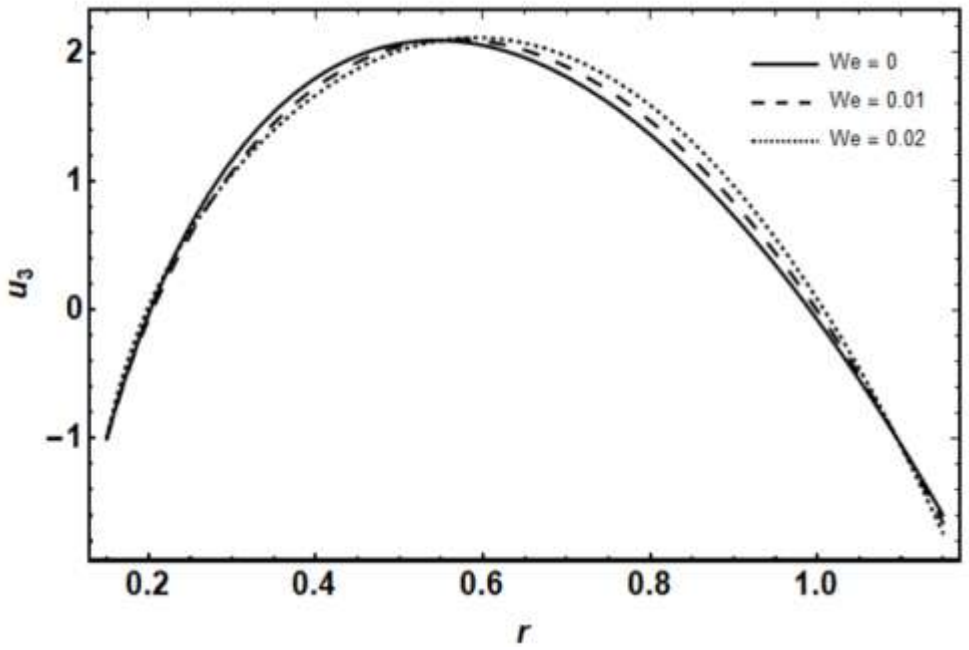

Fig. 3.3 Variation of We on velocity field at We = 0, 0.01, 0.02 with φ = 0.1, ϵ = 0.15, L_1= 0.1, z = 0.4, L_2 = 0.5, L_3 = 0.1, L_4 = 0.1, L_5 = 0.1, t = 0.1.

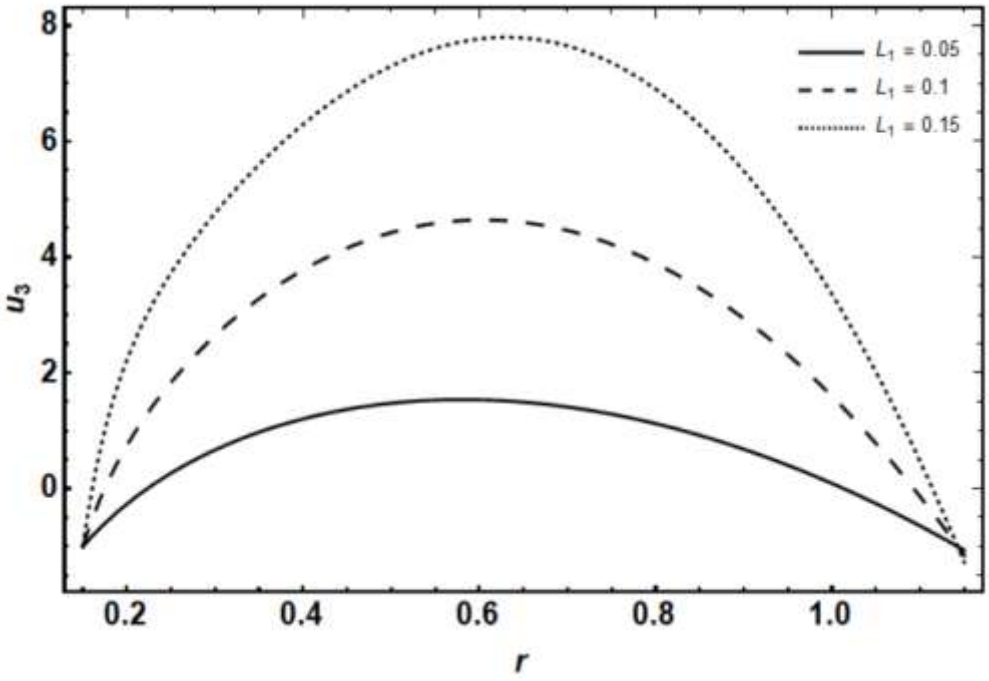

Fig. 3.4 Variation of L_1 on velocity field at L_1= 0.05, 0.1, 0.15 with φ = 0.1, ϵ = 0.15, We = 0.01, L_2 = 0.1, z = 0.4, L_3 = 0.1, L_4 = 0.1, L_5 = 0.1, t = 0.1.

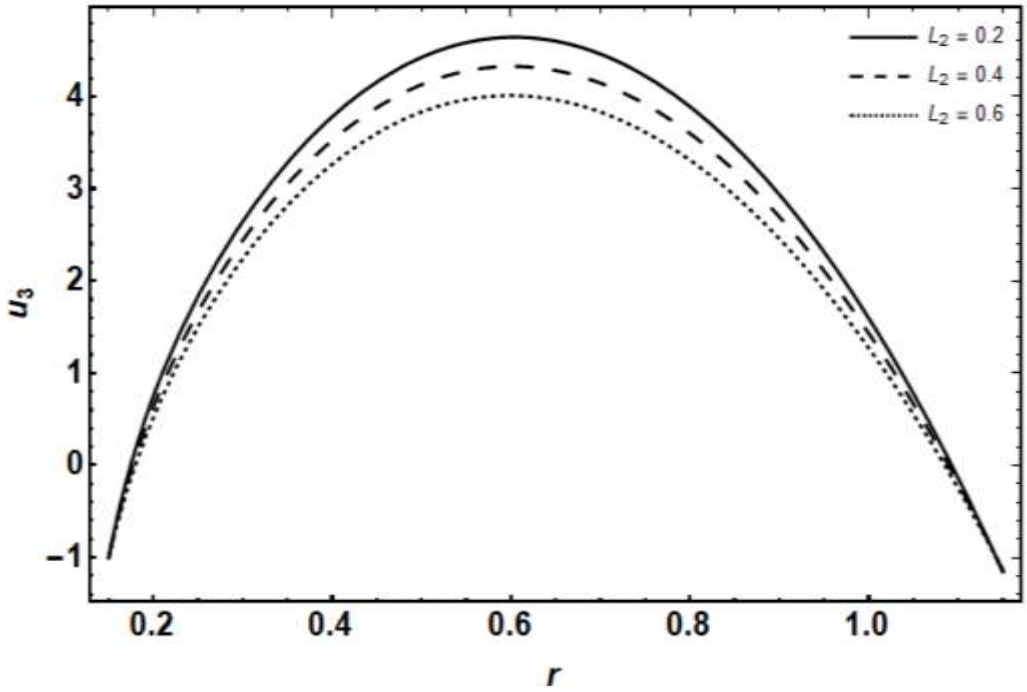

Fig. 3.5 Variation of L_2 on velocity field at L_2= 0.2, 0.4, 0.6 with φ = 0.1, ϵ = 0.15, We = 0.01, L_1 = 0.1, L_3 = 0.1, L_4 = 0.1, L_5 = 0.1, z = 0.4, t = 0.1.

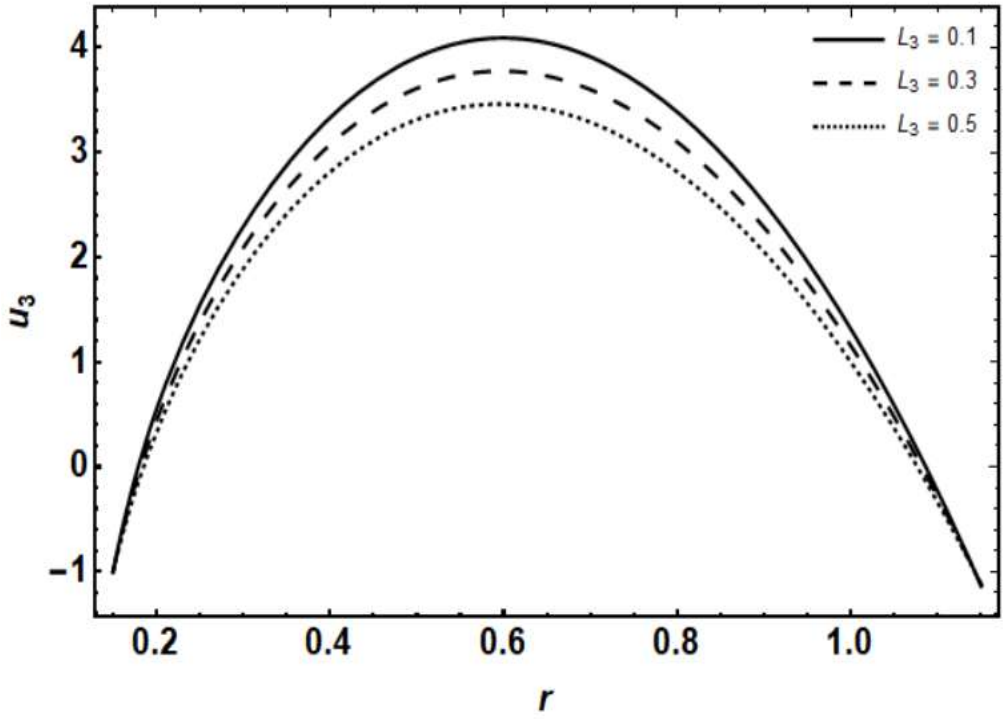

Fig. 3.6 Variation of L_3 on velocity field at $L_3 = 0.1, 0.3, 0.5$ with $\varphi = 0.1$, $\epsilon = 0.15$, We = 0.01, $L_1 = 0.1$, $L_2 = 0.5$, $L_4 = 0.2$, $L_5 = 0.1$, z = 0.4, t = 0.1.

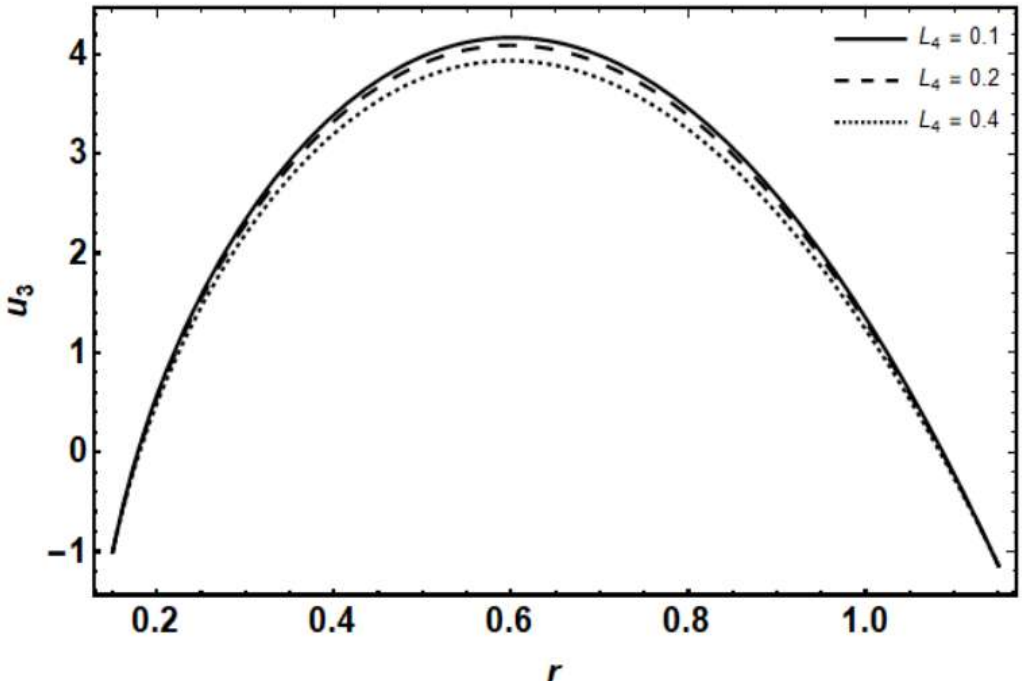

Fig. 3.7 Variation of L_4 on velocity field at $L_4 = 0.1, 0.2, 0.4$ with $\varphi = 0.15$, $\epsilon = 0.15$, We = 0.01, $L_1 = 0.1$, $L_2 = 0.5$, $L_3 = 0.1$, $L_5 = 0.1$, z = 0.4, t = 0.1.

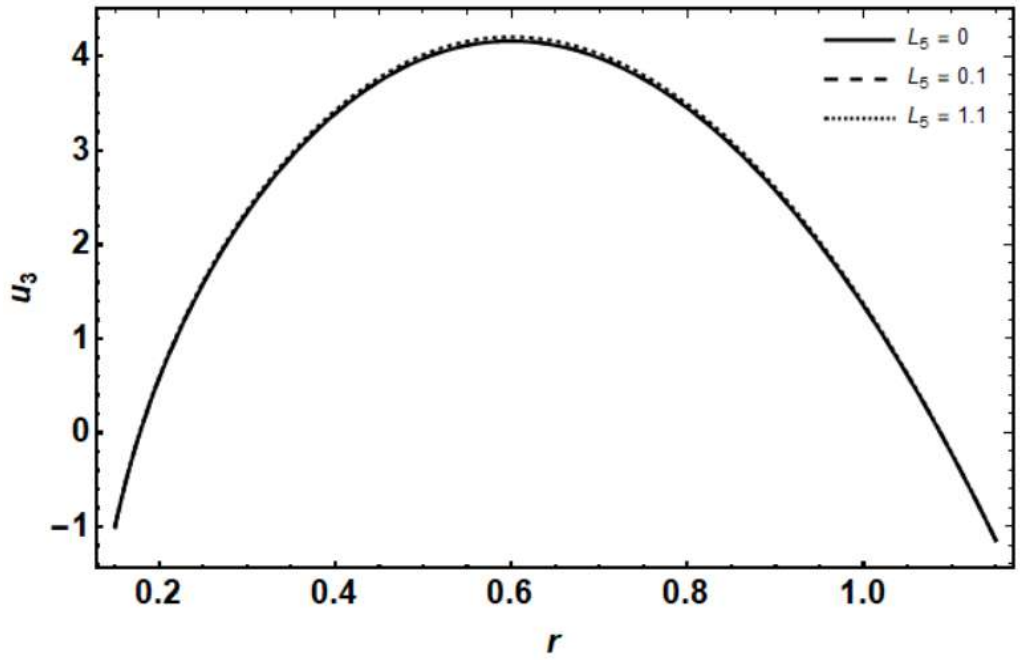

Fig. 3.8 Variation of L_5 on velocity field at L_5= 0, 0.1, 1.1 with φ = 0.15, ϵ = 0.15, We = 0.01, L_1 = 0.1, L_2 = 0.5, L_3 = 0.1, L_5 = 0.1, z = 0.4, t = 0.1.

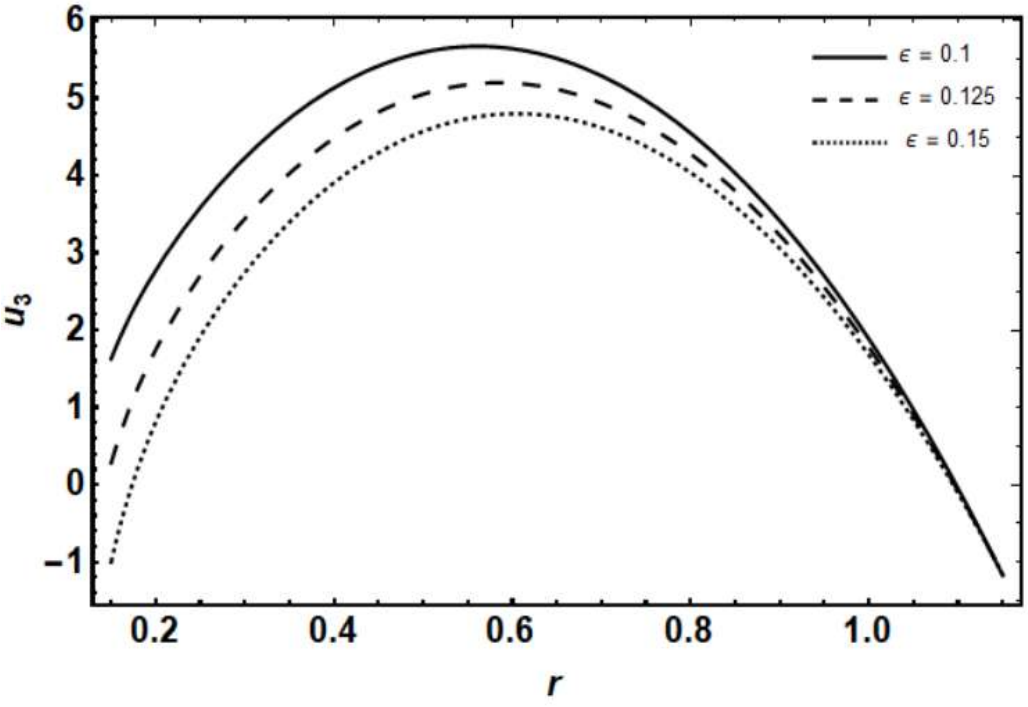

Fig. 3.9 Variation of ϵ on velocity field at ϵ = 0.1, 0.125, 0.15 with We = 0.01, φ = 0.15, L_1 = 0.1, L_2 = 0.5, L_3 = 0.1, L_4 =0.1, L_5 =0.1, z = 0.4, t = 0.1.

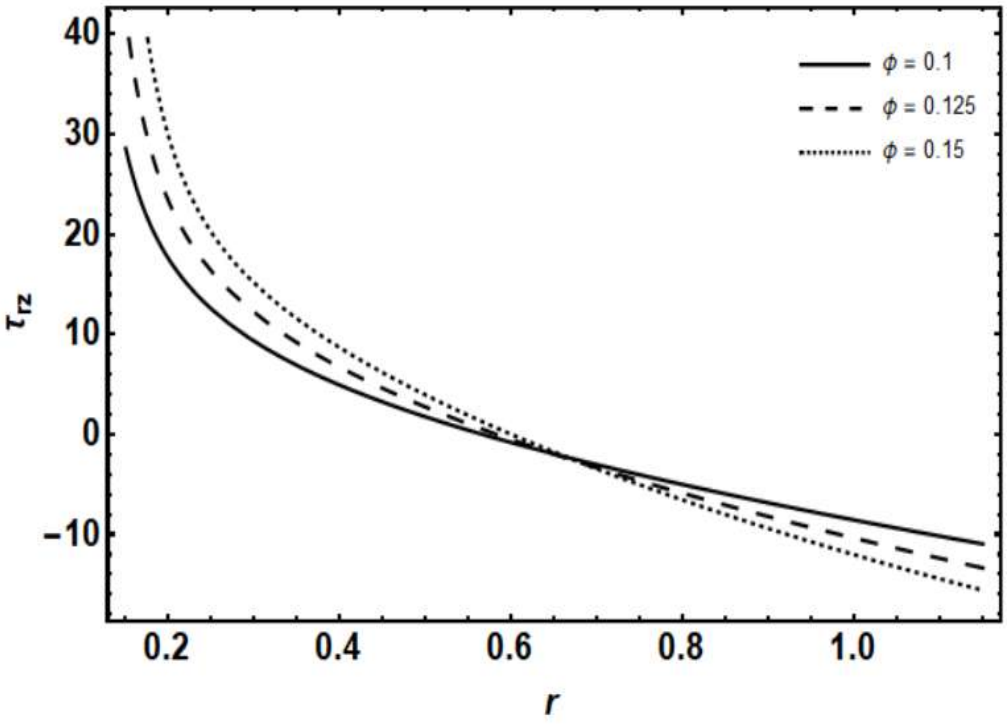

Fig. 3.10 Variation of φ on Shear-Stress at φ = 0.1, 0.125, 0.15 with We = 0.01, ϵ = 0.15, L_1 = 0.1, L_2 = 0.5, L_3 = 0.1, L_4 =0.1, L_5 = 0.1, z = 0.4, t = 0.1.

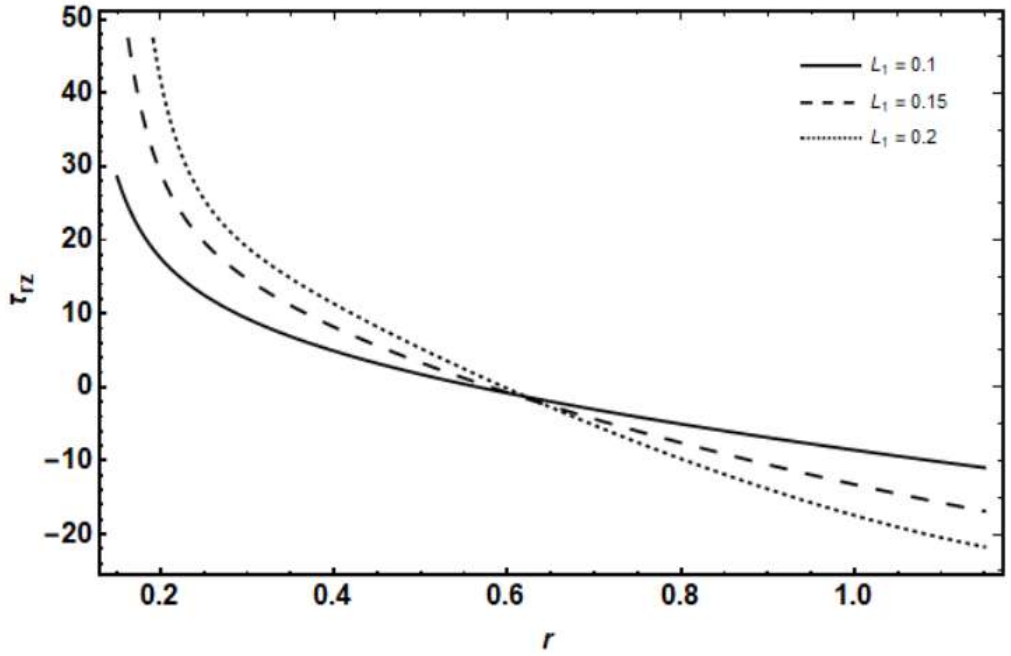

Fig. 3.11 Variation of L_1 on Shear-Stress at L_1= 0.1, 0.15, 0.2 with φ = 0.15, ϵ = 0.15, We = 0.01, L_2 = 0.5, L_3 = 0.1, L_4 = 0.1, L_5 = 0.1, z = 0.4, t = 0.1.

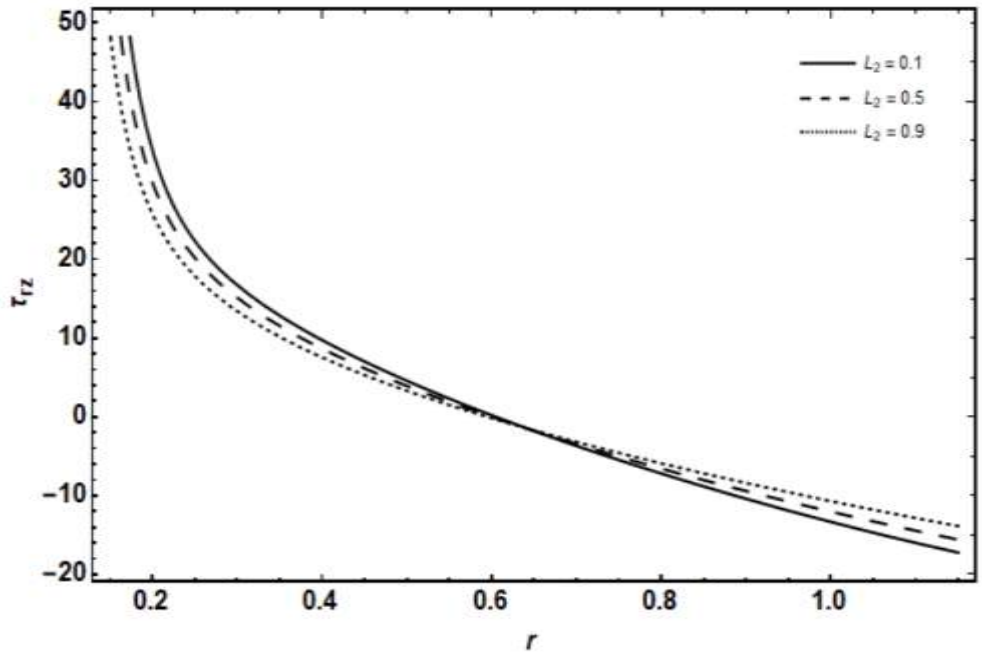

Fig. 3.12 Variation of L_2 on Shear-Stress at L_2= 0.1,0.5,0.9 with φ = 0.1, ϵ = 0.15, We = 0.01, L_1 = 0.1, L_3 = 0.1, L_4 = 0.1, L_5 = 0.1, z = 0.4, t = 0.1.

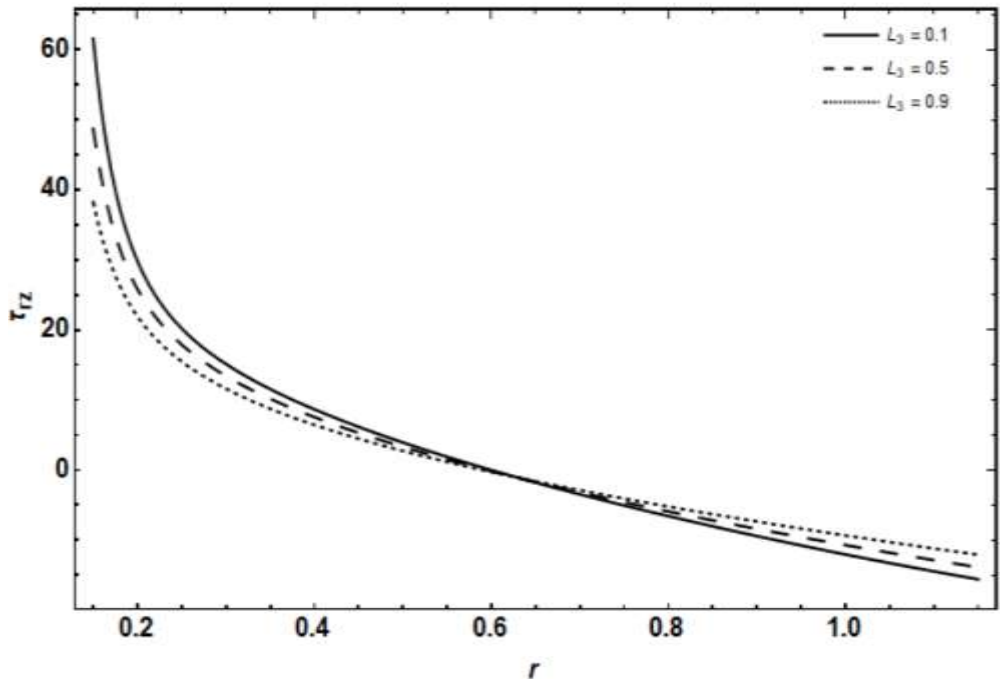

Fig. 3.13 Variation of L_3 on at Shear-Stress L_3= 0.1, 0.5, 0.9 with φ = 0.15, ϵ = 0.15, We = 0.01, L_1 = 0.1, L_2 = 0.5, L_4 = 0.2, L_5 = 0.1, z = 0.4, t = 0.1.

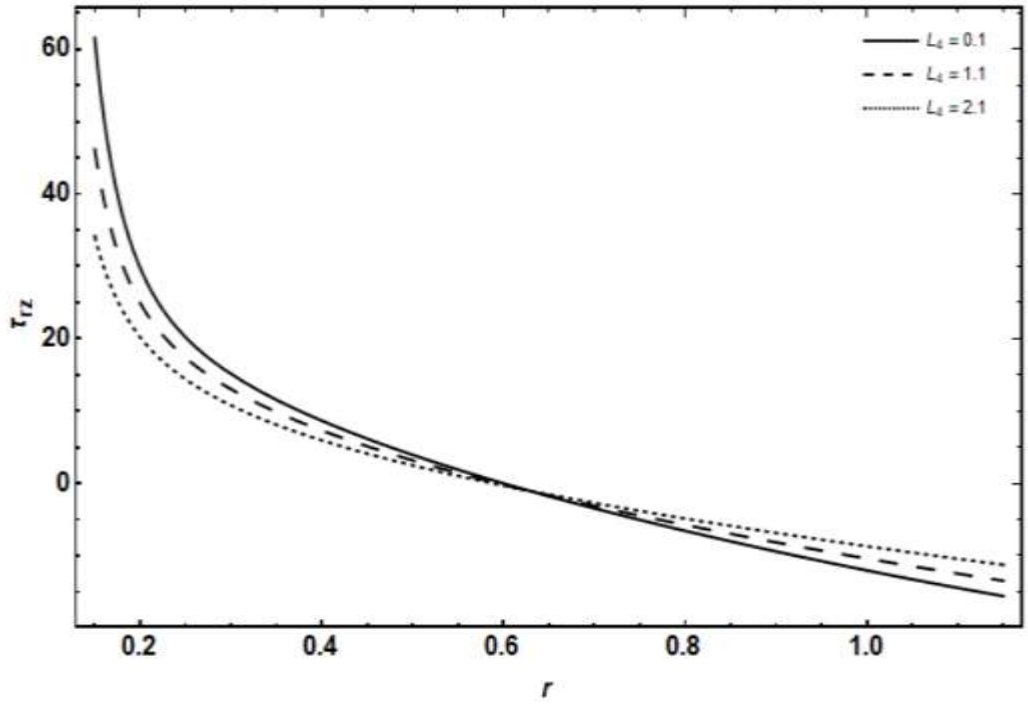

Fig. 3.14 Variation of L_4 on Shear-Stress at L_4= 0.1, 1.1, 2.1 with φ = 0.15, ϵ = 0.15, We = 0.01, L_1 = 0.1, L_2 = 0.5, L_3 = 0.1, L_5 = 0.1, z = 0.4, t = 0.1.

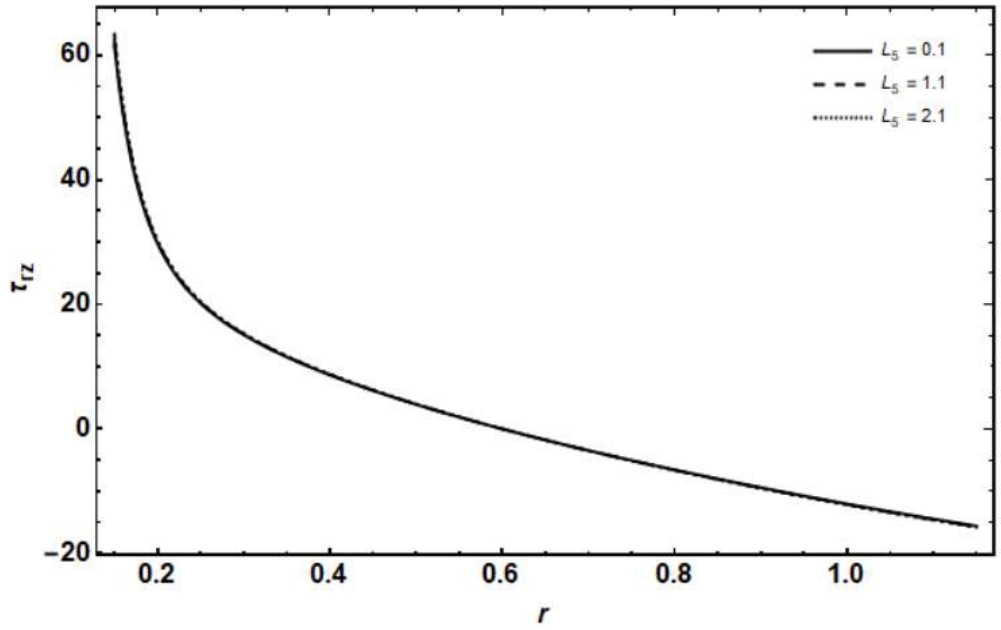

Fig. 3.15 Variation of L_5 on Shear-Stress at L_5 = 0.1, 1.1, 2.1 with φ = 0.15, ϵ = 0.15, We = 0.01, L_1 = 0.1, L_2 = 0.5, L_3 = 0.1, L_5 = 0.1, z = 0.4, t = 0.1.

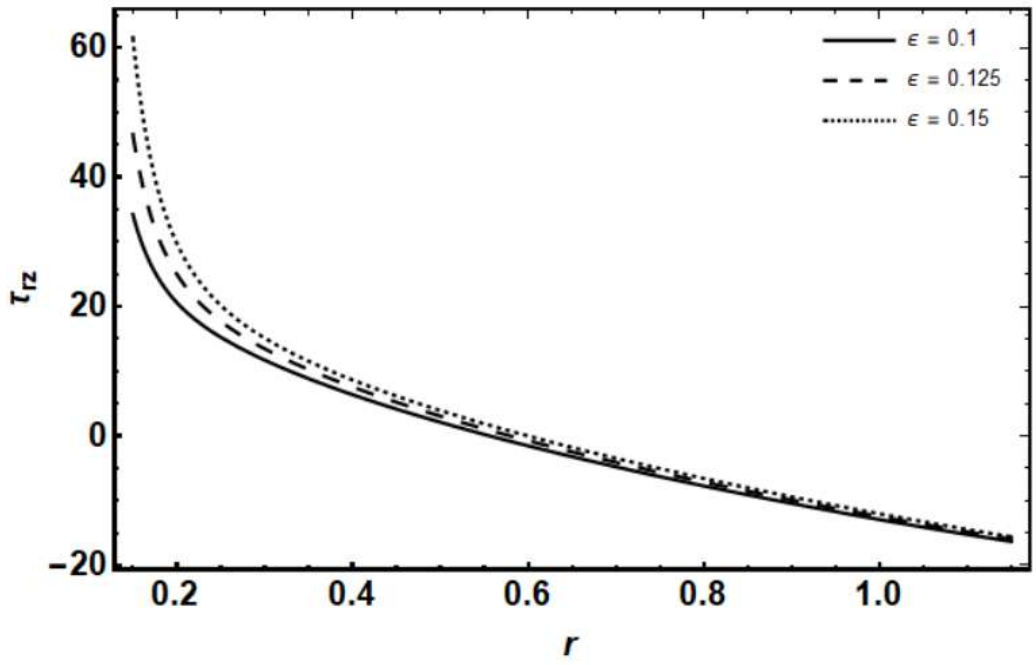

Fig. 3.16 Variation of ϵ on Shear-Stress at ϵ = 0.1, 0.125, 0.15 with We = 0.01, φ = 0.15, L_1 = 0.1, L_2 = 0.5, L_3 = 0.1, L_4 =0.1, L_5 =0.1, z = 0.4, t = 0.1.

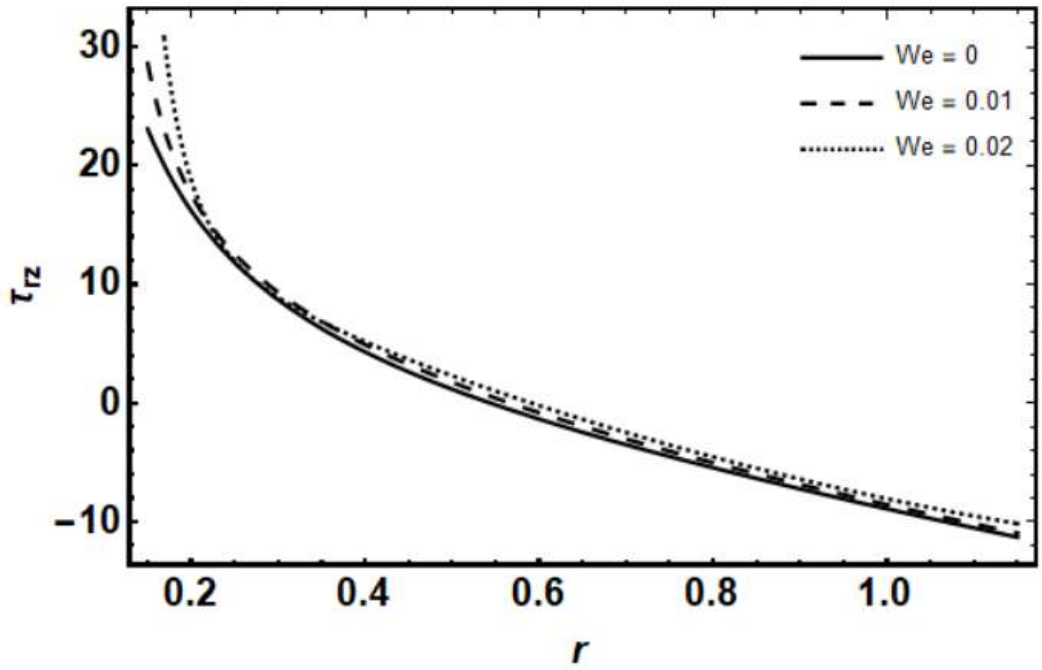

Fig. 3.17 Variation of We on Shear-Stress at We = 0,0.01,0.02 with φ = 0.1, ϵ = 0.15, L_1= 0.1, L_2 = 0.5, L_3 = 0.1, L_4 =0.1, L_5 =0.1, z = 0.4, t = 0.1.

CHAPTER 4

IMPACT OF ELASTIC PASSAGE ON THE PERISTALTIC TRANSPORT OF WILLIAMSON FLUID WITH SLIP EFFECTS

4.1 Introduction

In this chapter, extension of the work by (Al-Khafajy & Al-Delfi, 2023) in which the effect of an elastic outer wall on the peristaltic transport of a non-Newtonian Williamson fluid trapped between two concentric cylinders where the outer wall exhibits a sinusoidal wave pattern while the inner wall stays inelastic is examined. The effects of velocity slip at the boundaries, porosity, and magnetohydrodynamics (MHD) are taken into account. The mathematical formulation of the proposed model is done by using the momentum and energy equations in cylindrical coordinates while assuming a long wavelength and a low Reynolds number assumption. The series solutions of the produced differential systems are obtained using a regular perturbation technique due to their non-linear nature. Mathematica software is used to solve the governing equations and investigate the effects of important parameters including fluid rheology, wall elasticity, and wave amplitude. The findings show that the elastic behaviour of the outer wall causes notable differences in shear stress, streamlines, and velocity profiles.

4.2 Physical Model

The proposed model considers the flow of incompressible Williamson fluid passes through the tube exhibiting the peristaltic mechanism as illustrated in Fig. 4.1. The cylindrical coordinates $\hat{Z}$ in synchrony with the tube's axis and $\hat{R}$ with its radius.

$$\hat{R}(\hat{Z},\ \hat{t}) = a_2 + \ bsin\frac{2\pi}{l}(\hat{Z} - s\hat{t}) \tag{4.1}$$

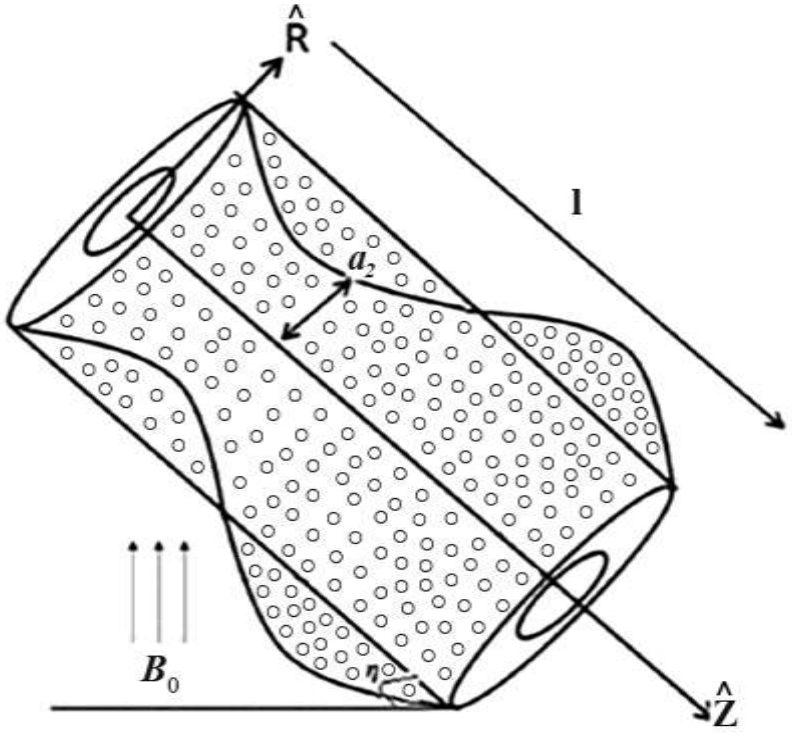

Fig. 4.1 Geometry of the Tube.

where wave propagation speed is s, wavelength is l, a_2 is the average radius of the tube, small holes shows the porous structure, time is $\hat{t}$ and b is the amplitude of a peristaltic wave, η is the inclination of the tube B_0 is the magnetic field.

In two-dimensional flow, the velocity field is defined as follows:

$$\widehat{\mathbf{V}} = \left[\widehat{U}_1\left(\widehat{R}, \widehat{Z}, \hat{t}\right), \widehat{U}_3\left(\widehat{R}, \widehat{Z}, \hat{t}\right)\right]. \tag{4.2}$$

The basic governing continuity along momentum and energy equations describing the fluid model are

$$\operatorname{div} \widehat{\mathbf{V}} = 0, \tag{4.3}$$

$$\rho\left(\frac{d\widehat{\mathbf{V}}}{d\hat{t}}\right) = \operatorname{div}\mathbf{S} + \rho\mathbf{f}, \tag{4.4}$$

$$\left(\rho c_p\right)\frac{d\widehat{T}}{d\hat{t}} = -\operatorname{div}\mathbf{q}^* + \mathbf{Q_0}, \tag{4.5}$$

where

$$q^* = -\mathbf{k}\nabla^2\widehat{T},$$

the velocity field is denoted by $\widehat{\mathbf{V}}$, the density by ρ, specific body force is denoted by **f**, and the material time derivative by $\frac{\mathrm{d}}{\mathrm{d}\hat{\mathrm{t}}}$. $\widehat{\mathrm{T}}$ denotes temperature, **k** is thermal conductivity, $\mathrm{c_p}$ is specific heat, $\mathbf{Q_0}$ heat generation, **q*** denotes heat flux, total heat flux div **q***.

The Cauchy stress tensor S for incompressible fluid can be expressed as:

$$\mathrm{S} = \left[-\widehat{\mathrm{P}}\hat{\mathrm{I}} + \hat{\tau}\right], \tag{4.6}$$

where Cauchy stress tensor by S pressure by $\widehat{\mathrm{P}}$, the identity tensor by $\hat{\mathrm{I}}$, $\hat{\tau}$ extra stress tensor.

The Williamson fluid constitutive equations and elastic wall's equations already discussed in chapter 03.

After substituting the velocity components in the shear stress equation for Williamson's fluid, the governing equations for fluid motion are obtained in equations (4.3) - (4.5), we have

$$\frac{\partial \widehat{\mathrm{U}}_1}{\partial \hat{\mathrm{R}}} + \frac{\widehat{\mathrm{U}}_1}{\hat{\mathrm{R}}} + \frac{\partial \widehat{\mathrm{U}}_3}{\partial \hat{\mathrm{Z}}} = 0\,, \tag{4.7}$$

$$\rho\left(\frac{\partial \widehat{\mathrm{U}}_1}{\partial \hat{\mathrm{t}}} + \widehat{\mathrm{U}}_1\,\frac{\partial \widehat{\mathrm{U}}_1}{\partial \hat{\mathrm{R}}} + \widehat{\mathrm{U}}_3\,\frac{\partial \widehat{\mathrm{U}}_1}{\partial \hat{\mathrm{Z}}}\right) = -\frac{\partial \widehat{\mathrm{P}}}{\partial \hat{\mathrm{R}}} + \frac{1}{\hat{\mathrm{R}}}\,\frac{\partial}{\partial \hat{\mathrm{R}}}\left(\hat{\mathrm{R}}\hat{\tau}_{\hat{\mathrm{R}}\hat{\mathrm{R}}}\right) + \frac{\partial}{\partial \hat{\mathrm{Z}}}\left(\hat{\tau}_{\hat{\mathrm{R}}\hat{\mathrm{Z}}}\right) + \rho\beta_0 \mathrm{g}\left(\widehat{\mathrm{T}}_1 - \widehat{\mathrm{T}}_0\right)\mathrm{Cos}\eta, \tag{4.8}$$

$$\rho\left(\frac{\partial \widehat{\mathrm{U}}_3}{\partial \hat{\mathrm{t}}} + \widehat{\mathrm{U}}_1\,\frac{\partial \widehat{\mathrm{U}}_3}{\partial \hat{\mathrm{R}}} + \widehat{\mathrm{U}}_3\,\frac{\partial \widehat{\mathrm{U}}_3}{\partial \hat{\mathrm{Z}}}\right) = -\frac{\partial \widehat{\mathrm{P}}}{\partial \hat{\mathrm{Z}}} + \frac{1}{\hat{\mathrm{R}}}\frac{\partial}{\partial \hat{\mathrm{R}}}\left(\hat{\mathrm{R}}\hat{\tau}_{\hat{\mathrm{R}}\hat{\mathrm{Z}}}\right) + \frac{\partial}{\partial \hat{\mathrm{Z}}}\left(\hat{\tau}_{\hat{\mathrm{Z}}\hat{\mathrm{Z}}}\right) + \rho\beta_0 \mathrm{g}\left(\widehat{\mathrm{T}}_1 - \widehat{\mathrm{T}}_0\right)\mathrm{Sin}\eta - \sigma B_0^2 \widehat{\mathrm{U}}_3 + \frac{\mu_0 \widehat{\mathrm{U}}_3}{\mathrm{k}}, \tag{4.9}$$

$$\rho \mathrm{c_P}\left(\frac{\partial \widehat{\mathrm{T}}}{\partial \hat{\mathrm{t}}} + \widehat{\mathrm{U}}_1\frac{\partial \widehat{\mathrm{T}}}{\partial \hat{\mathrm{R}}} + \widehat{\mathrm{U}}_3\frac{\partial \widehat{\mathrm{T}}}{\partial \hat{\mathrm{Z}}}\right) = \mathrm{K}\left(\frac{\partial \widehat{\mathrm{T}}}{\partial \hat{\mathrm{R}}^2} + \frac{1}{\hat{\mathrm{R}}}\frac{\partial \widehat{\mathrm{T}}}{\partial \hat{\mathrm{R}}} + \frac{\partial \widehat{\mathrm{T}}}{\partial \hat{\mathrm{Z}}^2}\right) + \mathrm{Q}_0\,, \tag{4.10}$$

The equation of the elastic passage is

$$\frac{\partial}{\partial \hat{z}}\left(\mathrm{E}\frac{\partial^4}{\partial \hat{\mathrm{Z}}^4} - \mathrm{F}\,\frac{\partial^2}{\partial \hat{\mathrm{Z}}^2} + \mathrm{G}\frac{\partial^2}{\partial \hat{\mathrm{t}}^2} + \mathrm{H}\,\frac{\partial^2}{\partial \hat{\mathrm{t}}} + \mathrm{I_L}\right)(\hat{\mathrm{r}}_2) = -\frac{\partial \widehat{\mathrm{P}}}{\partial \hat{\mathrm{Z}}} + \frac{1}{\hat{\mathrm{R}}}\frac{\partial}{\partial \hat{\mathrm{R}}}\left(\hat{\mathrm{R}}\hat{\tau}_{\hat{\mathrm{R}}\hat{\mathrm{Z}}}\right) + \frac{\partial}{\partial \hat{\mathrm{Z}}}\left(\hat{\tau}_{\hat{\mathrm{Z}}\hat{\mathrm{Z}}}\right)$$

$$+\ \rho\beta_0 \mathrm{g}\left(\widehat{\mathrm{T}}_1 - \widehat{\mathrm{T}}_0\right)\mathrm{Sin}\eta - \sigma\widehat{\mathrm{U}}_3 B_0^2 + \frac{\mu_0 \widehat{\mathrm{U}}_3}{\mathrm{K}},\ -\rho\left(\frac{\partial \widehat{\mathrm{U}}_3}{\partial \hat{\mathrm{t}}} + \widehat{\mathrm{U}}_1\,\frac{\partial \widehat{\mathrm{U}}_3}{\partial \hat{\mathrm{R}}} + \widehat{\mathrm{U}}_3\,\frac{\partial \widehat{\mathrm{U}}_3}{\partial \hat{\mathrm{Z}}}\right). \tag{4.11}$$

g is a gravitational acceleration, $\hat{T}_1$ is a fluid temperature , $\hat{T}_0$ refer to wall temperature, β_0 is a Thermal expansion coefficient, k refer to permeability, ρ is a fluid density, B_0^2 represents

applied magnetic field, specific heat is represented by c_p, K refer to thermal conductivity and heat source is represented by Q_0.

To convert the proposed model into a steady – state problem, the following transformations are used

$$\hat{r} = \hat{R}, \qquad \hat{z} = \hat{Z} - s\hat{t}, \qquad \hat{u}_1 = \hat{U}_1,$$

$$\hat{u}_3 = \hat{U}_3 - s, \qquad \hat{p} = \hat{P}(\hat{Z} - s\hat{t}, \hat{R}, \hat{t}). \tag{4.12}$$

The governing equations take the form as:

$$\frac{\partial \hat{u}_1}{\partial \hat{r}} + \frac{\hat{u}_1}{\hat{r}} + \frac{\partial \hat{u}_3}{\partial \hat{z}} = 0, \tag{4.13}$$

$$\rho\left(\hat{u}_1 \frac{\partial \hat{u}_1}{\partial \hat{r}} + \hat{u}_3 \frac{\partial u_1}{\partial \hat{z}}\right) = -\frac{\partial \hat{P}}{\partial \hat{r}} + \frac{1}{\hat{r}} \frac{\partial}{\partial \hat{r}}(\hat{r}\hat{\tau}_{\hat{r}\hat{r}}) + \frac{\partial}{\partial \hat{z}}(\hat{\tau}_{\hat{r}\hat{z}}) + \rho\beta_0 g(\hat{T}_1 - \hat{T}_0)\mathrm{Cos}\eta, \tag{4.14}$$

$$\rho\left(\hat{u}_1 \frac{\partial \hat{u}_3}{\partial \hat{r}} + \hat{u}_3 \frac{\partial \hat{u}_3}{\partial \hat{z}}\right) = -\frac{\partial \hat{P}}{\partial \hat{z}} \frac{1}{\hat{r}} \frac{\partial}{\partial \hat{r}}(\hat{r}\hat{\tau}_{\hat{r}\hat{z}}) \frac{\partial}{\partial \hat{z}}(\hat{\tau}_{\hat{z}\hat{z}}) + \rho\beta_0 g(\hat{T}_1 - \hat{T}_0)\,\mathrm{Sin}\eta - \sigma B_0^2(\hat{u}_3) - \frac{\mu_0(\hat{u}_3)}{k}, \tag{4.15}$$

$$\rho c_p\left(\hat{u}_1 \frac{\partial \hat{T}}{\partial \hat{r}} + \hat{u}_3 \frac{\partial \hat{T}}{\partial \hat{z}}\right) = K\left(\frac{\partial}{\partial \hat{r}}\left(\frac{\partial \hat{T}}{\partial \hat{r}}\right) + \frac{1}{\hat{r}}\frac{\partial \hat{T}}{\partial \hat{r}} + \frac{\partial \hat{T}}{\partial \hat{z}}\left(\frac{\partial \hat{T}}{\partial \hat{z}}\right)\right) + Q_0, \tag{4.16}$$

$$\left(E\frac{\partial^5}{\partial \hat{z}^5} - F\frac{\partial^3}{\partial \hat{z}^3} + G\frac{\partial^3}{\partial \hat{z}\,\partial \hat{t}^2} + H\frac{\partial^2}{\partial \hat{z}\,\partial \hat{t}} + I_L\frac{\partial}{\partial \hat{z}}\right)(\hat{r}_2) = \frac{1}{\hat{r}}\frac{\partial}{\partial \hat{r}}(\hat{r}\hat{\tau}_{\hat{r}\hat{z}}) + \frac{\partial}{\partial \hat{z}}(\hat{\tau}_{\hat{z}\hat{z}})$$

$$-\rho\beta g(\hat{T}_1 - \hat{T}_0)\,\mathrm{Sin}\eta - \sigma B_0^2(\hat{u}_3) - \frac{\mu_0(\hat{u}_3)}{K} - \rho\left(\hat{u}_1 \frac{\partial \hat{u}_3}{\partial \hat{r}} + \hat{u}_3 \frac{\partial \hat{u}_3}{\partial \hat{z}}\right). \tag{4.17}$$

And the components of the stress tensor are same in equation (3.30) - (3.33) in the chapter 03.

Following are the non-dimensional quantities used in the above system of equations.

$$u_1 = \frac{\hat{u}_1}{a_2 s}, \quad u_3 = \frac{\hat{u}_3}{s}, \quad r = \frac{\hat{r}}{a_2}, \quad z = \frac{\hat{z}}{l}, \quad t = \frac{s\hat{t}}{l}, \quad Pr = \frac{\mu_0 c_p}{K},$$

$$\tau = \frac{a_2\hat{\tau}}{s\mu_0}, \quad We = \frac{\Gamma s}{a_2}, \quad p = \frac{a^2{}_2\hat{P}}{sl\mu_0}, \quad \alpha = \frac{\hat{\alpha}a_2}{s}, \quad Re = \frac{\rho s a_2}{\mu_0}, \quad \delta = \frac{a_2}{l}$$

$$\varphi = \frac{b}{a_2}, \quad r_2 = h = \frac{\hat{r}_2}{a_2} = 1 + \varphi\sin(2\pi\hat{z}), \quad \tau = \frac{a_2^2\hat{P}}{s\mu_0}, \quad Da = \frac{k}{a_2}, \quad \theta = \frac{\hat{T} - \hat{T}_0}{\hat{T}_1 - \hat{T}_0},$$

$$M = \sqrt{\frac{\sigma}{\mu}}\,B_0\,a_2, \quad Gr = \frac{gp\beta_0 a_2^2(\hat{T}_1 - \hat{T}_0)}{s\mu_0}, \quad B = \frac{a^2 Q_0}{K(\hat{T}_1 - \hat{T}_0)}, \tag{4.18}$$

where u_1 is the dimensionaless radial velocity, u_3 is the dimensionaless axial velocity, r is the dimensionless radial coordinate, z is the dimensionless axial coordinate, t is the dimensionless time, τ is the dimensionless shear stress, φ is the amplitude ratio, δ is the dimensionless wave number, and We is the Weissenberg number, M is the Hartmann number, Gr is the Grashof Number, B is Biot number, θ is the dimensionless temperature, Re is the Reynolds number, Pr is prandtl number, α is the dimensionless shear rate, Da is the Darcy number.

By using these non-dimensional quantities in the equations (4.13) - (4.17) we get

$$\frac{\partial u_1}{\partial r} + \frac{u_1}{r} + \frac{\partial u_3}{\partial z} = 0, \tag{4.19}$$

$$Re\delta^3\left(u_1\frac{\partial u_1}{\partial r} + u_3\frac{\partial u_1}{\partial z}\right) = -\frac{\partial p}{\partial r} + \frac{1}{r}\frac{\partial}{\partial r}(r\tau_{rz}) + \delta\frac{\partial}{\partial z}(\tau_{zz}) + \delta Gr\theta Cos\eta, \tag{4.20}$$

$$Re\delta\left(u_1\frac{\partial u_3}{\partial r} + u_3\frac{\partial u_3}{\partial z}\right) = -\frac{\partial p}{\partial z} + \frac{1}{r}\frac{\partial}{\partial r}(r\tau_{rz}) + \delta\frac{\partial}{\partial z}(\tau_{zz}) + Gr\theta Sin\eta - \left(M^2 + \frac{1}{Da}\right)u_3, \tag{4.21}$$

$$RePr\delta\left(u_1\frac{\partial\theta}{\partial r} + u_3\frac{\partial\theta}{\partial z}\right) = \frac{1}{r}\frac{\partial\theta}{\partial r} + \frac{\partial^2\theta}{\partial r^2} + \delta^2\frac{\partial^2\theta}{\partial z^2} + B. \tag{4.22}$$

The equation of motion governing the elastic wall is

$$\left(\left(\frac{Ea_2^3}{\mu_0 sl^5}\right)\frac{\partial^5 r_2}{\partial z^5} - \left(\frac{Fa_2^3}{\mu_0 sl^3}\right)\frac{\partial^3 r_2}{\partial z^3} + \left(\frac{Gsa_2^3}{\mu_0 l^3}\right)\frac{\partial^3 r_2}{\partial z\,\partial t^2} + \left(\frac{Hsa_2^3}{\mu_0 l^2}\right)\frac{\partial^2 r_2}{\partial z\,\partial t} + \left(\frac{I_L a_2^3}{\mu_0 sl}\right)\frac{\partial r_2}{\partial z}\right) = \frac{1}{r}\frac{\partial}{\partial r}(r\tau_{rz}) + \delta\frac{\partial}{\partial z}(\tau_{zz}) + Gr\theta Sin\eta - \left(M^2 + \frac{1}{Da}\right) - Re\delta\left(u_1\frac{\partial u_1}{\partial r} + u_3\frac{\partial u_3}{\partial z}\right), \tag{4.23}$$

and the dimensionless boundary conditions are

$$\frac{\partial u_3}{\partial r} = 0, \qquad \frac{\partial\theta}{\partial r} = 0, \qquad \text{at} \qquad r = 0,$$

$$u_3 + \beta\tau_{rz} = -1, \qquad \frac{\partial\theta}{\partial r} = 0, \qquad \text{at} \qquad r = h. \tag{4.24}$$

We assume an extremely small wavenumber because it is exceedingly difficult to solve the problem in the latter form ($\delta \ll 1$), hence equations (4.19- 4.23) become

$$\frac{\partial p}{\partial r} = 0, \tag{4.25}$$

$$\frac{\partial p}{\partial z} = \frac{1}{r}\frac{\partial}{\partial r}(r\tau_{rz}) + Gr\theta Sin\eta - \left(M^2 + \frac{1}{Da}\right)u_3, \tag{4.26}$$

$$\frac{1}{r}\frac{\partial \theta}{\partial r} + \frac{\partial^2 \theta}{\partial r^2} + B = 0, \tag{4.27}$$

$$\left(L_1\frac{\partial^5 r_2}{\partial z^5} - L_2\frac{\partial^3 r_2}{\partial z^3} + L_3\frac{\partial^3 r_2}{\partial z\,\partial t^2} + L_4\frac{\partial^2 r_2}{\partial z\,\partial t} + L_5\frac{\partial r_2}{\partial z}\right) = \frac{1}{r}\frac{\partial}{\partial r}(r\tau_{rz}) + Gr\theta Sin\eta - \left(M^2 + \frac{1}{Da}\right)u_3. \tag{4.28}$$

where

$$L_1 = \frac{Ea_2^3}{\mu s l^5},\ L_2 = -\frac{Fa_2^3}{\mu s l^3},\ L_3 = \frac{Ga_2^3}{\mu l^3},\ L_4 = \frac{Ha_2^3}{\mu l^3},\ L_5 = \frac{I_l a_2^3}{\mu s l}, \tag{4.29}$$

$L_1$is flexural stiffness of the wall, L_2 is a longitudinal tension unit, L_3 is mass per unit area, L_4 is a coefficient of viscous damping and L_5 is spring stiffness.

The components of extra stress are

$$\tau_{rr} = \tau_{zz} = 0 \quad \text{and} \quad \tau_{rz} = \left(\frac{\partial u_3}{\partial r} + We\left(\frac{\partial u_3}{\partial r}\right)^2\right). \tag{4.30}$$

Replacing τ_{rz} into equation (4.28) we have:

$$r\frac{\partial^2 u_3}{\partial r^2} + \frac{\partial u_3}{\partial r} + We\left(\frac{\partial u_3}{\partial r}\right)^2 + 2rWe\left(\frac{\partial u_3}{\partial r}\right)\left(\frac{\partial^2 u_3}{\partial r^2}\right) - \left(M^2 + \frac{1}{Da}\right)u_3 = -Gr\theta Sin\eta + r\widetilde{K}, \tag{4.31}$$

where

$$\widetilde{K} = L_1\frac{\partial^5 r_2}{\partial z^5} - L_2\frac{\partial^3 r_2}{\partial z^3} + L_3\frac{\partial^3 r_2}{\partial z\,\partial t^2} + L_4\frac{\partial^2 r_2}{\partial z\,\partial t} + L_5\frac{\partial r_2}{\partial z}. \tag{4.32}$$

4.3 Solution Methodology

Equation (4.32) is difficult to solve analytically, therefore, to obtain the solution, we employ the regular perturbation strategy in terms of a second-order form of the Weissenberg number. To solve the perturbation problem, it has been expanded as follows:

$$u_3 = u_{03} + We\, u_{13} + We^2 u_{23} + O(We^3). \tag{4.33}$$

4.3.1 Zero order System

$$r\frac{\partial^2 u_{03}}{\partial r^2} + \frac{\partial u_{03}}{\partial r} = -\left(M^2 + \frac{1}{Da}\right) u_{03} - Gr\theta Sin\eta + r\widetilde{K}, \tag{4.34}$$

with boundary conditions as:

$$\frac{\partial u_{03}}{\partial r} = 0, \quad at \quad r = 0, \quad and \quad u_{03} + \beta\frac{\partial u_{03}}{\partial r} = -1, \quad at \quad r = h. \tag{4.35}$$

4.3.2 First order System

$$r\frac{\partial^2 u_{13}}{\partial r^2} + \frac{\partial u_{13}}{\partial r} = -2r\left(\frac{\partial^2 u_{03}}{\partial r^2}\right)\left(\frac{\partial u_{03}}{\partial r}\right) - \left(\frac{\partial u_{03}}{\partial r}\right)^2 - \left(M^2 + \frac{1}{Da}\right) u_{13}, \tag{4.36}$$

with boundary conditions as

$$\frac{\partial u_{13}}{\partial r} = 0, \quad at \quad r = 0, \quad and \quad u_{13} + \beta\frac{\partial u_{13}}{\partial r} = 0, \quad at \quad r = h. \tag{4.37}$$

4.4 Result and Discussion

The behavior of the parameters used in the temperature (θ), axial velocity (u), and streamline expressions is discussed. Specifically the effects of the magnetic parameter (M), porosity parameter (Da), slip parameter (β), Grashof number (Gr), Biot number (B) , Weissenberg number (We) , and wall properties are examined. To analyze their influence, graphs were generated using the MATHEMATICA software.

The first figure presents streamline patterns of Williamson fluid under the action of a magnetic field for different values of the magnetic parameter M. In Fig. 4.2 (a) when M = 0.1 the streamlines show a relatively larger bolus (trapped fluid region) near the channel center. At this stage, the magnetic resistance is weak, which allows the recirculation zone to expand and fluid particles to move more freely. In Fig. 4.2 (b) when M = 1, the bolus size decreases slightly and streamlines compress near the channel walls due to the Lorentz force, which resists fluid motion and reduces recirculation. In Fig. 4.2 (c) for M = 1.5 the bolus becomes even smaller, and streamlines shift closer to the axis. The stronger magnetic field further suppresses circulation, reducing trapped zones and restricting secondary flows.

Fig. 4.3 (a − c) illustrates the effect of the porosity parameter Da. In Fig. 4.3 (a) when Da = 0.1, the bolus is relatively small due to low porosity, which offers greater resistance to flow and limits fluid entrapment. In Fig. 4.3 (b) when Da = 1 the bolus size increases as porosity improves, allowing more fluid to be trapped and carried along by the peristaltic wave. In Fig. 4.3 (c) for Da = 1.5 the bolus becomes largest confirming that higher porosity reduces resistance and enhances fluid trapping.

Fig. 4.4 (a − c) show streamlines for different values of L_1. The closed loops represent trapped boluses that move with the peristaltic wave. In Fig. 4.4 (a) for L_1= 0.1 the bolus is small, indicating minimal trapping. When L_1 = 0.2 in Fig. 4.4 (b) the bolus size increases, and more fluid is trapped in the channel center. In Fig. 4.4(c) for L_1 = 0.3 the bolus reaches its maximum size, confirming that increasing L_1enhances fluid trapping. Fig. 4.5 (a − c) demonstrates the effect of on L_2 peristaltic flow. In Fig. 4.5 (a) for L_2= 0.1 the bolus is relatively small. As L_2 increases to 0.2 in Fig. 4.5 (b) the bolus expands significantly. At L_2 = 0.3 in Fig. 4.5 (c) the

trapped bolus is largest, showing that higher L_2 enhance fluid entrapment. Fig. 4.6 (a – c) show the effect of L_3. In Fig. 4.6 (a) when L_3 = 0.1 the trapped bolus is small. As L_3 increases to 0.2 in Fig. 4.6(b) the bolus expands, trapping more fluid. In Fig. 4.6 (c) at L_3= 0.3 the bolus reaches its largest size, indicating that higher L_3values increase fluid trapping.

Fig. 4.7 (a – c) shows the effect of L_4. In Fig. 4.7 (a) when L_4= 0.1 the bolus is relatively small. In Fig. 4.7 (b) when L_4= 0.2 the bolus size reduces noticeably, unlike the previous parameters. In Fig. 4.7 (c) at L_4= 0.3 the bolus is smallest. This indicates that L_4 acts differently representing resistance or damping which reduces fluid trapping. Fig. 4.8 (a – c) show the influence of L_5. In Fig. 4.8 (a) at L_4 = 0.1 the bolus is small. In Fig. 4.8 (b) for L_5 = 0.2 the bolus grows larger. In Fig. 4.8 (c) at L_5 = 0.3 the bolus is largest. This confirms that increasing L_5 enhances fluid trapping. Fig. 4.9 (a – c) presents the impact of the slip parameter β. In Fig. 4.9 (a) when β = 0.1 the bolus is smallest. Increasing β to 0.3 in Fig. 4.9 (b) reduces the bolus size. At β = 0.5 in Fig. 4.9 (c) the trapped bolus is largest, indicating that slip enhance trapping efficiency by stronger peristaltic pumping.

Fig. 4.10 displays velocity profiles for different slip parameter values. For $\beta = 0$ (solid line), the classic parabolic profile appears, with maximum velocity at $r = 0$ and zero velocity at the walls. When β = 0.02 (dashed line), velocity at the walls is non-zero, and the overall velocity increases. For β = 0.04 (dotted line), the velocity further increases, and wall slip becomes stronger.

Fig. 4.11 shows the effect of the Weissenberg number We. At We = 0 (solid line), the velocity profile is parabolic, characteristic of Newtonian fluids. At We = 0.02 (dashed line), velocity decreases across the channel and the profile flattens. At We = 0.04 (dotted line), the velocity reduces further, with the lowest peak at the center, showing stronger viscoelastic effects.

Fig. 4.12 shows velocity profiles for different magnetic parameter values. At M = 0.1 (solid line), velocity is maximum with a classic parabolic shape. At M = 2 (dashed line), velocity decreases due to Lorentz force. At M = 4 (dotted line), velocity reduces further, with the flattest profile, as magnetic resistance is strongest. Fig. 4.13 illustrates velocity profiles for different Darcy numbers Da. At Da = 0.1 (solid line), velocity is highest with a parabolic profile. At Da = 0.2 (dashed line), velocity decreases due to porous resistance. At Da = 0.4 (dotted line),

velocity reduces further, showing the strongest damping effect. Fig. 4.14 shows velocity profiles for various Grashof numbers Gr. At Gr = 0.1 (solid line), velocity is lowest. Increasing Gr to 0.3 (dashed line) raises velocity across the channel. At Gr = 0.5 (dotted line), velocity is highest, confirming that buoyancy effects enhance flow strength.

Fig. 4.15 the variation of velocity distribution with respect to different values of the parameter B is displayed in the figure. The horizontal axis represents the radial position r, while the vertical axis corresponds to the velocity component. For all cases, the velocity profile retains a parabolic nature, reaching its maximum at the channel centerline (r = 0) and gradually decreasing towards the walls (r = ±1), where it approaches zero due to the no-slip condition. The effect of parameter B is clearly visible: when B = 1 the velocity attains the highest peak, signifying faster fluid motion. Increasing B to 5 reduces the peak velocity, and a further increase to B = 10 produces a much flatter curve with a significantly lower magnitude of velocity. These observations indicate that larger values of B enhance the resistive influence on the flow, thereby suppressing the velocity throughout the domain, while smaller values of B allow the fluid to accelerate more freely.

Fig.4.16 demonstrates the influence of wall properties L_1, L_2, L_3, L_4, L_5 on velocity distribution. As wall property values increase, the velocity at the centerline decreases, and overall flow reduces due to enhanced wall rigidity and resistance. Fig. 4.17 presents temperature profiles for different Biot number values. At $B = 0.01$ (solid line), temperature is lowest, with nearly uniform distribution across the channel, indicating dominant conduction. At $B = 0.02$ (dashed line), temperature increases and becomes more parabolic. At $B = 0.03$ (dotted line), temperature is highest across all radial positions, showing stronger convective heat transfer at the boundaries.

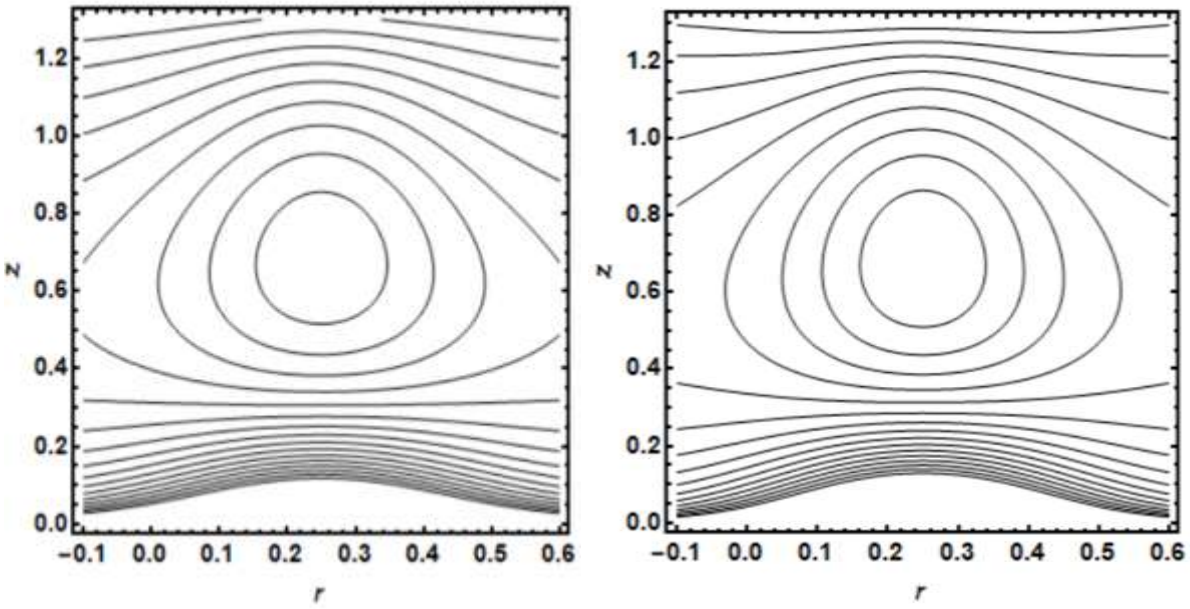

(a) M = 0.1 (b) M = 1

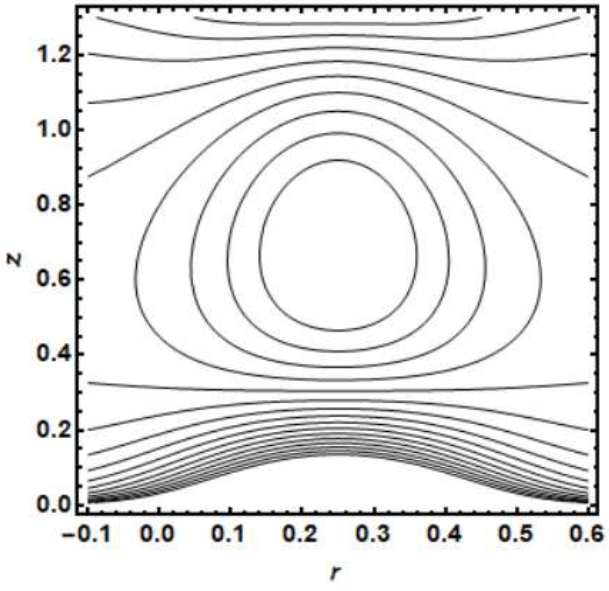

(c) M = 1.5

Fig. 4.2 Streamlines for the diverse values of magnetic parameter.

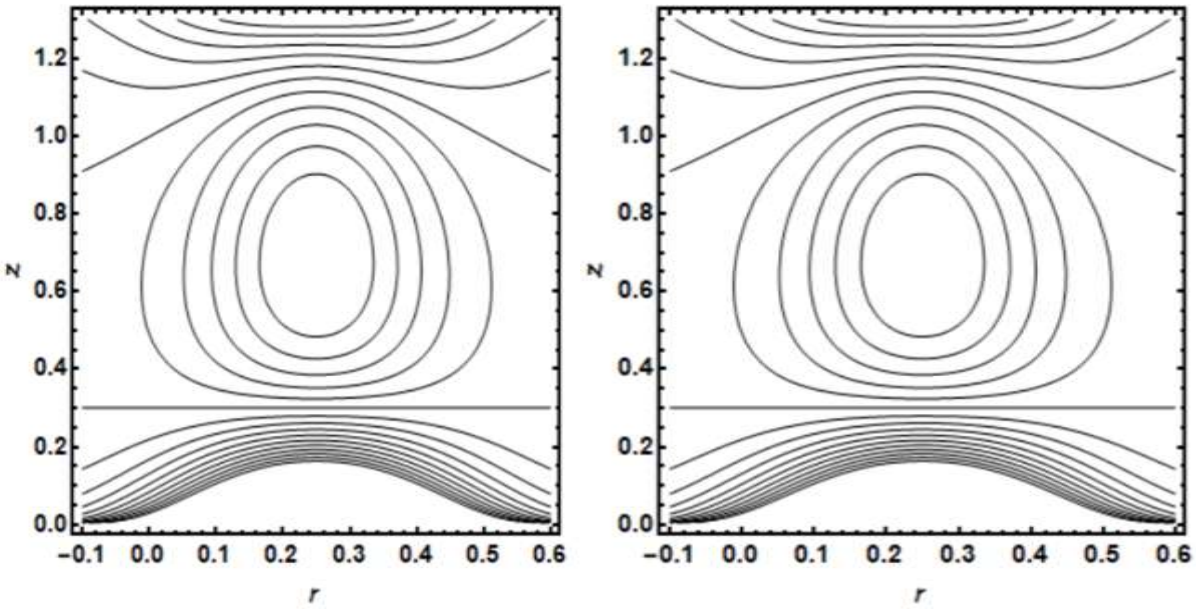

(a) Da = 0.1 (b) Da = 1

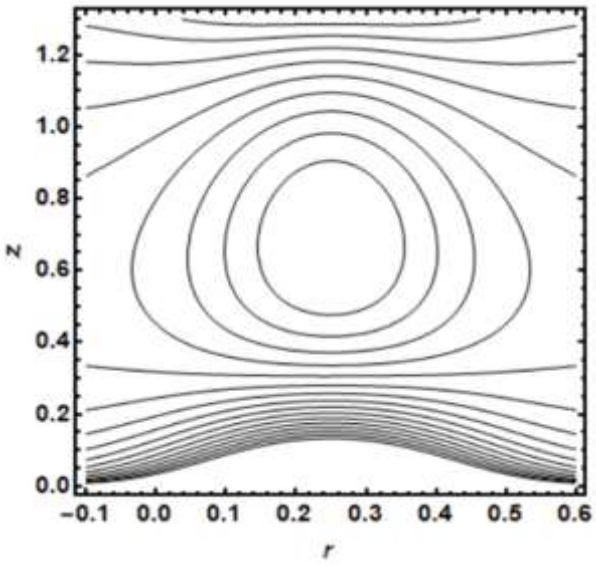

(c) Da = 1.5

Fig. 4.3 Streamlines for the diverse values of porosity parameter.

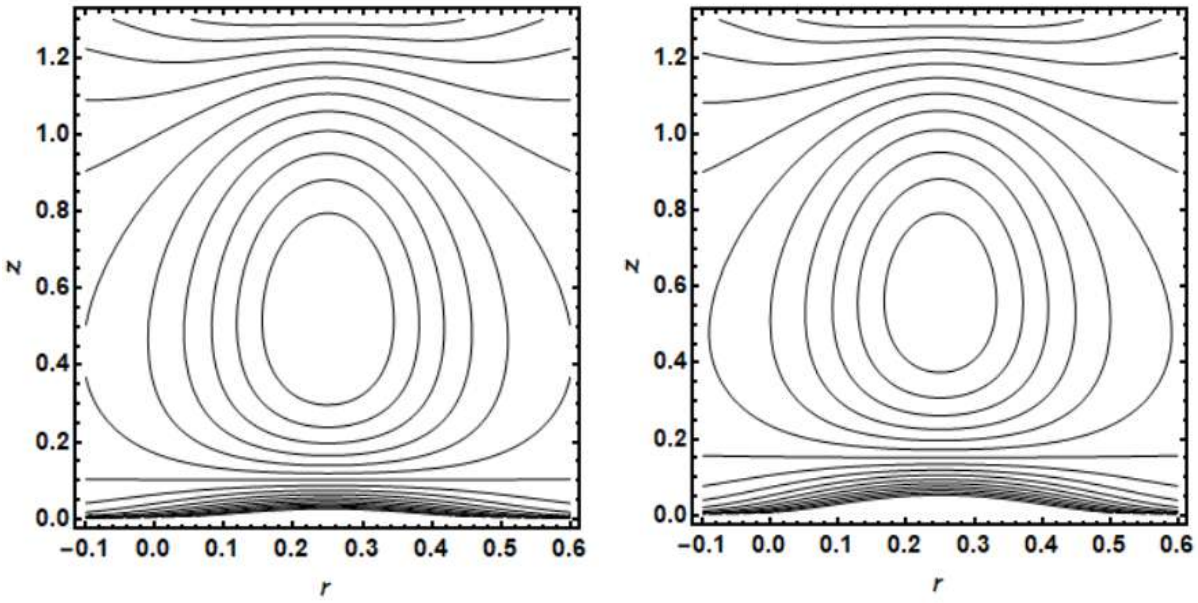

(a) $L_1 = 0.1$ (b) $L_1 = 0.2$

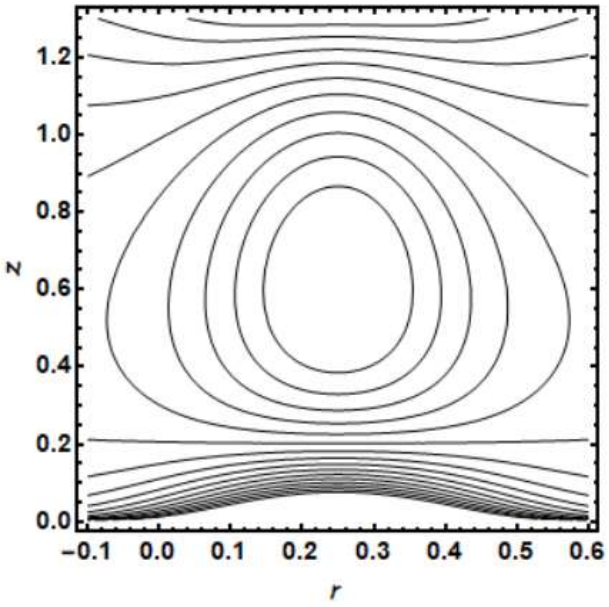

(c) $L_1 = 0.3$

Fig. 4.4 Streamlines for the diverse value of flexural stiffness of wall (L_1).

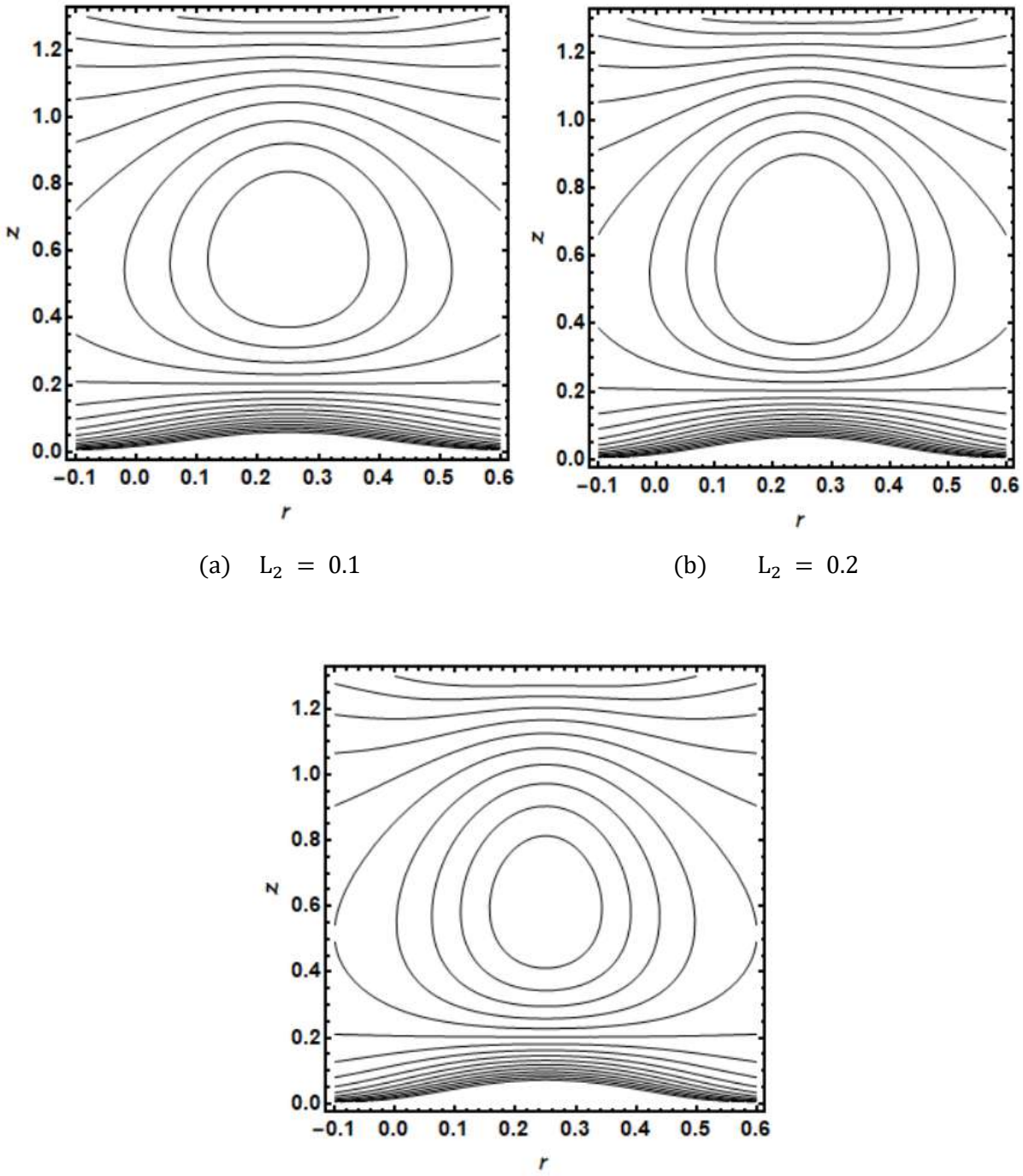

(a) $L_2 = 0.1$ (b) $L_2 = 0.2$

(c) $L_2 = 0.3$

Fig. 4.5 Streamlines for the diverse of longitudinal tension per unit width (L_2).

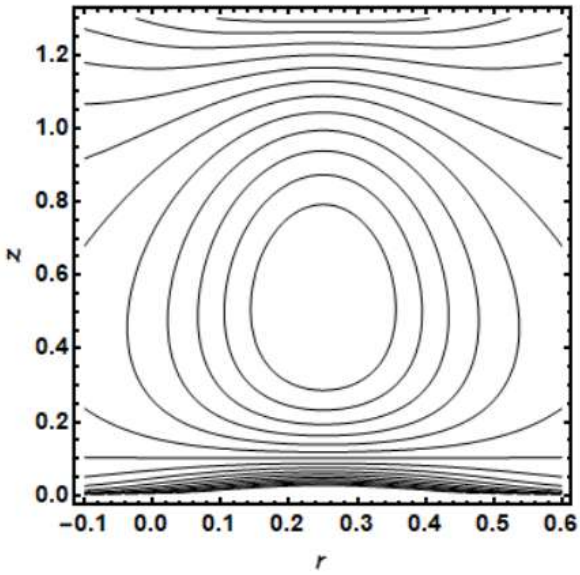

(a) $L_3 = 0.1$

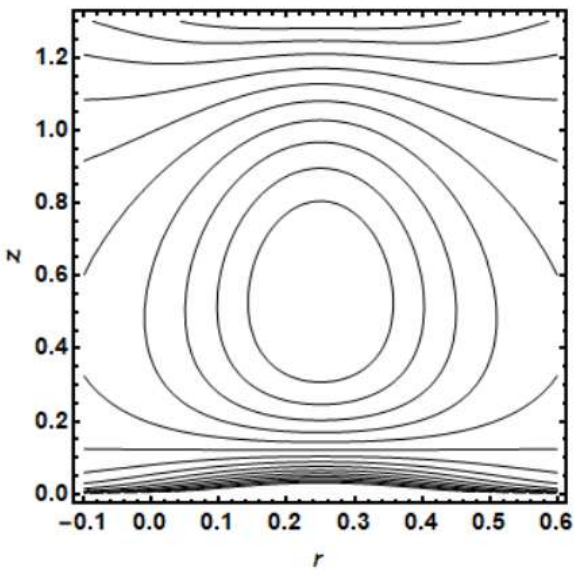

(b) $L_3 = 0.2$

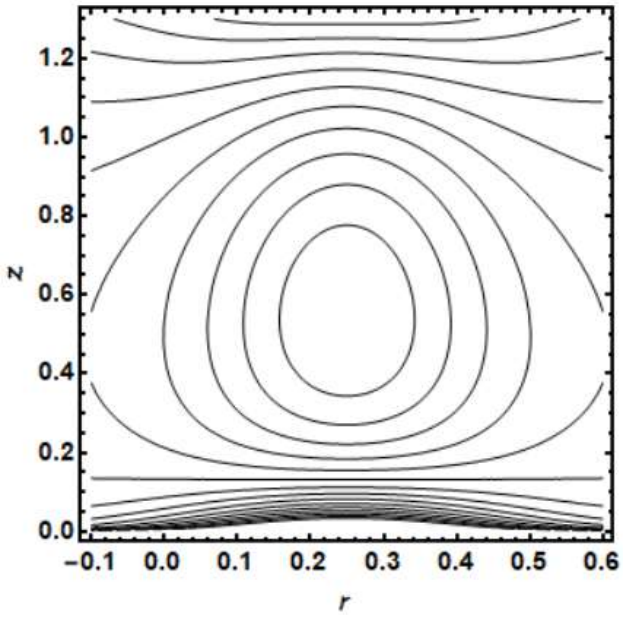

(c) $L_3 = 0.3$

Fig. 4.6 Streamlines for diverse of Mass per unit area (L_3).

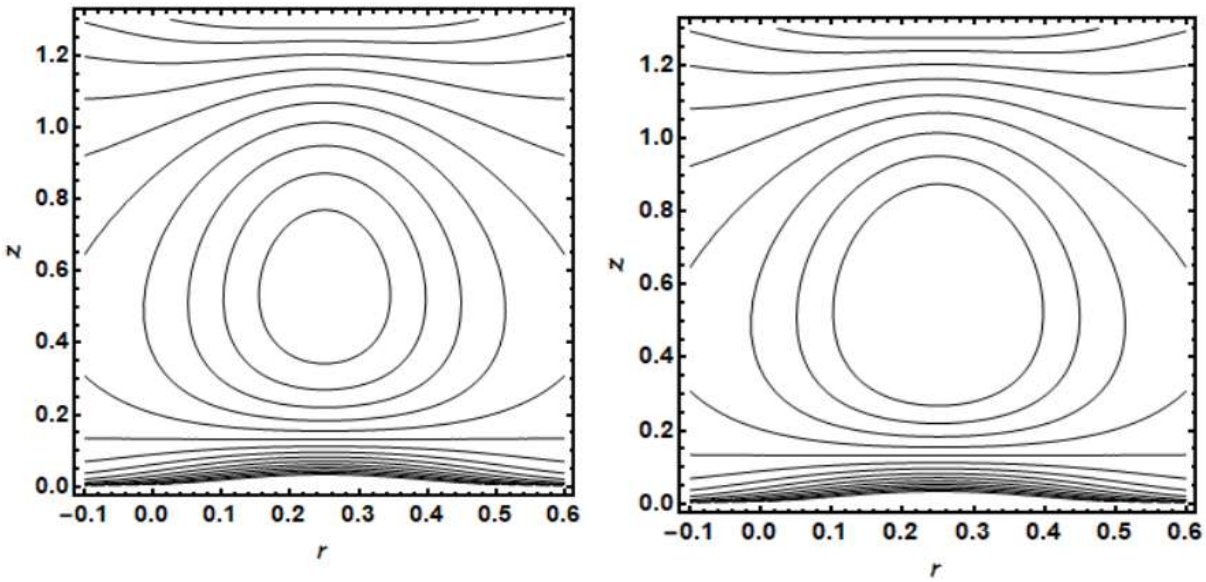

(a) $L_4 = 0.1$ (b) $L_4 = 0.2$

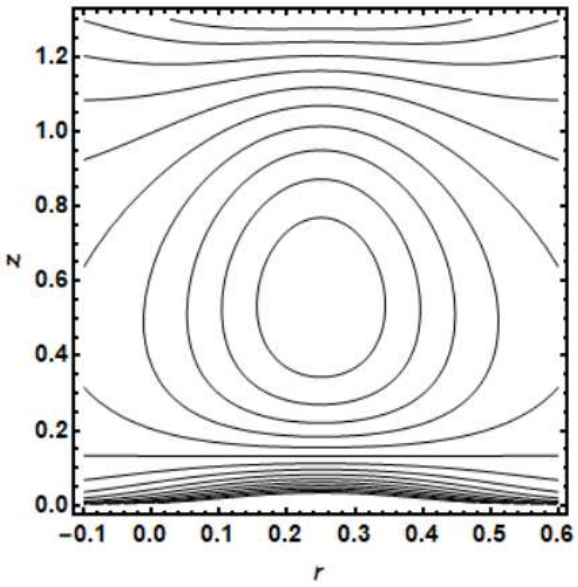

(c) $L_4 = 0.3$

Fig. 4.7 Streamlines for the diverse of coefficient of viscid damping (L_4).

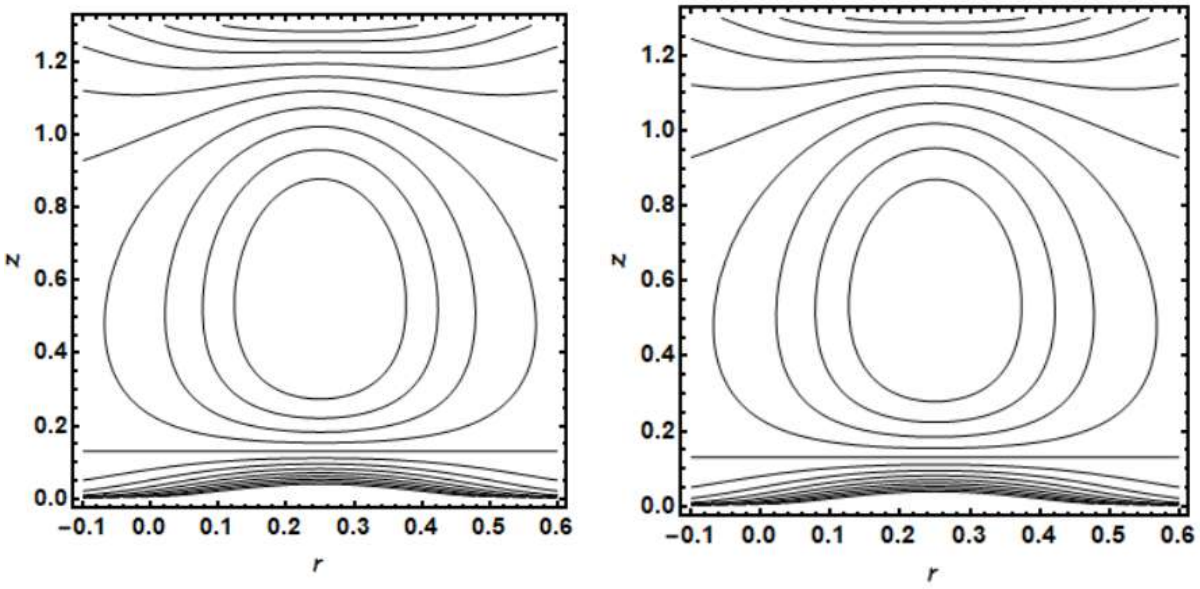

(a) $L_5 = 0.1$ (b) $L_5 = 0.2$

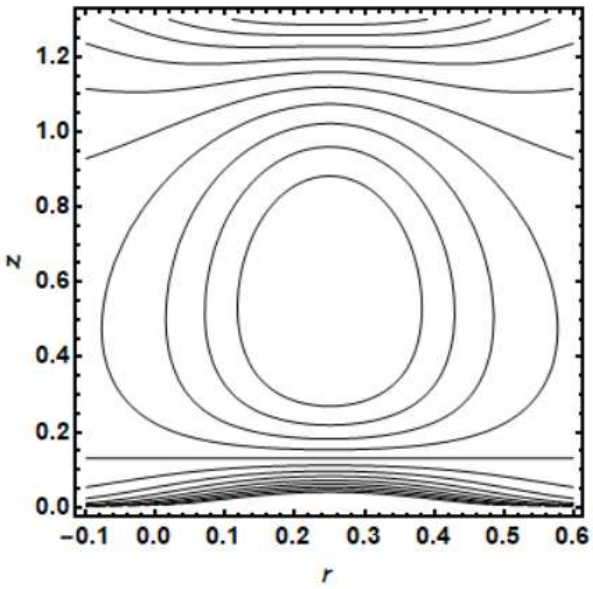

(c) $L_5 = 0.3$

Fig. 4.8 Streamlines for the diverse of Spring stiffness (L_5).

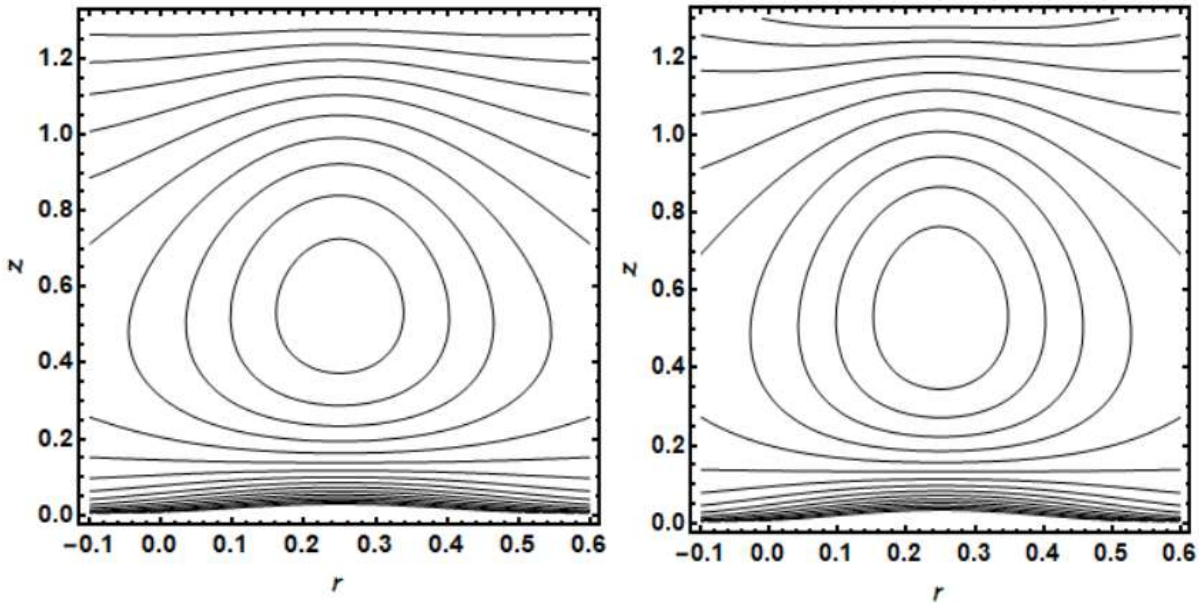

(a) Slip (β) = 0.1

(b) Slip (β) = 0.3

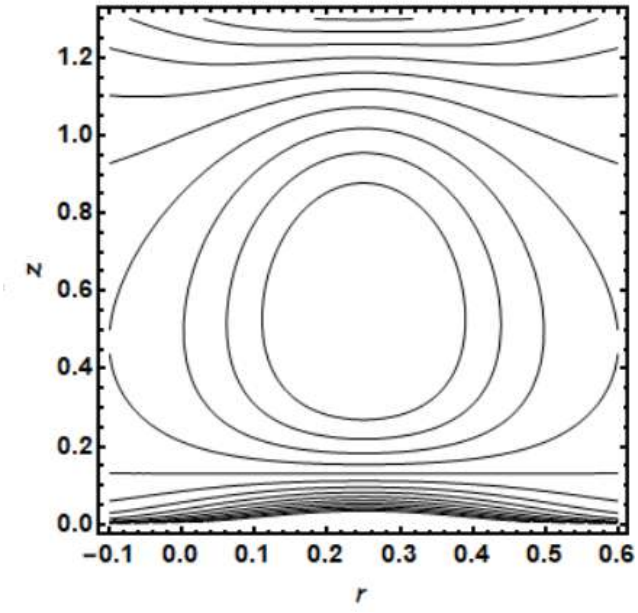

(c) Slip (β) = 0.5

Fig. 4.9 Streamlines for the diverse values of slip parameter.

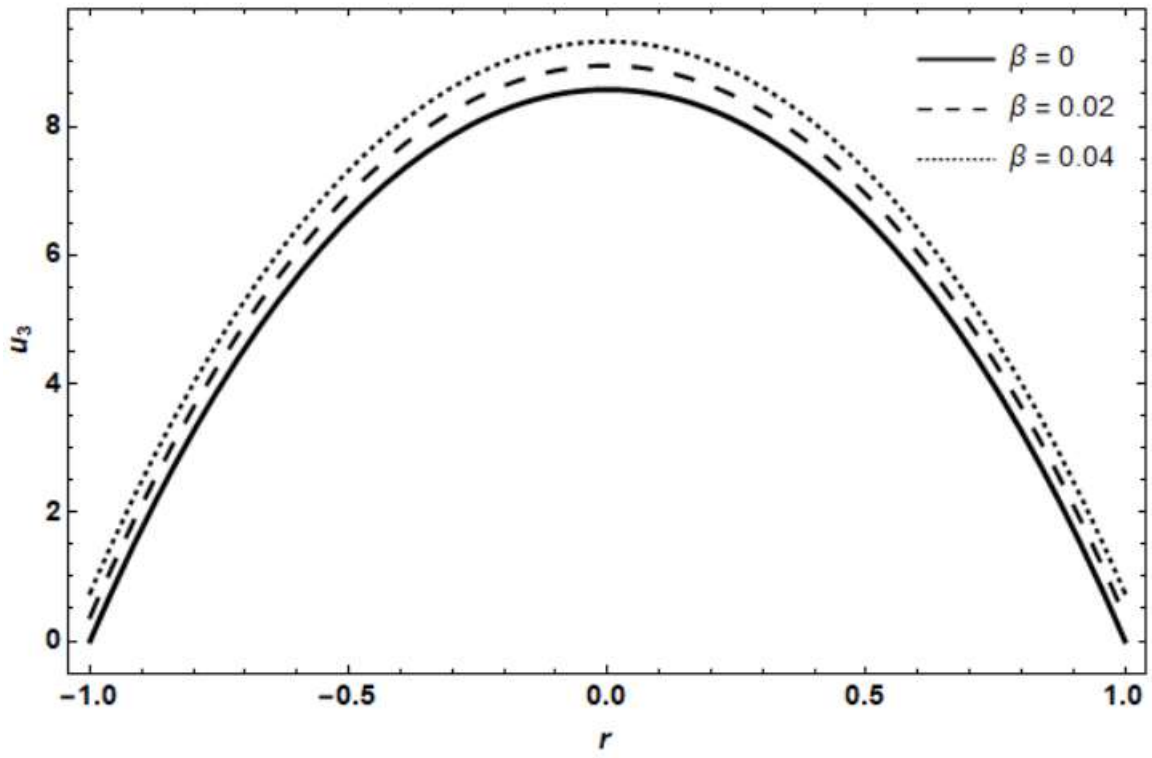

Fig. 4.10 Velocity distribution for the diverse values of slip parameter.

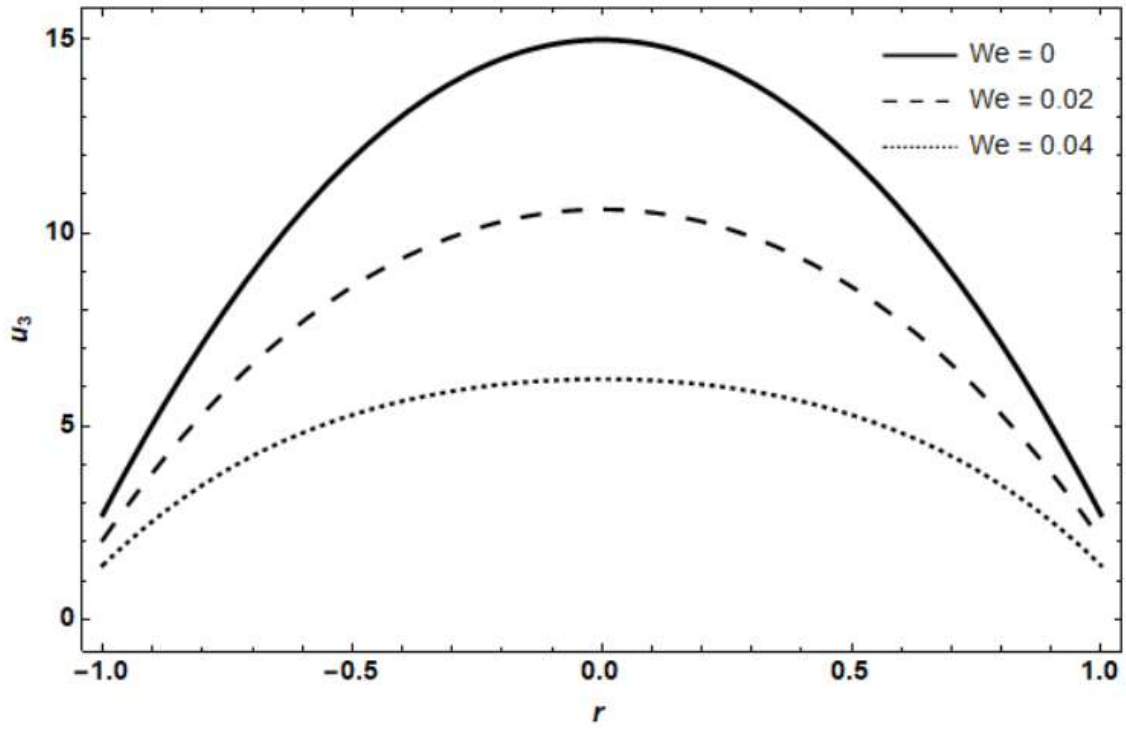

Fig. 4.11 Velocity distribution for the diverse values of Weissenberg number.

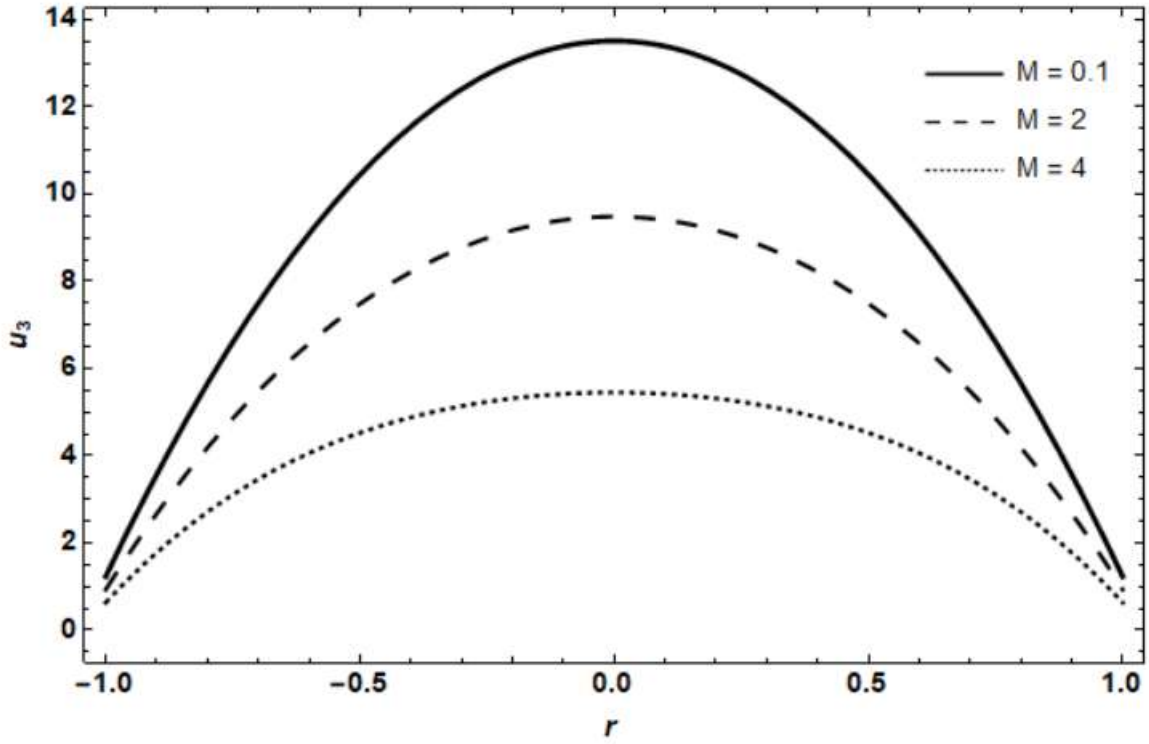

Fig. 4.12 Velocity distribution for the diverse values of magnetic parameter.

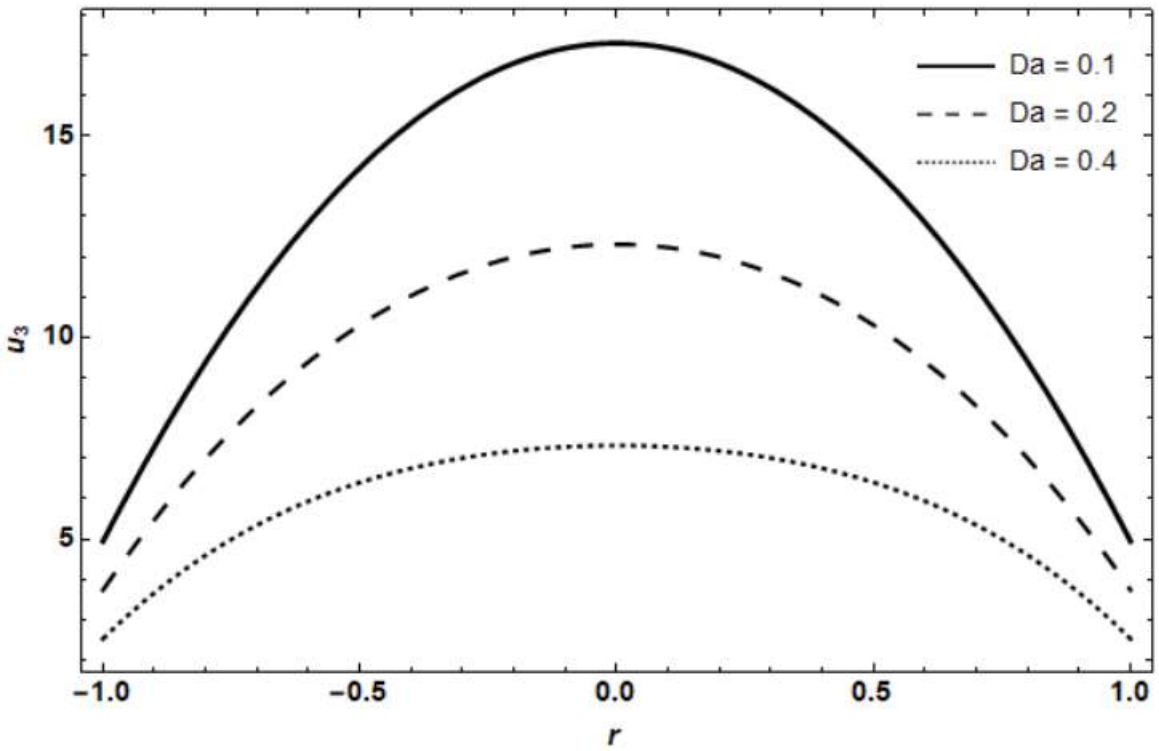

Fig. 4.13 Velocity distribution for the diverse values of porosity parameter.

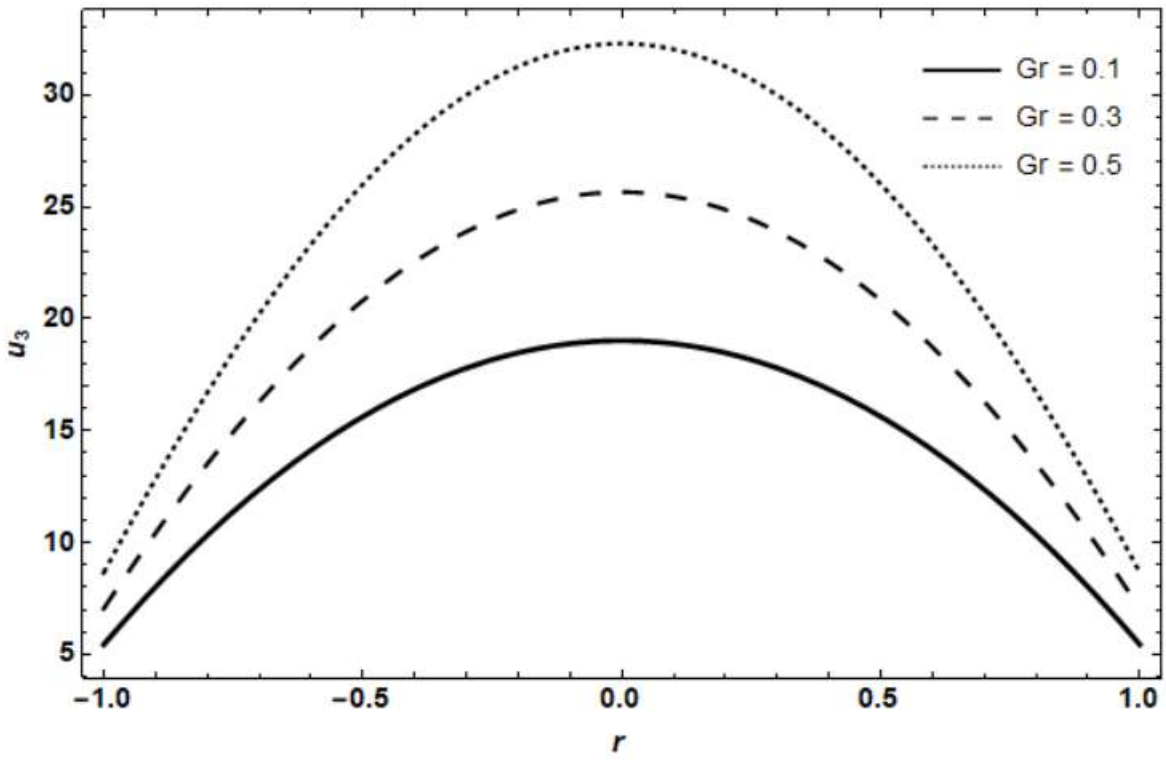

Fig. 4.14 Velocity distribution for the diverse values of Grashof number.

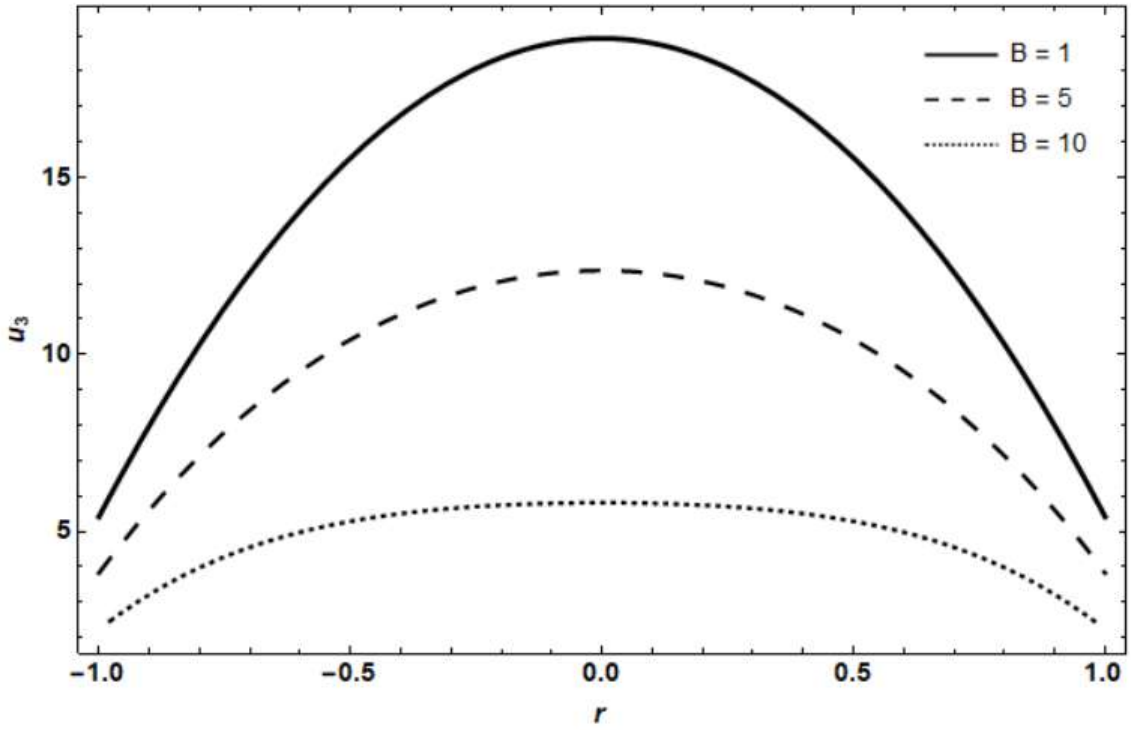

Fig. 4.15 Velocity distribution for the diverse values of Biot number.

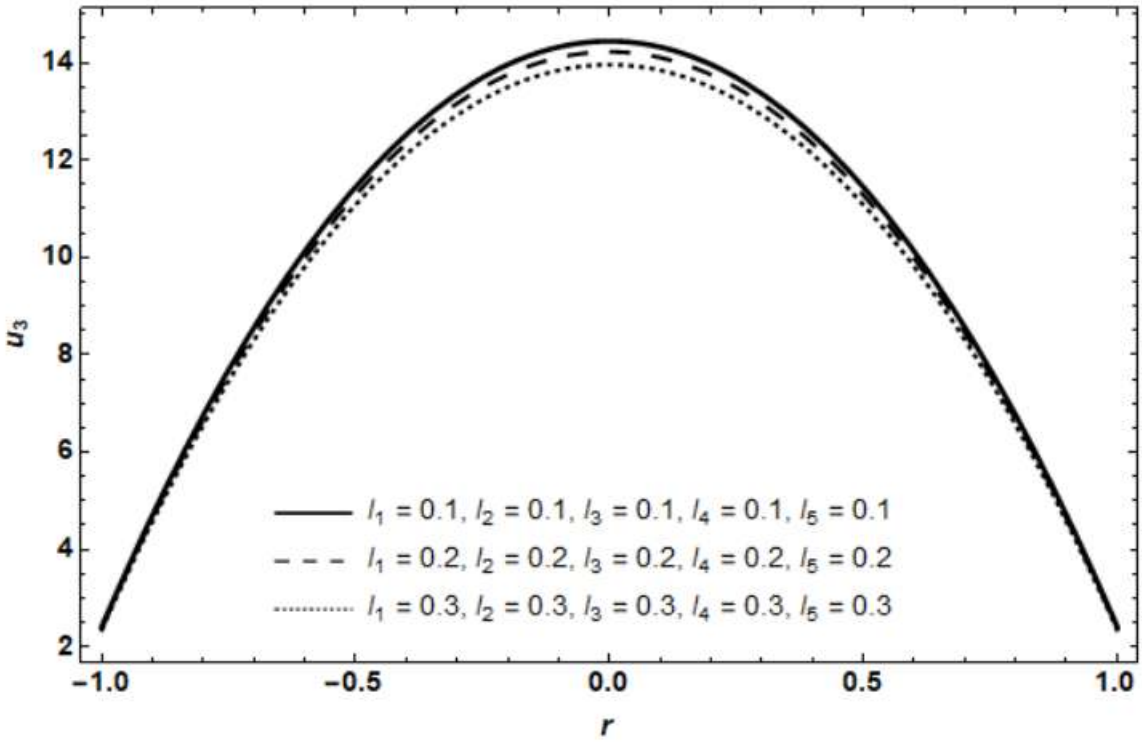

Fig. 4.16 Velocity distribution for the diverse values of wall properties.

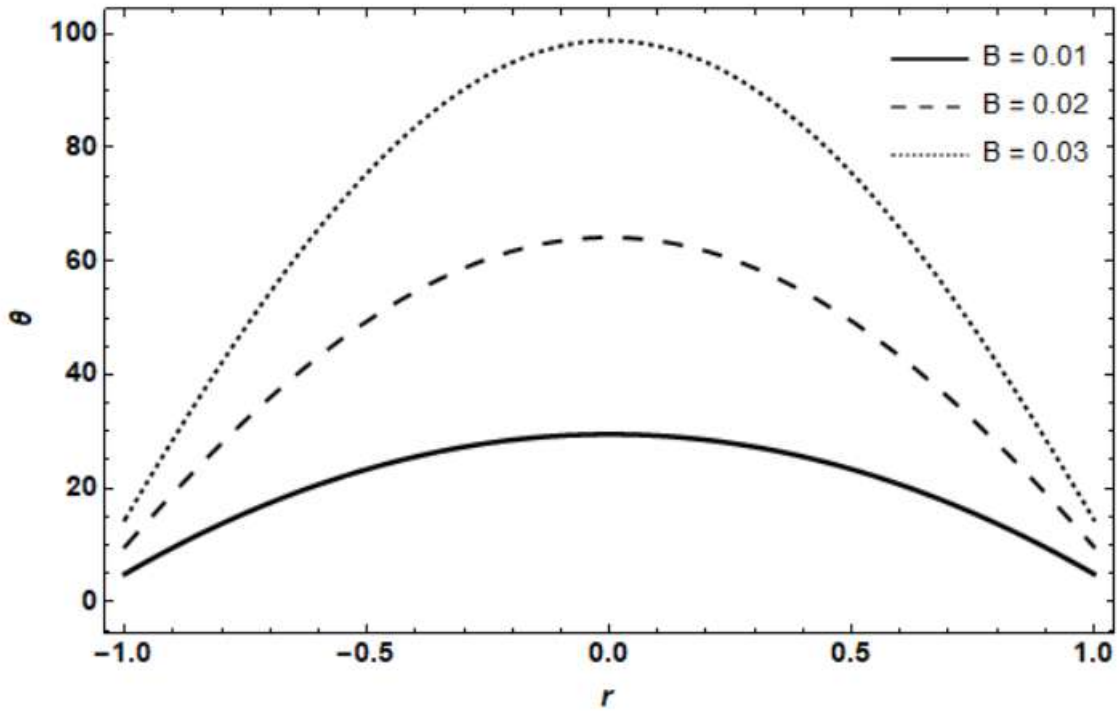

Fig. 4.17 Temperature distribution for the diverse values of Biot number.

CHAPTER 5
CONCLUSION AND FUTURE WORK

5.1 Conclusion

This thesis has examined the peristaltic flow of a non-Newtonian Williamson fluid, revealing a complex interdependence between porosity, magnetic effects, slip conditions, and the fluid's overall dynamics. Streamline analysis has proven particularly effective in illustrating the influence of these parameters on the trapped bolus a pocket of fluid carried by the peristaltic wave. The complexity of the governing equations has been addressed through lubrication approach and the perturbation techniques Furthermore, graphical representations of streamline patterns, velocity function and temperature profile, generated using Mathematica, provided meaningful insights into the flow characteristics under varying conditions.

The notable conclusions drawn this research are that the velocity of the Williamson fluid declined as the magnetic parameter enhanced. This shows that the increase in the Lorentz force created resistance in the fluid flow thus causing a significant decline in the velocity. The increase in Grashof Number (Gr) means the growing dominance of inertial over the viscous forces, which in turn increases the fluid's velocity. The surge in Weissenberg Number (We) shows that non-Newtonian effects are intensifying, thus decline in the fluid's velocity is observed as this number is elevated. Porosity parameter (Da) indicates that the void spaces in the medium are increasing. As these void spaces increase, fluid experiences interruption to flow freely through the channel, thus reduce in the velocity can be seen in the graphical representation. For the diverse wall properties like stiffness, damping, rigidity etc. It can be seen that the surge in these parameters causes declines in the fluid's velocity.

Impact of the slip parameter refers to the situation where the fluid slides along the channel's walls. The resistance near the wall declines allowing fluid to flow past the channel easily. Biot number is a non-dimensional number that helps to investigate if the temperature gradient inside the fluid is substantial or not. Velocity descended as Biot number was enhanced thus causing the convection process accelerate in the passage, this results elevation in the temperature profile as depicted in the graph.

5.2 Future Work

The model studied in this dissertation includes MHD, porosity and slip effects along with heat transfer. However, this model has potential to be extended for the future researches as well by including thermal effects and mass transfer.

- Investigating various fluid models, such as the Carreau and Walter's B fluid models, as well as non-Newtonian fluid models, could be part of this.
- As our current study focused on the effect of elastic passage properties, slip boundary conditions in a tube, the same model can be studied in an endoscope as well.
- Furthermore, adding boundary conditions like thermal slip and convective boundary conditions may help future researchers understand how peristaltic flow behaves in real-world situations.

References

Abbas, Z., Irshad, S., & Rafiq, M. (2023). Study of peristaltic activity in non-linear blood analysis of Williamson fluid in a microchannel. Waves in Random and Complex Media, 1-24.

Abd-Alla, A., Abbas, I. A., Abo-Dhab, S., Elmhedy, Y., Sapoor, H., & Abdelhafez, M. (2025). Effect of magnetic field and heat transfer on peristaltic flow of a micropolar fluid through a porous medium. Waves in Random and Complex Media, 35(2), 4070-4081.

Afifi, N., & Gad, N. (2001). Interaction of peristaltic flow with pulsatile magneto-fluid through a porous medium. Acta Mechanica, 149(1), 229-237.

Ajithkumar, M., Kuharat, S., Bég, O. A., Sucharitha, G., & Lakshminarayana, P. (2024). Catalytic effects on peristaltic flow of Jeffrey fluid through a flexible porous duct under oblique magnetic field: Application in biomimetic pumps for hazardous materials. Thermal Science and Engineering Progress, 49, 102476.

Akbar, N. S., Hayat, T., Nadeem, S., & Obaidat, S. (2012). Peristaltic flow of a Williamson fluid in an inclined asymmetric channel with partial slip and heat transfer. International Journal of Heat and Mass Transfer, 55(7-8), 1855-1862.

Akbar, N. S., & Nadeem, S. (2012). Characteristics of heating scheme and mass transfer on the peristaltic flow for an Eyring–Powell fluid in an endoscope. International Journal of Heat and Mass Transfer, 55(1-3), 375-383.

Akram, S., Razia, A., & Afzal, F. (2020). Effects of velocity second slip model and induced magnetic field on peristaltic transport of non-Newtonian fluid in the presence of double-diffusivity convection in nanofluids. Archive of Applied Mechanics, 90(7), 1583-1603.

Al-Khafajy, D., & Al-Delfi, W. N. (2023). The peristaltic flow of Williamson fluid through a flexible channel. Iraqi Journal of Science, 865-877.

Al-Khafajy, D. G. S., & Majeed Mashhadi, R. R. (2023). The peristaltic flow for Carreau fluid through an elastic channel. Journal of the Mechanical Behavior of Materials, 32(1), 20220257.

Alharbi, K. A. M., Adnan, A., Eldin, S. M., & Akgul, A. (2023). Investigation of Williamson nanofluid in a convectively heated peristaltic channel and magnetic field via method of moments. AIP Advances, 13(6).

Ali, N., & Hayat, T. (2007). Peristaltic motion of a Carreau fluid in an asymmetric channel. Applied Mathematics and Computation, 193(2), 535-552.

Ali, N., Wang, Y., Hayat, T., & Oberlack, M. (2009). Numerical solution of peristaltic transport of an Oldroyd 8-constant fluid in a circular cylindrical tube. Canadian Journal of Physics, 87(9), 1047-1058.

Alqarni, A. J., Abo-Elkhair, R., Elsaid, E. M., Abdel-Aty, A.-H., & Abdel-wahed, M. S. (2023). Effect of magnetic force and moderate Reynolds number on MHD Jeffrey hybrid nanofluid through peristaltic channel: application of cancer treatment. The European Physical Journal Plus, 138(2), 1-30.

Böhme, G., & Friedrich, R. (1983). Peristaltic flow of viscoelastic liquids. Journal of Fluid Mechanics, 128, 109-122.

Bradford, J., & Gupta, S. (1986). Compressibility. Methods of Soil Analysis: Part 1 Physical and Mineralogical Methods, 5, 479-492.

Brown, T. D., & Hung, T.-K. (1977). Computational and experimental investigations of two-dimensional nonlinear peristaltic flows. Journal of Fluid Mechanics, 83(2), 249-272.

Burns, J., & Parkes, T. (1967). Peristaltic motion. Journal of Fluid Mechanics, 29(4), 731-743.

Civan, F. (2011). Porous media transport phenomena. John Wiley & Sons.

El-Hamid, M. A., Abo-El Dahab, E. M., Abd El-Aziz, M., & Salem, A. M. (2025). Finite difference versus unsupervised machine learning approach for exploring trihybrid non-Newtonian nanofluid flow around spinning cone. International Communications in Heat and Mass Transfer, 168, 109435.

El-Shehawey, E., & Husseny, S. Z. (2002). Peristaltic transport of a magneto-fluid with porous boundaries. Applied Mathematics and Computation, 129(2-3), 421-440.

El-Shehawy, E., El-Dabe, N., & El-Desoky, I. (2006). Slip effects on the peristaltic flow of a non-Newtonian Maxwellian fluid. Acta Mechanica, 186(1), 141-159.

El Misery, A., & El Shamy, I. (2004). Effects of an endoscope and fluid with variable viscosity on peristaltic motion. Applied Mathematics and Computation, 158(2), 497-511.

Eldabe, N., Moatimid, G., Abouzeid, M., ElShekhipy, A., & Abdallah, N. F. (2020). A semianalytical technique for MHD peristalsis of pseudoplastic nanofluid with temperature-dependent viscosity: Application in drug delivery system. Heat Transfer—Asian Research, 49(1), 424-440.

Eldesoky, I., Abumandour, R., Kamel, M., & Abdelwahab, E. (2019). The combined influences of heat transfer, compliant wall properties and slip conditions on the peristaltic flow through tube. SN Applied Sciences, 1(8), 897.

Ellahi, R., Riaz, A., & Nadeem, S. (2014). Three-dimensional peristaltic flow of a Williamson fluid in a rectangular channel having compliant walls. Journal of Mechanics in Medicine and Biology, 14(01), 1450002.

Elshehawey, E., Eldabe, N. T., Elghazy, E., & Ebaid, A. (2006). Peristaltic transport in an asymmetric channel through a porous medium. Applied Mathematics and Computation, 182(1), 140-150.

Farank, w. (1996). fluid mechnics.

Granger, R. A. (2012). Fluid mechanics. Courier Corporation.

Gupta, B., & Seshadri, V. (1976). Peristaltic pumping in non-uniform tubes. Journal of Biomechanics, 9(2), 105-109.

Hafez, N. (2024). EHD peristaltic flow of Sisko fluid under the effects of convection and endoscope. Ain Shams Engineering Journal, 15(5), 102647.

Hanin, M. (1968). The flow through a channel due to transversally oscillating walls(Mean flow rate calculated for flow in two dimensional channel generated by transverse deflection oscillations along walls). Israel Journal of Technology, 6, 67-71.

Hariharan, P., Seshadri, V., & Banerjee, R. K. (2008). Peristaltic transport of non-Newtonian fluid in a diverging tube with different wave forms. Mathematical and Computer Modelling, 48(7-8), 998-1017.

Hayat, T., Hussain, Q., & Ali, N. (2008). Influence of partial slip on the peristaltic flow in a porous medium. Physica A: Statistical Mechanics and its Applications, 387(14), 3399-3409.

Hayat, T., Saleem, A., Tanveer, A., & Alsaadi, F. (2017). Numerical study for MHD peristaltic flow of Williamson nanofluid in an endoscope with partial slip and wall properties. International Journal of Heat and Mass Transfer, 114, 1181-1187.

Jaffrin, M., & Shapiro, A. (1971). Peristaltic pumping. Annual Review of Fluid Mechanics, 3(1), 13-37.

Jaffrin, M. Y. (1973). Inertia and streamline curvature effects on peristaltic pumping. International Journal of Engineering Science, 11(6), 681-699.

Janna, W. S. (2009). Introduction to fluid mechanics. CRC press.

Kwang-Hua Chu, W., & Fang, J. (2000). On the peristaltic transport in small-Knudsen-number flow. Meccanica, 35, 69-74.

Latham, T. W. (1966). Fluid motions in a peristaltic pump Massachusetts Institute of Technology.

Lykoudis, P. (1971). Peristaltic pumping: A bioengineering model. Proceeding Workshop Hydrodynamic Upper Urinary Tract, Nat. Acad. Sci., Washington, DC,

Macagno, E. O., & Christensen, J. (1980). Fluid mechanics of the duodenum. Annual Review of Fluid Mechanics, 12(1), 139-158.

Mekheimer, K. S. (2005). Peristaltic transport of a Newtonian fluid through a uniform and non-uniform annulus. Arabian Journal for Science and Engineering, 30(1), 69-83.

Misra, J., & Pandey, S. (2001). A mathematical model for oesophageal swallowing of a food-bolus. Mathematical and Computer Modelling, 33(8-9), 997-1009.

Nadeem, S., Ashiq, S., & Ali, M. (2012). Williamson fluid model for the peristaltic flow of chyme in small intestine. Mathematical Problems in Engineering, 2012(1), 479087.

Nadeem, S., Maraj, E., & Akbar, N. S. (2014). Investigation of peristaltic flow of Williamson nanofluid in a curved channel with compliant walls. Applied Nanoscience, 4(5), 511-521.

Nuwairan, M. A., & Souayeh, B. (2022). Simulation of gold nanoparticle transport during MHD electroosmotic flow in a peristaltic micro-channel for biomedical treatment. Micromachines, 13(3), 374.

Paterson, W. G. (2006). Esophageal peristalsis. GI Motility online.

Pritchard, P. J., & Leylegian, J. C. (2011). Introduction to fluid mechanics. ISBN-13 9780470547557.

Rafiq, M., Shaheen, A., Trabelsi, Y., Eldin, S. M., Khan, M. I., & Suker, D. K. (2023). Impact of activation energy and variable properties on peristaltic flow through porous wall channel. Scientific Reports, 13(1), 3219.

Rajput, R. (2010). A textbook of fluid mechanics and hydraulic machines: in SI units. (No Title).

Raju, K. K., & Devanathan, R. (1972). Peristaltic motion of a non-Newtonian fluid. Rheologica Acta, 11(2), 170-178.

Raju, K. S. N. (2011). Fluid mechanics, heat transfer, and mass transfer: chemical engineering practice. John Wiley & Sons,.

Ridha, S. R., & Solagh, H. N. (2025). Effect of Inclined MHD Peristaltic Transport for non-Newtonian model in a Non-Uniform Channel Through Porous Medium As: HTF. Iraqi Journal of Science, 635-651.

Roshani, H., Dabhoiwala, N., Tee, S., Dijkhuis, T., Kurth, K., Ongerboer de Visser, B., de Jong, J., & Lamers, W. (1999). A study of ureteric peristalsis using a single catheter to record EMG, impedance, and pressure changes. Techniques in urology, 5(1), 61-66.

Shaheen, A., Muhammad Hussain, S., Ghazwani, H. A., Huma, Z., & Siddique, I. (2024). Analytical solution of non-Newtonian Williamson fluid under the effect of magnetohydrodynamics. Modern Physics Letters B, 38(13), 2450103.

Siddiqui, A., & Schwarz, W. (1994). Peristaltic flow of a second-order fluid in tubes. Journal of Non-Newtonian Fluid Mechanics, 53, 257-284.

Srinivas, A., Selvi, C., & Sreenadh, S. (2017). Peristaltic pumping of a generalized Newtonian fluid in an elastic tube. Journal of Applied Fluid Mechanics, 10(6), 1785-1798.

Srivastava, L., & Srivastava, V. (1985). Interaction of peristaltic flow with pulsatile flow in a circular cylindrical tube. Journal of Biomechanics, 18(4), 247-253.

Taber, L. A., Zhang, J., & Perucchio, R. (2007). Computational model for the transition from peristaltic to pulsatile flow in the embryonic heart tube.

Takabatake, S., Ayukawa, K., & Mori, A. (1988). Peristaltic pumping in circular cylindrical tubes: a numerical study of fluid transport and its efficiency. Journal of Fluid Mechanics, 193, 267-283.

Tanveer, A., Hayat, T., Alsaedi, A., & Ahmad, B. (2017). On modified Darcy's law utilization in peristalsis of Sisko fluid. Journal of Molecular Liquids, 236, 290-297.

Tanveer, A., Rasheed, I., & Jarral, S. (2024). Peristaltic flow of Williamson nanofluid on a rough surface. Advances in Mechanical Engineering, 16(1), 16878132231222793.

Tripathi, D., & Bég, O. A. (2014). A study on peristaltic flow of nanofluids: Application in drug delivery systems. International Journal of Heat and Mass Transfer, 70, 61-70.

Vajravelu, K., Sreenadh, S., Devaki, P., & Prasad, K. (2016). Peristaltic pumping of a Casson fluid in an elastic tube. Journal of Applied Fluid Mechanics, 9(4), 1897-1905.

Veera Krishna, M., & Swarnalathamma, B. (2016). Convective heat and mass transfer on MHD peristaltic flow of Williamson fluid with the effect of inclined magnetic field. AIP Conference Proceedings,

Weinberg, S. L. (1970). A theoretical and experimental treatment of peristaltic pumping and its relation to ureteral function Massachusetts Institute of Technology].

Weisstein, E. W. (2005). Cylindrical coordinates. https://mathworld. wolfram. com/.

Williamson, R. V. (1929). The flow of pseudoplastic materials. Industrial & Engineering Chemistry, 21(11), 1108-1111.

Yasmin, H., & Nisar, Z. (2023). Mathematical analysis of mixed convective peristaltic flow for chemically reactive Casson nanofluid. Mathematics, 11(12), 2673.